Norwegian University of Life Sciences

Master's Thesis 2020 30 ECTS
Faculty of Science and Technology

Mie ripples and wiggles in infrared spectroscopy of cells and tissues

Simen Rønnekleiv Eriksen
Teacher Education in Natural Sciences

If I have seen further than others, it is by standing upon the shoulders of giants.

Sir Isaac Newton (1643–1727)

Preface

This thesis is the fulfillment of my Master's degree in Teacher Education in Natural Sciences at the Norwegian University of Life Sciences (NMBU). I am also currently a co-author of two articles being written by the BioSpec Group Norway and soon to be published. One regarding inverted peaks in absorbance spectra, and another where the integration with regard to the numerical aperture is done for evaluating the extinction efficiency factor.

I'd like to thank my supervisor, Prof. Achim Kohler for great guidance. A special thanks to PhD Candidate Maren Anna Brandsrud for excellent advice and cooperation. Thank you all in the BioSpec Group Norway for an educational cooperation, and regular coffee and quiz meetings. It has been a pleasure and a privilege to get to know you all.

Thank you Dag, for your inputs and encouragement. Thank you mom and dad for all the love and support.

Ås, June, 2020

Simen Rønnekleiv Eriksen

Summary

Micro-spectroscopy yields chemical information about the microscopic structures in biological tissues in its native form. The great challenge of it is to understand the dynamics of scattered and absorbed light, which makes the extinguished light. The extinguished light is the light apparently absorbed from raw data. Hence the understanding of scattering and absorbance can make out what part of this raw spectrum was pure absorbance. Tools such as Extended Multiplicative Signal Correction (EMSC) and Mie Extinction EMSC (ME-EMSC) does the job of recovering pure absorbance spectra from raw spectra. This thesis uses Mie Theory to examine the scattering and absorbance from three microscopic particles: A sphere and two cylinders with different refractive indexes and radii. The dominant scattering effects from μm-sized particles are ripples and wiggles. Ripples are sharp peaks (thin needles) in the extinction efficiency factor, while wiggles are the greater variance in the extinction efficiency factor (wide oscillations). Absorption bands are modeled by the Lorentz model, and moved into places where ripples are found originally on the particles. This thesis predicts by Mie Theory that the absorbance bands creates inverted peaks in the extinction efficiency factor when placed in place with ripples on the top of a wiggle, and a peak when the ripple is placed on the bottom of a wiggle. The inverted peaks are found in apparent absorbance spectra from μ Fourier Transform Infrared (FTIR) imaging, which earlier have been discarded as artefacts, but are in fact signatures of absorption bands. When the absorption band is moved into a ripple which is placed mid-way on the wiggle, the ripple disappear, leaving almost no trace of neither absorbance band or ripple. The role of the numerical aperture (NA) is studied as well, and it is found that ripples are not affected by the NA.

Samandrag

Mikro-spektroskopi gjev kjemisk informasjon om dei mikroskopiske strukturane i biologiske vev, i deira originale form. Den store utfordringa er å forstå dynamikken mellom spreidt og absorbert lys, som til saman utgjer lyset som er kverva. Det kverva lyset er det lyset som ser ut til å ha blitt absorbert basert på det målte absorpsjonsspektrumet. Dermed kan kjennskapen om spreiing og absorpsjon avgjere kva del av det målte spektrumet var rein absorpsjon. Verktøy som "Extended Multiplicative Signal Correction" (EMSC) og "Mie Extinction EMSC" (ME-EMSC) hentar ut reine absorpsjonsspektrum utifrå målte absorpsjonsspektrum. Denne masteroppgåva nyttar Mie teori til å utforske spreiinga og absorpsjonen frå tre mikroskopiske partiklar: Ei kule og to sylindrar med ulike brytningsindeks og radiusar. Mesteparten av spreiing ifrå partiklar i μm-ordenen kjem ifrå fenomena "ripples" og "wiggles". "Ripples" er tynne nålar som stikk opp av effektivitetsfaktoren for kverving, medan "wiggles" er ein større variasjon i effektivitetsfaktoren for kverving (vide svingningar). Absorpsjonband er modellert ved hjelp av Lorentzmodellen, og flytta inn der "ripples" originalt vart funnen. Denne masteroppgåva føreser ved hjelp av Mie teori at absorpsjonsband skapar omvendte toppar i effektivitetsfaktoren for kverving når dei er plassert på toppen av ein "wiggle", og ein vanleg topp når dei er på botnen av ein "wiggle". Omvendte toppar er funnen i målte absorpsjonsspektrum ifrå μ Fourier Transform Infraraud (FTIR) bilete, som tidlegare har blitt forkasta som artefaktar, men som visar seg å vere signaturar for absorpsjonsband. Når eit absorpsjonsband blir flytta inni ein "ripple" som er plassert på midten av ein "wiggle", forsvinnar "ripple"-en og etterlatar seg knapt noko spor etter seg, ei heller absorpsjonsbandet. Rolla til numerisk apertur (NA) er også blitt studert, og det er funnen at NA ikkje påverkar "ripple"-ar.

List of Figures

Nomenclature

A	Absorbance
C	Cross section
F	Scattering Function
$H_n^{(+)}$	First Hankel Function of nth order
$H_n^{(2)}$	Second Hankel Function of nth order
I	Intensity of transmitted wave
I_0	Intensity of incoming wave
J_n	Bessel Function of first kind in nth order
Q_{abs}	Absorption Efficiency Factor
Q_{ext}	Extinction Efficiency Factor
Q_{sca}	Scattering Efficiency Factor
$T(\theta)$	Amplitude Function for cylinder case
X	Cartesian direction
Y	Cartesian direction
Z	Cartesian direction
Γ	Adjustable parameter corresponding to FWHM of Lorentz function
$\Im$	Imaginary part
Λ	Adjustable parameter proportional to Lorentz peak
Ψ	Wave Function
$\Re$	Real part
$\tilde{\epsilon}$	Real part of the Complex Dielectric Function
$\tilde{\nu_0}$	Wavenumber corresponding to Lorentz peak
$\tilde{\nu}$	Wavenumber
β_n	Phase angle
χ_n	Second Riccati-Bessel Function of nth order

ϵ	Complex Dielectric Function
μ_0	Permeability in vacuum
∇	Gradient
∇^2	Laplacian operator
ω	Angular frequency
∂	Partial derivative
ψ_n	First Riccati-Bessel Function of nth order
ρ	Charge density in vacuum
θ	Spherical coordinate: angle
ε	Scalar electric field
ε_0	Amplitude of scalar electric field
φ	Spherical coordinate: angle
ζ_n	Third Riccati-Bessel Function of nth order
a_n	Coefficient determining the efficiency factors
b_n	Coefficient determining the efficiency factors
c	Speed of electromagnetic waves in vacuum
d	Optical path length
i	Imaginary unit
k	Angular wavenumber
m	Complex refractive index
n	Integer
n_r	Real refractive index
n_i	Imaginary refractive index / Absorptivity
n_{max}	Maximum absolute value of n
r	Spherical coordinate: distance
t	Time
v	Frequency in units of s^{-1}
x	Scaling factor
y	Scaling factor
M	Amplitude for the wave function
$\boldsymbol{B}$	Magnetic Field in vector form
$\boldsymbol{E}$	Electric Field in vector form
$\boldsymbol{J}$	Current density in vector form

EM	Electro Magnetic
EMSC	Extended Multiplicative Signal Correction
FTIR	Fourier Transform Infrared Spectroscopy
FWHM	Full Width Half Mid
IR	Infrared
ME-EMSC	Mie Extinction Extended Multiplicative Signal Correction
NA	Numerical Aperture
PMMA	Polymethyl methacrylate
WGM	Whispering Gallery Mode

1. Introduction

Infrared (IR) spectroscopy has proven to be a great tool for determining chemical properties in biological samples in medical and life science studies. The great advantage of spectroscopy versus a strictly chemical analysis, is that the biological sample can be analysed in its native form. When analysing cells with IR spectroscopy, scattering phenomena occur. Since cells are of the same size-order as the wavelengths of the infrared light, the scattering effects are especially strong. When the cell has a quasi-spherical shape, this scattering phenomenon is called Mie scattering (Mohlenhoff et al., 2005). The dynamics of this light scattering was explained in detail by Gustav Mie already in 1908 (van de Hulst, 1981). In IR spectroscopy of cells, the challenge is to understand which contribution of the measured extinction efficiency or absorbance derives from scattering and which one from pure chemical absorption by the sample.

The understanding of the interplay between scattering and absorption that causes extinction is important in order to understand measured absorbance spectra. Since measured absorbance spectra always contain contributions from scattering, the raw spectra are therefore often called apparent absorbance spectra. While scatter-free spectra, i.e. spectra where the scatter contributions have been separated and removed are called pure absorbance spectra. Extended Multiplicative Signal Correction (EMSC) is a methof frequently used in infrared spectroscopy of cells and tissues to model absorbance spectra and to separate the pure absorbance and the scattering part from apparent absorbance spectra. EMSC was introduced to mid-infrared spectroscopy already in 2005 and successfully used to determine the chemical differences of raw and cooked beef loins from images from Fourier Transform Infrared Microscopy (FTIR) (Kohler et al., 2005). EMSC has been used as a platform for modelling Mie-type scattering in the following years (Kohler et al., 2008), (Bassan et al., 2009), (Bassan et al., 2010), (van Dijk et al., 2013), (Lukacs et al., 2015), (Konevskikh et al., 2016), (Solheim et al., 2019). When modelling Mie scattering, the challenge is that parameters relating to morphology of the sample such as shape and effective thickness of the sample need to be estimated in the modelling process. Another iterative approach for recovery of the imaginary part of the complex refractive index was introduced in 2013 to recover the pure absorbance spectra from

PMMA (Polymethyl methacrylate) spheres (van Dijk et al., 2013). This method was subsequently tested for recovery of pure absorbance spectra of pollen grains (Lukacs et al., 2015). The disadvantage of the method is that it requires an *a priori* knowledge of model parameters. Finally, an EMSC algorithm was developed to correct Mie scattering in single cell infrared spectroscopy in 2016 by using the van de Hulst approximation formulae for calculating the extinction efficiency, Q_{ext} with a complex refractive index, m (Konevskikh et al., 2016).

The Mie theory describes the scattering and absorption of electromagnetic radiation and spherically shaped particles exactly and is the theory that is mostly used in IR spectroscopy of cells and tissues to describe and model scattering phenomena (van de Hulst, 1981), (Kohler et al., 2008), (Bassan et al., 2010), (van Dijk et al., 2013), (Konevskikh et al., 2016), (Blümel et al., 2018), (Solheim et al., 2019). The Mie scattering signatures shows so-called wiggles and ripples. A ripple refers to a sharp peak in the efficiency factor for scattering and for absorption, Q_{sca} and Q_{abs}, and hence also extinction, Q_{ext} (van de Hulst, 1981). These ripples in the efficiency factors are caused by standing waves along the circumference of a spherical or circular scatterer, called Whispering Gallery Modes (WGMs) (Brandsrud, 2016). This is a phenomenon which often appears in infrared spectroscopy, as it is caused by small particles with low imaginary part of the complex refractive index. The higher the real refractive index, n_r, the sharper are the ripples, as the WGMs becomes more dominant (Brandsrud, 2016). Wiggles are a result of the interference between the incident IR light, and the scattered light in the forward direction. This scattering results in larger oscillations creating a background in the extinction efficiency for ripples and absorption bands to manifest on (van de Hulst, 1981).

Since the extinction efficiency of infrared spectra contains sharp chemical absorption bands as well, it is interesting to study what happens when sharp absorption bands, sharp ripples and wiggles appear in the same wavelength range. Since wiggles are causing an underlying baseline carrying ripples and absorption bands, it is interesting to investigate how the ripples and absorption bands are affected by the wiggles. It is further interesting to understand how the absolute peak height of absorption bands is affected by the ripples and wiggles, since infrared spectroscopy is used as a technique to estimate concentration of chemical analytes in a sample and the basic assumption in the ideal case is that the absorbance is proportional to the analyte concentration.

The plan of action for the theoretical exploration in this thesis is to examine two different cylindrical particles and one spherical, in the order of $a = 5 - 10\mu$m, where a is the radius of the particle. Obviously, cells are neither perfectly spherical nor cylindrical. Therefore, a core assumption of this thesis is that the infrared spectrum of cells with quasi-cylindrical and -spherical morphology is comparable to that of perfectly cylindrical or spherical particles. The first cylinder, named cylinder1, has a real refractive index of $n_r = 1.3$, which resembles that of water, and thus also that of most biological samples, (Skaar, 2019). The second cylinder, called cylinder2, has a a real refractive index of $n_r = 1.8$, a parameter setting that produces sharp ripples (Brandsrud, 2016). A refractive index of 1.8 gives us possibility to investigate the sharpest ripples, which do not appear in the situations where the difference between the refractive index of the scatterer and the refractive index of the surroundings are lower. The sphere will be mimicking that of a PMMA sphere which has a real refractive index of around $n_r = 1.5$ in the infrared region (Lukacs et al., 2015). Using different analytical models, the particles will be subject to IR light in the range $\tilde{\nu} = 1000 - 4000$ cm^{-1}. This is the region typically used for FTIR spectroscopy (Blümel et al., 2018). The efficiency factors will be compared to each other for three different assumptions for the pure absorbance, $A = 0, A = 0.3$ and $A = 0.5$.

2. Theory

2.1 Maxwell's Equations in vacuum

The fundament for studying electromagnetic waves, are Maxwell's equations. The Mie Theory which describes the scattering of infrared (IR) light from small particles is derived from answering Maxwell's equations for a plane wave colliding with a dielectric sphere (van de Hulst, 1981). The set of Maxwell's equations consists of four differential equations describing the mutual dependency of electric fields and magnetic fields (Hollesbekk and Skaar, 2018). The first is Gauss' Law:

$$\epsilon_0 \nabla \cdot \boldsymbol{E} = \rho, \tag{2.1}$$

where the vector $\boldsymbol{E}$ is the electric field, ϵ_0 is the dielectric constant and ρ the charge density in vacuum, respectively.

The second is the no magnetic monopole law, also called Gauss Law for magnetism. It states

$$\nabla \cdot \boldsymbol{B} = 0, \tag{2.2}$$

where the vector $\boldsymbol{B}$ is the magnetic field.

Faraday's Law is the third equation. It describes how a varying magnetic field induces a circulating electric field

$$\nabla \times \boldsymbol{E} = -\frac{\partial \boldsymbol{B}}{\partial t}, \tag{2.3}$$

where t is time.

Lastly, The Ampére-Maxwell Law describes how a current or varying electric field induces a circulating magnetic field

$$\nabla \times \boldsymbol{B} = \mu_0 \boldsymbol{J} + \epsilon_0 \mu_0 \frac{\partial \boldsymbol{E}}{\partial t}, \tag{2.4}$$

where μ_0 is the permeability in vacuum and $\boldsymbol{J}$ is the current density. From (Hollesbekk and Skaar, 2018).

2.2 The Wave Function

2.2.1 The Electric Field

The electric field in vacuum with no electric charge propagating in the X-direction satisfies the wave equation

$$\frac{\partial^2 \varepsilon}{\partial X^2} - \frac{1}{c^2}\frac{\partial^2 \varepsilon}{\partial t^2} = 0, \tag{2.5}$$

by Maxwells Equations. The solution to Eq. (2.5) is a simple harmonic wave in the real plane.

$$\varepsilon = \varepsilon_0 \cos{(kX - \omega t)}, \tag{2.6}$$

where k is the angular wavenumber, and ω is the angular frequency (Townsend, 2010).

2.2.2 The Electromagnetic Field

The wave function, $\Psi(X,t)$, describes either the magnetic or the electric field of the light. For a plane wave of constant intensity and amplitude M, the equation is

$$\Psi(X,t) = Me^{i\omega t - ikX}, \tag{2.7}$$

where i is the imaginary unit, (van de Hulst, 1981). The more common symbol for amplitude, A, has been reserved for absorbance in this thesis.

2.3 Absorbance

2.3.1 Definition

Different chemical groups are absorbing specific levels of energy, energy quanta, from EM-waves. The energy quanta are determined through the photon energy

$$E = hv, \tag{2.8}$$

where v is the frequency in units of s^{-1} and h is Planck's constant. This relation was famously explained by Einstein in 1905 (Townsend, 2010). In spectroscopy, the wavenumber is usually given in cm^{-1} and has the symbol $\tilde{\nu}$. The relation between the wavenumber (in cm^{-1}) and the frequency of the EM-wave is then

$$\tilde{\nu} = \frac{2\pi v}{100c}, \tag{2.9}$$

where c is the speed of light in vacuum (Tanner, 2019). Combining (2.8) and (2.9) gives the energy absorbed by a chemical group from an EM-wave with wavenumber $\tilde{\nu}$

$$E = h\frac{100c\tilde{\nu}}{2\pi} \tag{2.10}$$

i.e. the light absorbed is dependent on the wavenumber, which is the basis for the theory of spectroscopy.

The absorbance, $A(\tilde{\nu})$ of a sample being radiated by monochromatic light, is given by

$$A(\tilde{\nu}) = -\log\frac{I(\tilde{\nu})}{I_0(\tilde{\nu})}, \tag{2.11}$$

where $I(\tilde{\nu})$ is the intensity transmitted through the sample and $I_0(\tilde{\nu})$ is the intensity of the incident light, (Kohler et al., 2005). From Beer's Law, the absorbance is related to the imaginary part of the refractive index, $n_i(\tilde{\nu})$, and the effective thickness of the sample, d by

$$A(\tilde{\nu}) = \frac{4\pi\tilde{\nu}n_i(\tilde{\nu})d}{\ln(10)}. \tag{2.12}$$

(van Dijk et al., 2013). Some simple algebra from (2.12) yields a function for the imaginary part of the refractive index, n_i:

$$n_i(\tilde{\nu}) = \frac{A\ln 10}{4\pi d\tilde{\nu}}. \tag{2.13}$$

The d is based on the effective thickness of a cylinder, and approximated as the same for a sphere. It is given by Eq. (2.14).

$$d = \frac{\pi a}{2} \tag{2.14}$$

The complex refractive index, m, is written as:

$$m = n_r - in_i, \tag{2.15}$$

where n_r is the real part of the refractive index. This thesis uses the notation of van de Hulst (1981), meaning the sign of the imaginary part is negative. The complex refractive index, m is defined

$$m \equiv \sqrt{\epsilon}, \tag{2.16}$$

where ϵ is the complex dielectric function (Tanner, 2019).

2.3.2 The Lorentz model

In spectroscopy, the Lorentz model is often used to model absorption. According to the Lorentz model, the complex dielectric function ϵ is calculated as

$$\epsilon = \tilde{\epsilon} + \sum \frac{\Lambda}{\tilde{\nu}_0^2 - \tilde{\nu}^2 - i\tilde{\nu}\Gamma}, \tag{2.17}$$

where $\tilde{\epsilon}$ is the real part of the complex dielectric function, Γ is the width of the Lorentz function and is adjusted to the known Full Width Half Mid (FWHM) value of the absorption band, Λ is proportional to the pure absorbance A. By assuming an absorbance A, the parameter Λ can be obtained from fitting the Lorentz maxima to the corresponding n_i from equation (2.13). $\tilde{\nu}_0$ is the wavenumber of the center of the Lorentz function and $\tilde{\nu}$ is the frequency in wavenumber (Lukacs et al., 2015).

Chemical bands are forces that stretches the elements or molecules bonded, causing them to oscillate. This oscillation is called molecular vibration and absorbs specific amounts of energy from (IR) light. The bands that are being used in vibrational spectroscopy are called stretching bands. At $\tilde{\nu} = 1750\text{cm}^{-1}$ the typical FWHM value of C=O stretching IR band related to lipids is approximately 15 cm^{-1}. For O-H stretching IR band around $\tilde{\nu} = 3250$ cm^{-1} related to water and carbohydrates is several hundred cm^{-1}(Kohler et al., 2020).

2.4 Light Extinction

This section, 2.4, and 2.5 is based on the extensive work of (van de Hulst, 1981).

2.4.1 Definitions

Materials are not only absorbing, but also scattering light. Then it is common to refer to light that is extinguished by some sample. Let the energy scattered in all directions be equal to the energy of the incident wave on to the cross section area C_{sca}. Then let the cross section C_{abs} be such that it covers the amount of light being absorbed, and hence the energy absorbed. Finally, the energy extinguished from the light has a corresponding cross section area C_{ext} covering the light. We get

$$C_{ext} = C_{sca} + C_{abs}. \tag{2.18}$$

The figure 2.1 shows an illustration of these cross sections. The actual geometrical cross section of the sample being radiated is G. The relation between the energy-related cross sections and the geometrical cross section gives the efficiency factors

$$Q_{sca} = \frac{C_{sca}}{G}, \tag{2.19}$$

$$Q_{abs} = \frac{C_{abs}}{G}, \tag{2.20}$$

and

$$Q_{ext} = \frac{C_{ext}}{G}, \tag{2.21}$$

where Q_{sca} is the scattering efficiency factor, Q_{abs} is the absorbance efficiency factor and Q_{ext} is the extinction efficiency factor. The efficiency factors are related by

$$Q_{ext} = Q_{sca} + Q_{abs}. \tag{2.22}$$

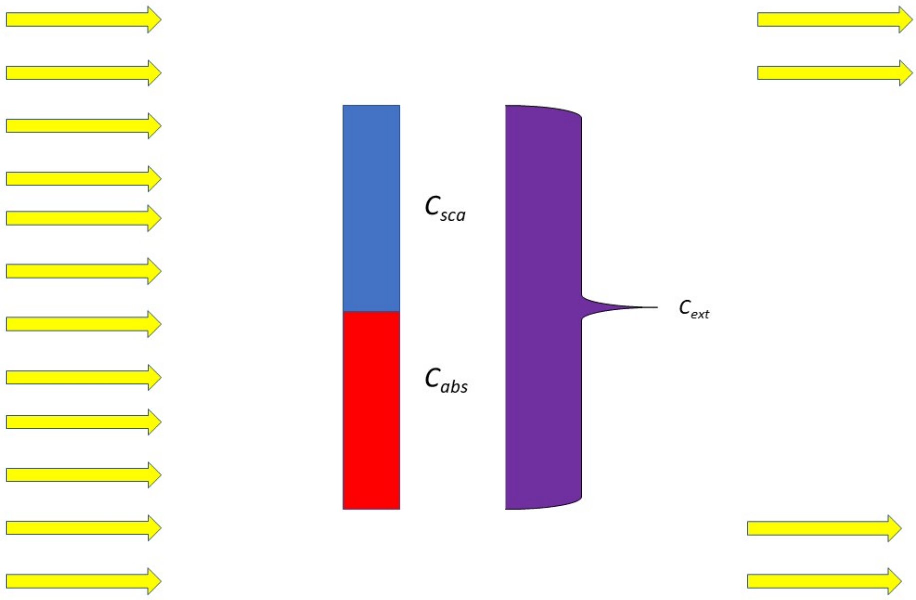

Figure 2.1: The cross sections illustrating the fraction of an incident beam that is absorbed and scattered. The incoming beam is indicated by the yellow arrows to the left. The yellow arrows to the right correspond to the amount of light that travelled through the sample undisturbed. The cross section of the scattered radiation is in blue, and the cross section of the absorbed radiation is in red. The actual area has a depth in to the paper, and a length equal to the vertical axis. The horizontal axis has only a thickness for graphical visibility. The purple summation arrow shows how the extinction cross section is the sum of the other two cross sections

2.5 Light scattering

When incident light with intensity I_0 is colliding with some particle in space, the light scattered has an intensity I at a large distance r away from the particle with an angle

θ with the line of propagation and azimuth angle φ. The light has a wavelength λ and corresponding angular wavenumber in m^{-1}, k, in the surrounding medium. Then

$$I = \frac{I_0 F(\theta, \varphi)}{k^2 r^2}. \tag{2.23}$$

The dimensionless function $F(\theta, \varphi)$ of the direction and depends on the orientation of the particle with respect to the incident wave, and on the polarization of the wave. Then the general expression for C_{sca} can be made

$$C_{sca} = \frac{1}{k^2} \int F(\theta, \varphi) d\omega. \tag{2.24}$$

The integral in 2.24 is taken over all directions and

$$d\omega = \sin(\theta) d\theta d\varphi, \tag{2.25}$$

is the element of solid angle. In order to find the amplitude and phase of the scattered waves, the scattering functions $S_1(\theta, \varphi)$ and $S_2(\theta, \varphi)$ are used. These functions will vary from particle to particle, and hence will be specified for the relevant particle in later sections, 2.6 and 2.7.

2.6 Cylinder

The Mie Theory describing the scattering from a cylindrical particle is derived by answering Maxwell's equations (sec. 2.1) for a plane wave scattered from a dielectric cylinder (van de Hulst, 1981).

2.6.1 Efficiency Factors by exact Mie Theory, Case I

This section regards a cylinder particle with an incident plane wave with the $\boldsymbol{E}$-field parallel to the cylinder axis, as shown in Fig. 2.2 and is referred to as Case I. From trigonometry, the angle θ and distance r away from the center of the cylinder are given by the Cartesian XY-plane, X and Y are given by

$$X = r \cos \theta, \tag{2.26}$$

and

$$Y = r \sin \theta. \tag{2.27}$$

Regarding a distance $r >> a$, where a is the radius of the cylinder, the expressions for

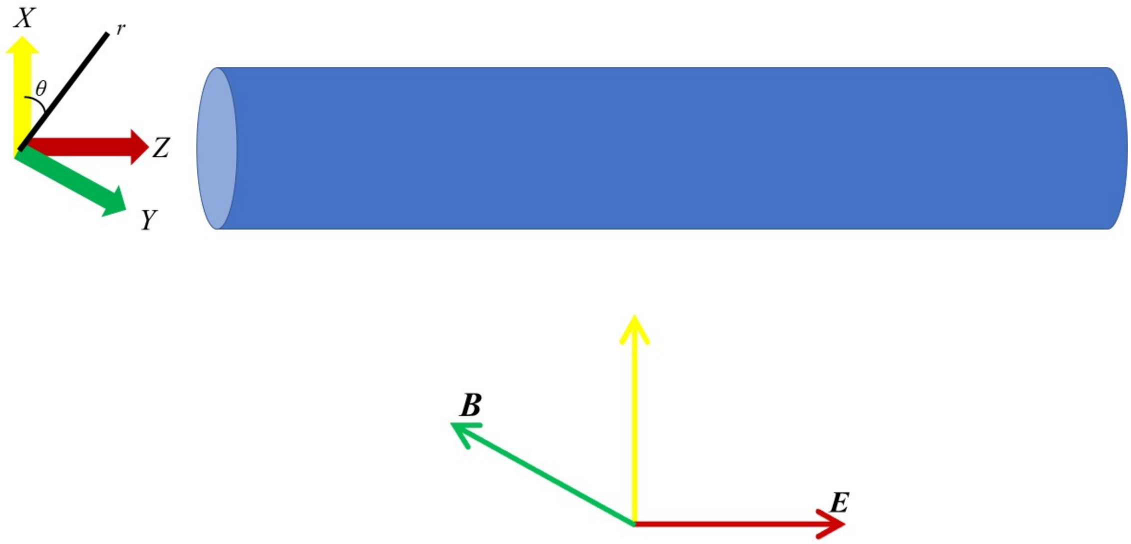

Figure 2.2: A cylinder-shaped particle with an incident EM-wave with ***E***-field parallel to the cylinder axis. The ***B***-field is perpendicular to the cylinder axis. The yellow vector indicates the propagation direction of the EM-wave which is perpedicular to the cylinder axis. The red and green vectors indicate the absolute maxima of the sinusoidal fields. The arrows on the left are the cartesian coordinates X, Y and Z.

Q_{ext} and Q_{sca} are

$$Q_{ext} = \frac{2}{x} \sum_{n=-\infty}^{\infty} \Re(b_n), \tag{2.28}$$

and

$$Q_{sca} = \frac{2}{x} \sum_{n=-\infty}^{\infty} |b_n|^2, \tag{2.29}$$

where n is some integer, b is a coefficient (described below) and x is the scaling factor

$$x = \frac{2\pi a}{\lambda}. \tag{2.30}$$

a is the radius of the cylinder and λ is the wavelength (van de Hulst, 1981). The wavelength λ is calculated by

$$\lambda = \frac{1}{100\tilde{\nu}}. \tag{2.31}$$

From these expressions and Eq. 2.22 the expression of Q_{abs} is found to be

$$Q_{abs} = \frac{2}{x} \sum_{n=-\infty}^{n=\infty} \Re(b_n) - \frac{2}{x} \sum_{n=-\infty}^{n=\infty} \Re(|b_n|^2). \tag{2.32}$$

The coefficients b_n are determined by

$$b_n = \frac{\tan \beta_n}{\tan \beta_n - i} \tag{2.33}$$

where β_n is the phase angle given by

$$\tan \beta_n = \frac{mJ_n'(y)J_n(x) - J_n(y)J_n'(x)}{mJ_n'(y)N_n(x) - J_n(y)N_n'(x)} \tag{2.34}$$

where y is another scaling factor

$$y = mx. \tag{2.35}$$

The functions J_n and N_n are Bessel functions of the first and second kind, respectively, in the nth order (van de Hulst, 1981).

2.6.2 Efficiency Factors by exact Mie theory, Case II

In Case II, it is the $\boldsymbol{B}$-field which is parallel to the cylinder axis, and the $\boldsymbol{E}$-field which is perpendicular to it as shown in figure 2.3.

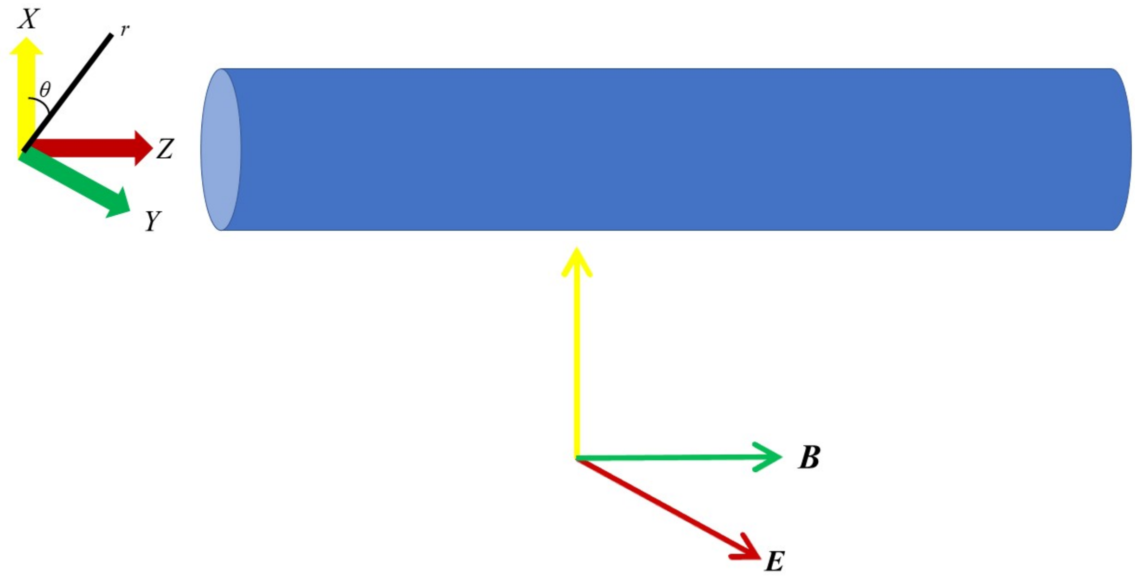

Figure 2.3: A cylinder-shaped particle with an incident EM-wave with $\boldsymbol{B}$-field parallel to the cylinder axis. The $\boldsymbol{E}$-field is perpendicular to the cylinder axis. The yellow vector indicates the propagation direction of the EM-wave, and the red and green vectors indicate the absolute maxima of the sinusoidal fields. The arrows on the left are the Cartesian coordinates X, Y and Z.

Q_{ext} and Q_{sca} in this scenario are given in equations 2.36 and 2.37.

$$Q_{ext} = \frac{2}{x} \sum_{n=-\infty}^{n=\infty} \Re(a_n), \tag{2.36}$$

and

$$Q_{sca} = \frac{2}{x} \sum_{n=-\infty}^{n=\infty} |a_n|^2, \tag{2.37}$$

where x and y are scaling factors given by Eqs (2.30) and (2.35), and the coefficient a_n is given as

$$a_n = \frac{\tan \alpha_n}{\tan \alpha_n - i}. \tag{2.38}$$

The phase angle $\tan \alpha_n$ is calculated by equation 2.39.

$$\tan \alpha_n = \frac{J_n'(y)J_n(x) - mJ_n(y)J_n'(x)}{J_n'(y)N_n(x) - mJ_n(y)N_n'(x)}. \tag{2.39}$$

2.6.3 Efficiency Factor for scattering by integral

The Q_{sca} is given by the integral over the angle θ, see Fig. 2.4, in all directions

$$Q_{sca} = \frac{1}{\pi x}\int_0^{2\pi} |T(\theta)|^2 d\theta, \tag{2.40}$$

where $T(\theta)$ is a type of amplitude function. For Case I, it is given by

$$T(\theta) = \sum_{n=-\infty}^{\infty} b_n e^{in\theta}. \tag{2.41}$$

Here, the coefficients b_n are given in terms of the Hankel function of second kind, $H_n^{(2)}$,

$$H_n^{(2)}(Z) = J_n(Z) - iN_n(Z) \tag{2.42}$$

$$b_n = \frac{mJ_n'(y)J_n(x) - J_n(y)J_n'(x)}{mJ_n'(y)H_n^{(2)}(x) - J_n(y)H_n^{(2)\prime}(x)}. \tag{2.43}$$

Since it is impossible to calculate for infinitely many n's, the restriction for n is given as

$$n_{max} = \max\left(x + 4(x)^{\frac{1}{3}} + 2\right) \tag{2.44}$$

This formula gives $n \geq 10 + x$ for the a's and $\tilde{\nu}$'s examined in this thesis (for which makes out the scaling factor x). At those high orders, the Bessel function becomes negligible for each order.

The formula for Q_{sca} in 2.29 and 2.40 both take into account for the waves scattered in all directions, based on C_{sca} from 2.24. However, in an experiment, the result is based on the waves reaching the detector. The detector's surface for detection is described by its NA (numerical aperture), defined as

$$\mathrm{NA} = \sin \theta \tag{2.45}$$

(Tipler and Mosca, 2008). In order to mimic experimental results, the integral in 2.40

may be restricted by the area from $-\theta$ to θ

$$Q_{sca} = \frac{1}{\pi x} \int_{-\theta}^{\theta} |T(\theta)|^2 d\theta. \tag{2.46}$$

This integration area is illustrated by figure 2.4. The restriction for the angle θ will be given by the NA. The values of NA used in this paper are 0.2, 0.35, 0.5 and 0.65, inspired by common minimum and maximum values of NA (van Dijk et al., 2013).

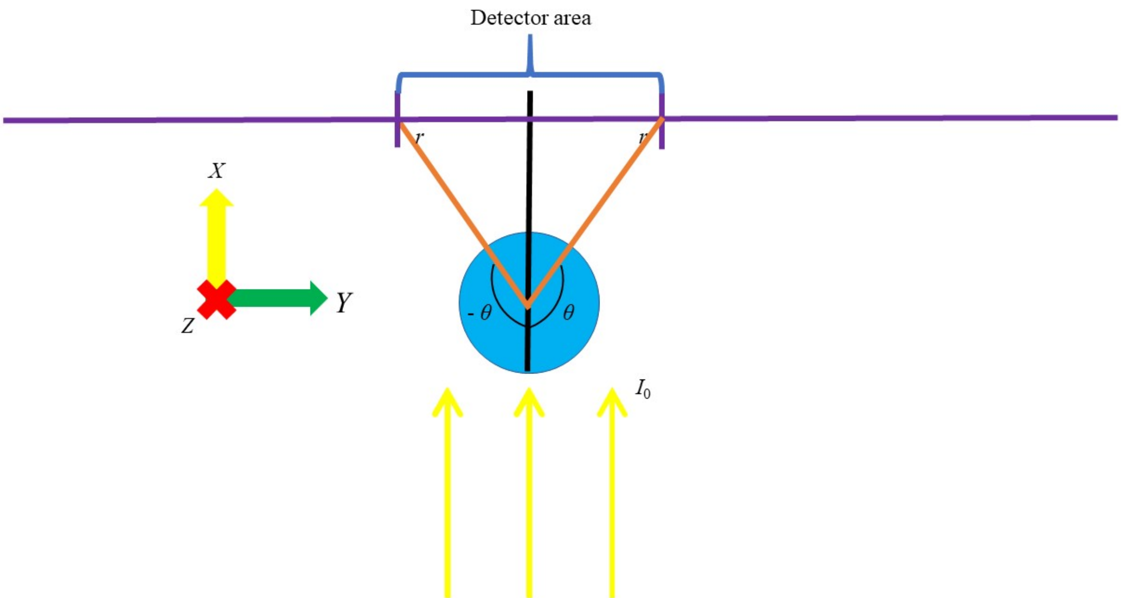

Figure 2.4: Illustration of the integration area. The perspective is along the Z-axis (red cross representing the "feathers" of the Z-arrow), from the side of the cylinder, making it look like a disk (light blue). The orange lines are light scattered at the angle $-\theta$ and θ a distance r away from the center of the cylinder. The black line is perpendicular to the cylinder axis, and the purple one is perpendicular to both the cylinder axis and the black line, representing the line of which the detector area lies. The blue brace shows the detector area. The three yellow arrows represent the direction of the incoming light with intensity I_0.

2.6.4 The near $\boldsymbol{E}$-field of a disk-shaped scatterer

The time-independent form of the wave equation (Eq. (2.5)) is known as the Helmholtz equation.

$$(\nabla^2 + k^2)\boldsymbol{E}(\boldsymbol{r}) = 0, \tag{2.47}$$

where ∇^2 is the Laplacian operator, $\boldsymbol{E}(\boldsymbol{r})$ is the plane vector wave and $\boldsymbol{r}$ being the position vector in the Cartesian plane. The Helmholtz equation can be simplified by replacing the plane vector wave $\boldsymbol{E}(\boldsymbol{r})$ by the single component scalar wave function $\Psi(\boldsymbol{r})$ (scalar version of Eq. (2.7)). The simplified Helmholtz equation (Eq. (2.47)) then becomes

$$(\nabla^2 + k^2)\Psi(\boldsymbol{r}) = 0, \tag{2.48}$$

(Torgersen, 2016).

In order to study more in-depth the scattering from a cylindrical particle, the close $\boldsymbol{E}$-field around a cylinder is studied. A simplification can only be done for Case I with $\boldsymbol{E}$-field of the incoming plane wave parallel to the cylinder axis, and thus is the only case studied in-depth in this thesis. The simplification is that the cylinder can be regarded as a disk, since the cylinder is a disk from the $\boldsymbol{E}$-fields perspective in that scenario. The disk considered is one with a potential $V = V_0$ inside, a so called "soft" disk, i.e. the light can penetrate through the sample. The refractive index inside the disk is $m > 1$, while it is $m = 1$ outside the disk (vacuum). The analytical solution to this problem has been derived by Prof. Reinhold Blümel and presented in his lecture notes from June 26, 2012 (Torgersen, 2016).

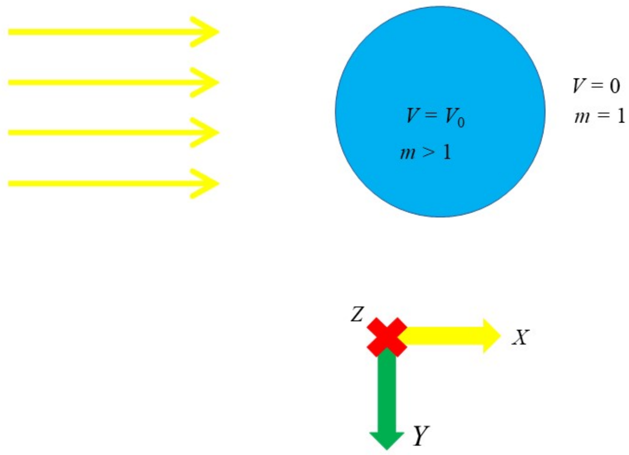

Figure 2.5: Illustration of a "soft" disk. The perspective is along the Z-axis, from the side of the cylinder, making it look like a disk (light blue). The yellow vectors indicates the propagation direction of the incoming light, along the X-axis. The arrows under the disk are the Cartesian coordinates, with the Z-axis into the paper (red cross indicating the "feathers" of the arrow). The $\boldsymbol{E}$-field is along the Z-axis.

For $r > a$, i.e. outside the disk, the wave function is given by

$$\Psi_{out}(r, \theta) = \sum_{n=-\infty}^{\infty} i^n J_n(kr) e^{in\theta} + \sum_{n=-\infty}^{n\infty} A_n H_n^{(+)}(kr) e^{in\theta}, \tag{2.49}$$

where $H_n^{(+)}$ is the Hankel functions of first kind of nth order, and A_n are coefficients derived from the quantum mechanical boundary conditions given by

$$A_n = \frac{i^n(J_n'(x)J(mx) - mJ_n'(mx)J_n(x))}{mJ_n'(mx)H_n^{(+)}(x) - H_n^{(+)}{}'(x)J_n(mx)}, \tag{2.50}$$

where x is the scaling factor in Eq (2.30), i.e. $x = ka$. The first part of equation 2.49 represents the incoming plane wave and the second part represents the outgoing, scattered wave.

For $r < a$, i.e. inside the disk, the wave function is given by

$$\Psi_{in}(r,\theta) = \sum_{n=-\infty}^{\infty} B_n J_n(mx)e^{in\theta}, \tag{2.51}$$

where B_n are coefficients determined by the quantum mechanical boundary conditions as

$$B_n = \frac{i^n(H_n^{(+)}{}'(x)J_n(x) - J_n'(x)H_n^{(+)}(x))}{H_n^{(+)}{}'(x)J_n(mx) - mJ_n'(mx)H_n^{(+)}(x)}, \tag{2.52}$$

(Torgersen, 2016). The same restriction for n_{max} as for calculating the a_n's and b_n's for the cylinder is set here, with calculations stopping after $n \geq x + 10$.

2.7 Sphere - Mie Theory

The Mie Theory is derived by answering Maxwell's equations (sec: 2.1) for scattered plane wave from a dielectric sphere (van de Hulst, 1981).

2.7.1 Efficiency Factors by series

The scattering of waves from an arbitrary sphere is explained through Mie Theory (van de Hulst, 1981). The extinction efficiency factor Q_{ext} and scattering efficiency factor, Q_{sca} are in this instance given by the series

$$Q_{ext} = \frac{2}{x^2}\sum_{n=1}^{n=\infty}(2n+1)\Re(a_n + b_n) \tag{2.53}$$

and

$$Q_{sca} = \frac{2}{x^2}\sum_{n=1}^{n=\infty}(2n+1)\Re(|a_n|^2 + |b_n|^2). \tag{2.54}$$

Here, another set of coefficients are needed, a_n, in addition to the b_n's. In this instance they are given by

$$a_n = \frac{\psi_n'(y)\psi_n(x) - m\psi_n(y)\psi_n'(x)}{\psi_n'(y)\zeta_n(x) - m\psi_n(y)\zeta_n'(x)}, \tag{2.55}$$

and

$$b_n = \frac{m\psi_n'(y)\psi_n(x) - \psi_n(y)\psi_n'(x)}{m\psi_n'(y)\zeta_n(x) - \psi_n(y)\zeta_n'(x)}. \quad (2.56)$$

where ψ_n and ζ_n are the first and third Riccati-Bessel function, which along the Z-axis is given by

$$\psi_n(Z) = (\frac{\pi Z}{2})^{\frac{1}{2}} J_{n+\frac{1}{2}}(Z), \quad (2.57)$$

$$\zeta_n(Z) = (\frac{\pi Z}{2})^{\frac{1}{2}} H^{(2)}_{n+\frac{1}{2}}(Z). \quad (2.58)$$

The second Riccati-Bessel function is

$$\chi_n(Z) = -(\frac{\pi Z}{2})^{\frac{1}{2}} N_{n+\frac{1}{2}}(Z). \quad (2.59)$$

From 2.42, 2.58 and 2.59, ζ_n can be expressed as

$$\zeta_n(Z) = \psi_n(Z) + i\chi_n(Z). \quad (2.60)$$

Thus, Q_{ext} and Q_{sca} can be computed (van de Hulst, 1981). Since the sum can not be calculated numerically for infinitely many n's, the calculations stops after $n \geq x + 10$.

3. Results

3.1 Cylinder

3.1.1 Ripple and b_n pairs

The extinction efficiency factor, Q_{ext}, consists of broad oscillations, called wiggles, and sharp oscillations called ripples. The black line in Fig. 3.1 shows Q_{ext} as a function of wavenumber $\tilde{\nu}$ for a cylinder with a radius 10 μm and a refractive index equal to 1.3, this will be referred to as "cylinder1". The evaluation is done for "Case I" as described in the Sec 2.6.1.

Q_{ext} is found by Eq. 2.28 and is made up of a sum of the coefficient b_n (described by Eq. 2.33). As e.g. $\Re(b_{12})$ (cyan dotted line) in Fig. 3.1 shows, do the peak in $\Re(b_{18})$ (magenta dotted line) correspond with a ripple in Q_{ext} and make up a *ripple and* b_n *pair*. The rightmost peak of the coefficient b_{12} coincides with the ripple at $\tilde{\nu} = 1807$ cm^{-1}for this cylinder. The rightmost peak of b_{18} coincides with the ripple at $\tilde{\nu} = 2600$ cm^{-1}. This ripple is at the top of a wiggle, while the ripple at 1808 cm^{-1}is at the bottom of a wiggle. An additional b_n-ripple pair for this scenario is b_{22} (magenta dotted line) and a ripple at $\tilde{\nu} = 3128$ cm^{-1}, midway between the bottom and peak of a wiggle, as shown in Fig. 3.2. The figures in this subsection is calculated by the MatLab script in appendix B.

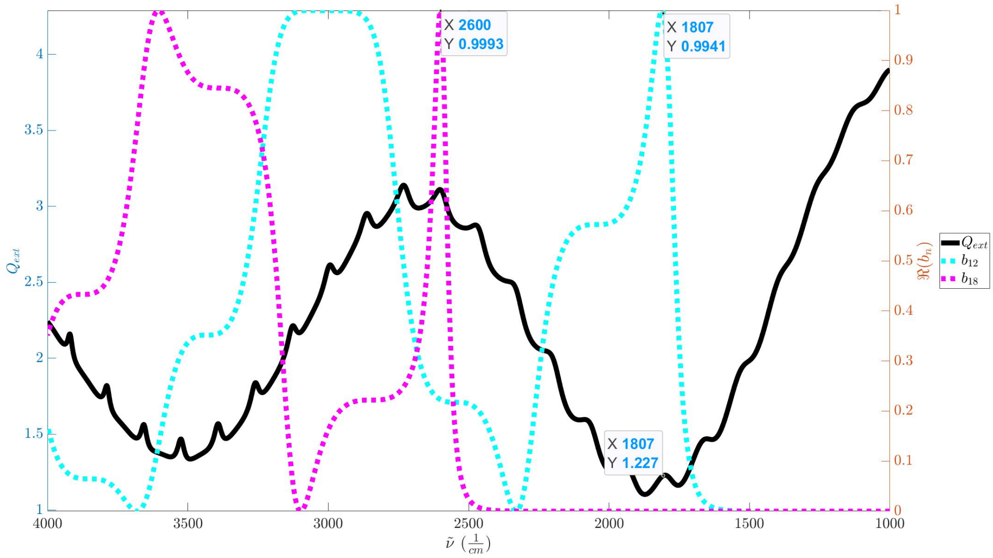

Figure 3.1: b_n-ripple pair for cylinder1. The left y-axis shows Q_{ext} (black line) as a function of wavenumber and right y-axis shows $\Re(b_n)$ as a function of wavenumber for $n = 12$ (cyan dotted line) and $n = 18$ (pink dotted line). The data tips shows the position of the peak in b_n which corresponds to a ripple in Q_{ext}.

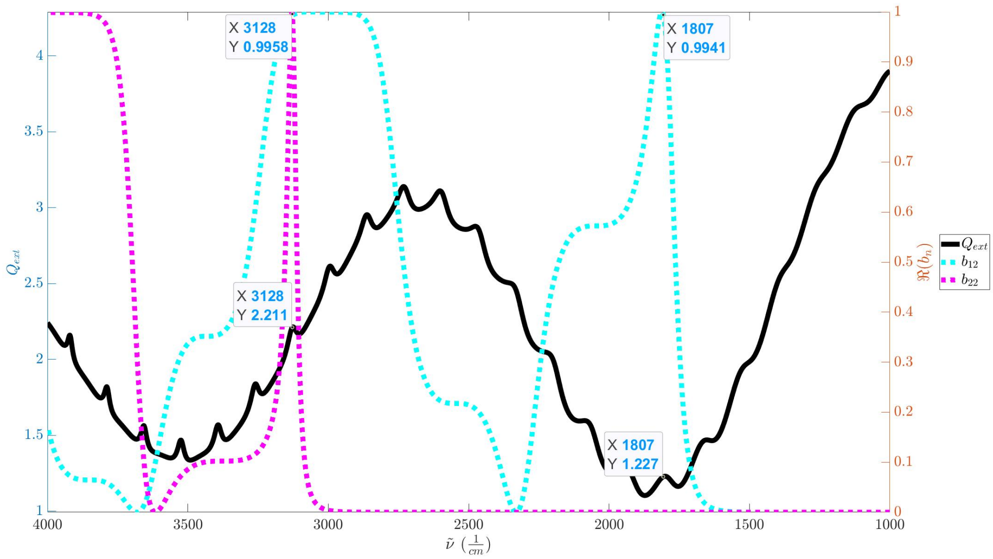

Figure 3.2: b_n-ripple pair for cylinder1. The left y-axis shows Q_{ext} (black line) as a function of wavenumber and right y-axis shows $\Re(b_n)$ as a function of wavenumber for $n = 12$ (cyan dotted line) and $n = 22$ (pink dotted line). The data tips shows the position of the peak in b_n which corresponds to a ripple in Q_{ext}, and the position of the ripple.

Another system investigated is an infinite cylinder with a refractive index $n_r = 1.8$ and radius $a = 5\mu$m. This will be referred to as "cylinder2". The coefficient b_{12} (cyan dotted line) now pairs with the sharp ripple at $\tilde{\nu} = 2696$ cm^{-1}and is at the bottom of a wiggle. A sharp ripple at the top of a wiggle, at $\tilde{\nu} = 3287$ cm^{-1}coincides with the peak of b_{18} (magenta dotted line) as shown in Fig. 3.3.

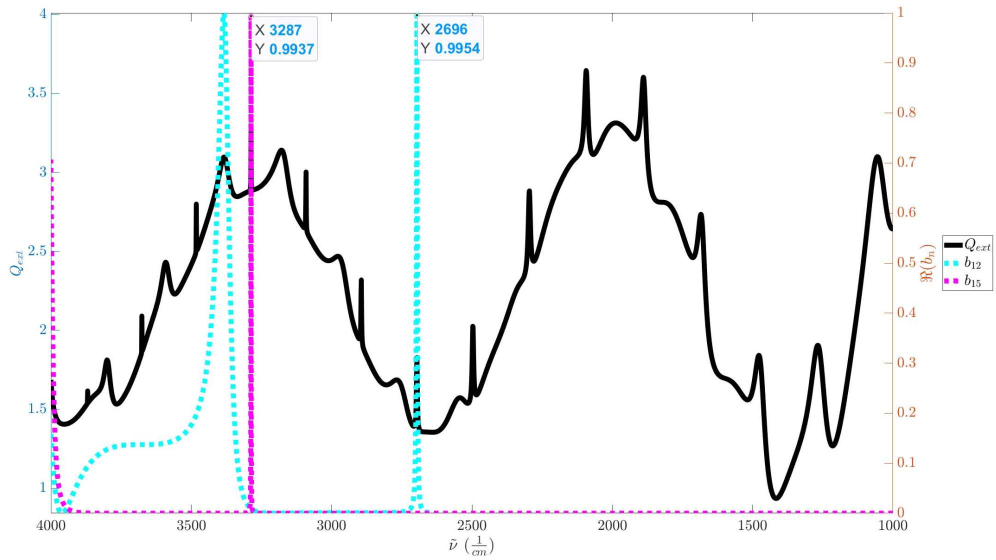

Figure 3.3: b_n-ripple pair for cylinder2. The left y-axis shows Q_{ext} (black line) as a function of wavenumber and right y-axis shows $\Re(b_n)$ as a function of wavenumber for $n = 12$ (cyan dotted line) and $n = 15$ (pink dotted line). The data tips shows the position of the peak in b_n which corresponds to a ripple in Q_{ext}.

3.1.2 The imaginary part of the refractive index for a constant absorbance and absorbance bands

For a constant absorbance equal to $A = 0.3$, the imaginary part of the refractive index, n_i, can be calculated by Eq. 2.13. For cylinder1 the wavenumbers corresponding to a ripple are $\tilde{\nu}_0 = 1807$ cm^{-1} and $\tilde{\nu}_0 = 3128$ cm^{-1}. The d used to calculate n_i is given by Eq. (2.14). The Fig. 3.4 shows how the imaginary part of the refractive index, found by Eq. (2.13), of cylinder1 varies with wavenumbers when the absorbance is assumed to be constant for all wavenumbers (green dashed line). This increases exponentially with lesser wavenumbers $\tilde{\nu}$, as they are inverse proportional. In Fig. 3.4 this line is plotted together with appropriate Lorentz functions at the relevant wavenumbers for the ripples (blue solid line). The n_i that varies with the two Lorentz functions were calculated by adding together the Eq. (2.17) with the two different central wavenumbers, $\tilde{\nu}_0 = 1807$ cm^{-1} and $\tilde{\nu}_0 = 3128$ cm^{-1}, and then found by Eq. (2.16). $\Gamma = 15$ cm^{-1} was used, which is related to lipids at around $\tilde{\nu} = 1750$ cm^{-1} (Kohler et al., 2020). Adjusted to a pure absorbance $A = 0.3$, this resulted in a $\Lambda = 1400$ cm^{-2}. This absorption band was then copied and put at the other ripple at $\tilde{\nu}_0 = 3128$ cm^{-1}, as indicated by the data tips. Notice the peaks of the Lorentz functions reaches the same $A = 0.3$. The MatLab script in appendix A was used to calculate the figures in this subsection.

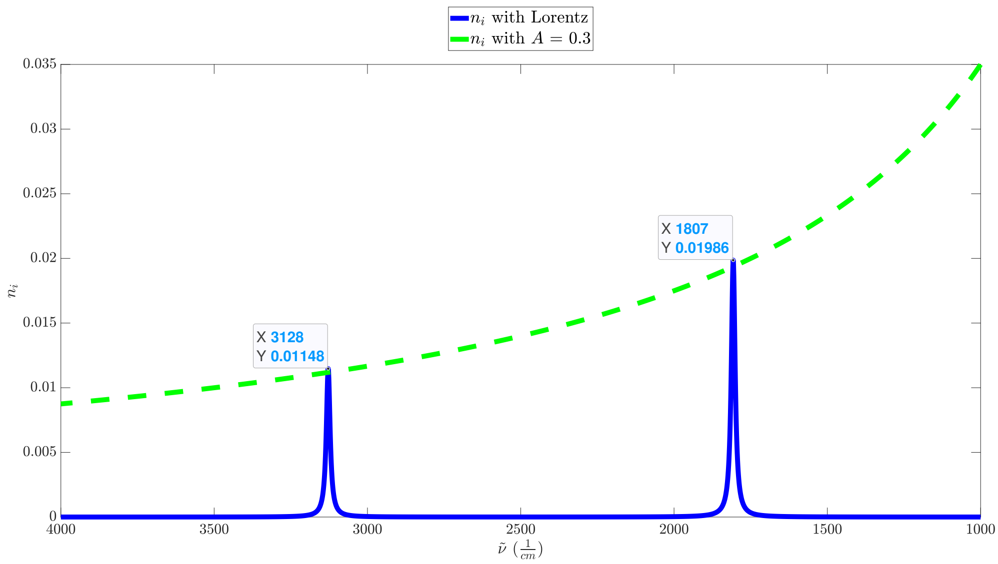

Figure 3.4: Lorentz function for cylinder1 with $\Gamma = 15$ cm^{-1}, $\Lambda = 1400$ cm^{-2} and $\tilde{\nu}_0 = 1807$ cm^{-1} and 3128 cm^{-1} plotted in blue solid line. n_i with constant $A = 0.3$ plotted in green dashed line. The data tips shows the peaks of the Lorentz functions, where the n_i-value corresponds to $A = 0.3$.

The pure absorbance is increased to $A = 0.5$ for cylinder1. Thus, the parameter Λ increases proportional to A by a factor of $\frac{5}{3}$ to 2300 cm^{-2} in order to reach a peak corresponding to $A = 0.5$, as seen by the blue solid lines reaching the green dotted line, and highlighted by the data tips. This absorption band is put at the ripple at $\tilde{\nu}_0 = 2600$ cm^{-1}, together with $\tilde{\nu} = 1807$ cm^{-1}in Fig. 3.5.

The pure absorbance, A, for cylinder2 is put to 0.5. The same $\Gamma = 15$ cm^{-1} was used, corresponding to the FWHM and thus giving a similar sharp absorption band. The Λ for this scenario becomes 6300 cm^{-2}. The absorption bands are centered on the ripples at $\tilde{\nu}_0 = 2696$ cm^{-1} and $\tilde{\nu}_0 = 3287$ cm^{-1}, giving the Lorentzian n_i in the blue solid line in Fig. 3.6. The resulting imaginary part of the refractive index, n_i, for constant A of cylinder2 is shown in green dotted line. Once more, the peak of the Lorentzian n_i reaches the same value for which they have been adjusted for as indicated by the data tips.

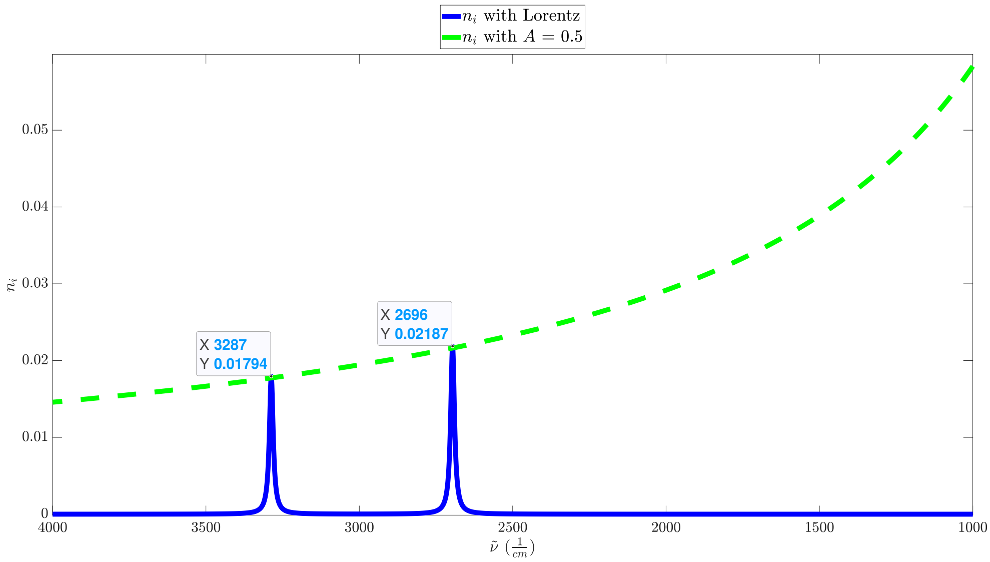

Figure 3.5: Lorentz function for cylinder1 with $\Gamma = 15$ cm^{-1}, $\Lambda = 2300$ cm^{-2} and $\tilde{\nu}_0 = 1807$ cm^{-1} and 2600 cm^{-1} plotted in blue solid line. n_i with constant $A = 0.5$ plotted in green dashed line. The data tips shows the peaks of the Lorentz functions, where the n_i-value corresponds to $A = 0.5$.

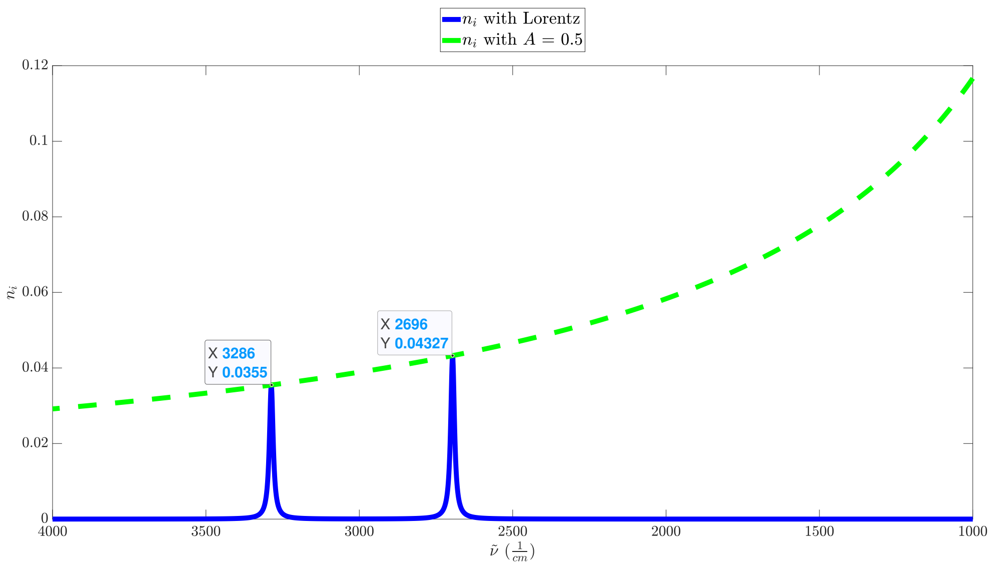

Figure 3.6: Lorentz function for cylinder2 with $\Gamma = 15$ cm^{-1}, $\Lambda = 6300$ cm^{-2} and $\tilde{\nu}_0 = 2696$ cm^{-1} and 3287 cm^{-1} plotted in blue solid line. n_i with constant $A = 0.5$ plotted in green dashed line. The data tips shows the peaks of the Lorentz functions, where the n_i-value corresponds to $A = 0.5$.

3.1.3 Efficiency factors found by Mie theory

Q_{ext} was evaluated for both cylinder1 and cylinder2 with Eq. (2.28) for two cases: (i) with constant A and (ii) with Lorentzian absorption bands with peaks corresponding to the same A, the position of peaks are identical to the ones shown in the figures in Sec. 3.1.2.

The extinction efficiency factor Q_{ext} for cylinder1 was plotted in the Fig. 3.7 against the left y-axis. Figure 3.7 shows Q_{ext} with constant $A = 0.3$ plotted with green dotted line, and the Q_{ext} with a Lorentzian absorbance band at $\tilde{\nu}_0 = 1807$ cm^{-1} and $\tilde{\nu}_0 = 3128$ cm^{-1} with $\Gamma = 15$ cm^{-1} and $\Lambda = 1400$ cm^{-2} plotted in a solid blue line. The $\Re(b_n)$'s from Fig. 3.1 are plotted against the right y-axis. $\Re(b_{12})$ for constant $A = 0.3$ is plotted in dotted magenta line, and for the Lorentzian n_i $\Re(b_{12})$ is plotted in a solid cyan line. For $A = 0.3$, $\Re(b_{22})$ is plotted in a dotted yellow line, and with the Lorentzian n_i it is plotted in a solid black line. The Q_{ext} with a Lorentz-shaped absorption band at $\tilde{\nu}_0 = 1807$ cm^{-1} has a peak reaching up towards the level of the Q_{ext} with constant A. The $\Re(b_{12})$ is lessened at this wavenumber, meaning the peak must come from an increase in most of the other $\Re(b_n)$'s at this point. This makes sense as the curve is quite smooth for the green dotted line of Q_{ext} with constant A, indicating it is a sum of several $\Re(b_n)$'s with some positive value. The leftmost peak of $\Re(b_{12})$ is influenced by the absorption band at $\tilde{\nu}_0 = 3128$ cm^{-1}, but the $\Re(b_{22})$ is not affected by the absorption band at $\tilde{\nu}_0 = 1807$ cm^{-1}. Since both $\Re(b_{12})$ and $\Re(b_{22})$ is lessened at by the Lorentz-shaped absorption band centered at $\tilde{\nu}_0 = 3128$ cm^{-1}, the ripple in Q_{ext} disappear. They are not however, lessened so much as to leave a dent in Q_{ext}. Rather, Q_{ext} has a smooth curve at this wavenumber.

The scattering efficiency factor Q_{sca} was calculated by Eq. (2.29) for the same parameters and plotted in Fig. 3.8. In these figures, the green dotted line is the Q_{sca} with constant $A = 0.3$. The solid blue line is the Lorentzian Q_{sca} with $\tilde{\nu}_0 = 1807$ cm^{-1} and $\tilde{\nu} = 3128$ cm^{-1} in Fig. 3.8. The absorbance efficiency factor Q_{abs} was calculated by subtracting Q_{sca} from Q_{ext}, rearranging Eq. (2.32), and plotted in the Fig. 3.9. The green dotted line is the Q_{abs} with constant $A = 0.3$. The solid blue line is the Q_{abs} with the same Lorentz parameters. It is apparent from Fig. 3.8 that with increasing absorbance, the amount of scattered light is lessened. The absorption bands creates inverted peaks in the Lorentzian Q_{sca} and moves it towards the Q_{sca} value for constant A, since they must be equal at the meeting points indicated by the data tips. The absorption bands are clearly visible in the Q_{abs} in Fig. 3.9. The Lorentzian Q_{abs} reaches towards the same values of Q_{abs}, since the peak corresponds to the same amount of absorbance, as indicated by the data tips.

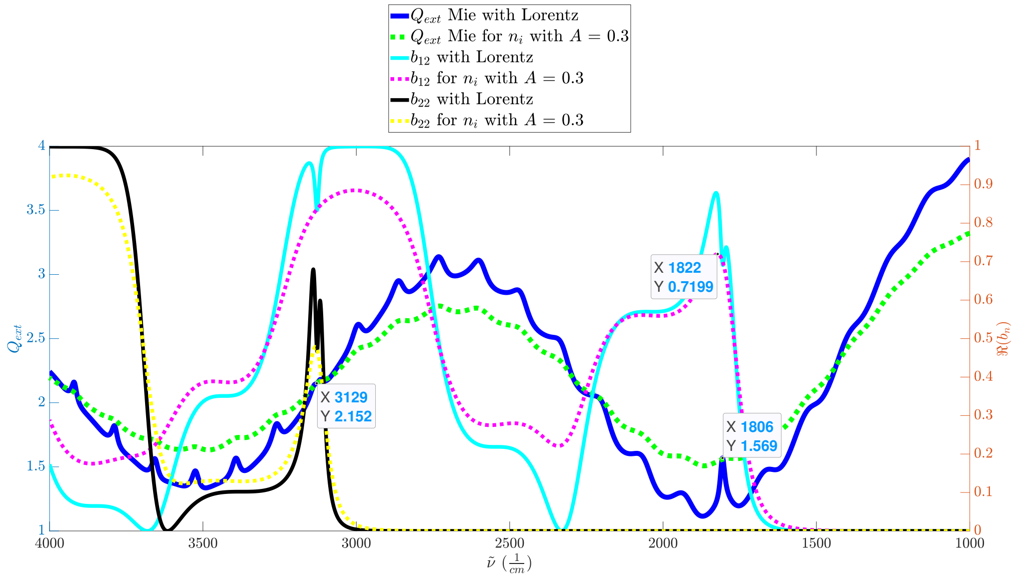

Figure 3.7: Two Q_{ext} for cylinder1 is plotted against the left y-axis. The dotted green line is Q_{ext} with $A = 0.3$ for all wavenumbers $\tilde{\nu}$, and the solid blue line is Q_{ext} with Lorentzian n_i. The $\Re(b_n)$'s are plotted against the right y-axis for $n = 12$ and $n = 22$ for cylinder1. $\Re(b_{12})$ with constant $A = 0.3$ is in dotted magenta line, and in solid cyan for Lorentzian n_i. $\Re(b_{22})$ with constant $A = 0.3$ is plotted in a dotted yellow line, and in a solid black line for the Lorentzian n_i. The Lorentzian n_i was calculated by two Lorentz functions summed together, one with $\tilde{\nu}_0 = 1807$ cm^{-1} and the other with $\tilde{\nu}_0 = 3128$ cm^{-1}. Both had $\Gamma = 15$ cm^{-1} and $\Lambda = 1400$ cm^{-2}.

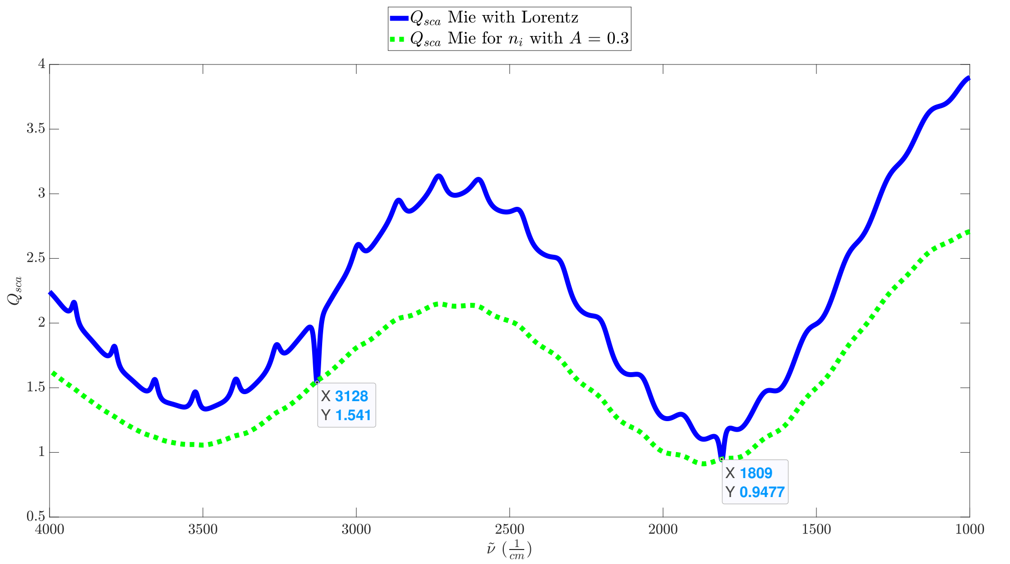

Figure 3.8: Two Q_{sca} is plotted for cylinder1. The dotted green line is Q_{sca} with $A = 0.3$ for all wavenumbers $\tilde{\nu}$, and the solid blue line is Q_{sca} with Lorentzian n_i. The Lorentzian n_i was calculated by two Lorentz functions summed together, one with $\tilde{\nu}_0 = 1807$ cm^{-1} and the other with $\tilde{\nu}_0 = 3128$ cm^{-1}. Both had $\Gamma = 15$ cm^{-1} and $\Lambda = 1400$ cm^{-2}.

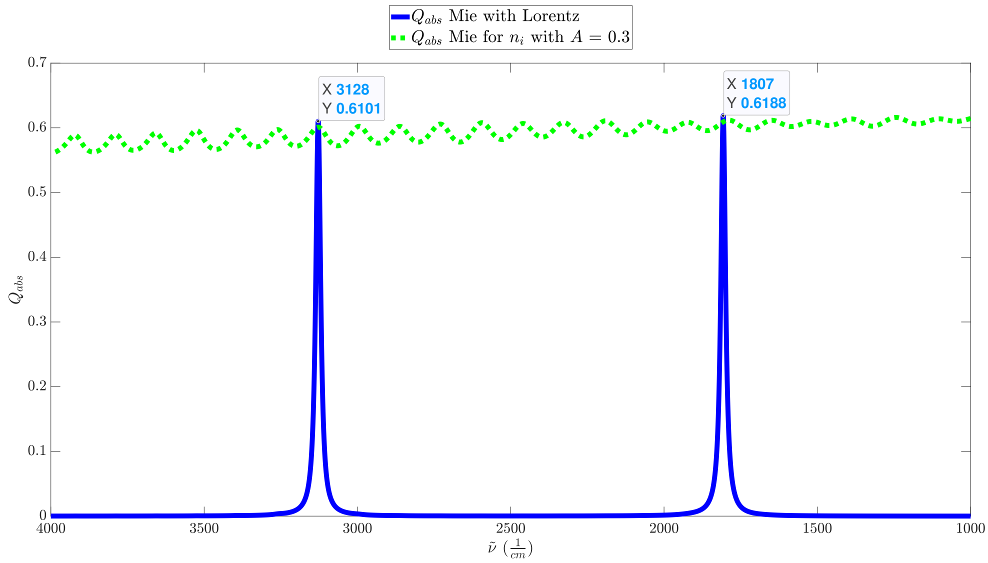

Figure 3.9: Two Q_{abs} is plotted for cylinder1. The dotted green line is Q_{abs} with $A = 0.3$ for all wavenumbers $\tilde{\nu}$, and the solid blue line is Q_{abs} with Lorentzian n_i. The Lorentzian n_i was calculated by two Lorentz functions summed together, one with $\tilde{\nu}_0 = 1807$ cm^{-1} and the other with $\tilde{\nu}_0 = 3128$ cm^{-1}. Both had $\Gamma = 15$ cm^{-1} and $\Lambda = 1400$ cm^{-2}.

Increasing the pure absorbance, A, from 0.3 to 0.5, the Q_{ext} for cylinder1 is calculated by Eq. (2.28) and plotted versus the left y-axis in the Fig. 3.10. As before, Q_{ext} with constant A (green dashed line) is compared with Q_{ext} calculated with Lorentzian n_i (blue solid line). The two Lorentz functions summed together in Fig. 3.10 has $\tilde{\nu}_0 = 1807$ cm^{-1}and $\tilde{\nu}_0 = 2600$ cm^{-1}. Both have $\Gamma = 15$ cm^{-1}. Λ is increased by a factor of $\frac{5}{3}$ to 2300 cm^{-2}. The $\Re(b_n)$'s are calculated by Eq. (2.33), and plotted versus the right y-axis for the n's corresponding to ripples. Figure 3.10 has for $n = 12$ with constant $A = 0.5$ (magenta dotted line), $n = 12$ with Lorentzian n_i (cyan dotted line), $n = 18$ with constant $A = 0.5$ (yellow dotted line) and $n = 18$ with Lorentzian n_i (black dotted line). The same peak at $\tilde{\nu}_0 = 1807$ cm^{-1} is shown here as in Fig. 3.7, only greater due to the greater absorbance. At $\tilde{\nu}_0 = 2600$ cm^{-1}, an inverted peak is created in the Q_{ext}. The wiggles in Q_{ext} is damped when an absorbance is present. When the Lorentzian Q_{ext} reaches for the same value for $A = 0.5$, it goes downwards, creating the inverted peak. Both the Lorentzian $\Re(b_{12})$ and $\Re(b_{18})$ reacts to the absorption band at $\tilde{\nu} = 2600$ cm^{-1}. The $\Re(b_{18})$, which had a peak corresponding to the ripple at this wavenumber, is greatly decreased, and $\Re(b_{12})$ is somewhat increased. The net difference in the $\Re(b_n)$'s is seen as the decrease in the Lorentzian Q_{ext} at this point.

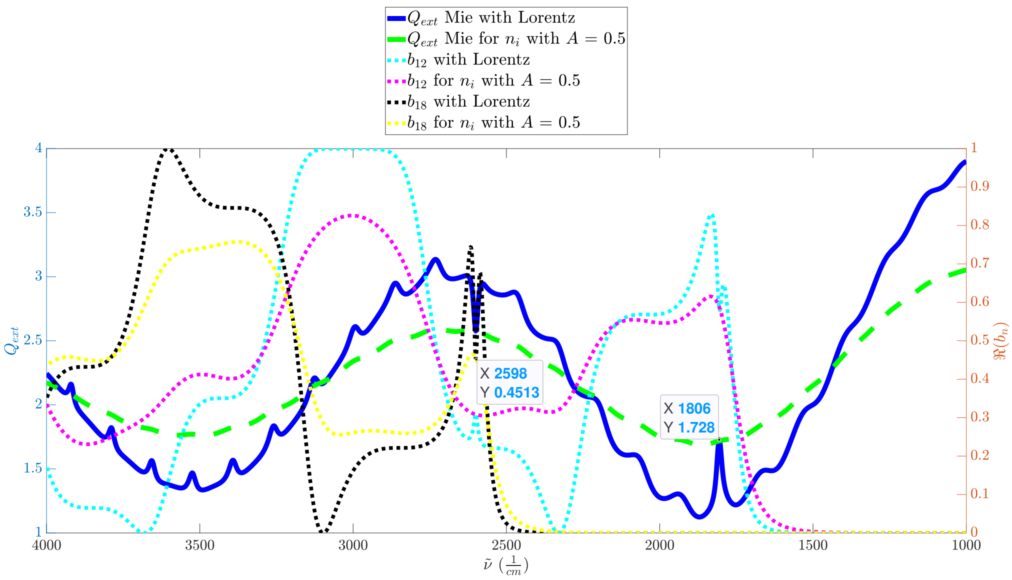

Figure 3.10: Two Q_{ext} for cylinder1 is plotted against the left y-axis. The dotted green line is Q_{ext} with $A = 0.5$ for all wavenumbers $\tilde{\nu}$, and the solid blue line is Q_{ext} with Lorentzian n_i. The $\Re(b_n)$'s are plotted against the right y-axis for $n = 12$ and $n = 18$ for cylinder1. $\Re(b_{12})$ with constant $A = 0.5$ is in dotted magenta line, and in solid cyan for Lorentzian n_i. $\Re(b_{18})$ with constant $A = 0.5$ is plotted in a dotted yellow line, and in a solid black line for the Lorentzian n_i. The Lorentzian n_i was calculated by two Lorentz functions summed together, one with $\tilde{\nu}_0 = 1807$ cm^{-1} and the other with $\tilde{\nu}_0 = 2600$ cm^{-1}. Both had $\Gamma = 15$ cm^{-1} and $\Lambda = 2300$ cm^{-2}.

The Q_{sca} with constant A (green dotted line) and with Lorentzian n_i (blue solid line) are calculated by Eq. (2.29) with the same parameters and plotted in the Fig. 3.11. With both the Q_{ext} and the Q_{sca} known, the Q_{abs} with constant A (green dashed line) and Lorentzian n_i (blue solid line) are calculated as before by Eq. (2.32) and is plotted in Fig. 3.12. From these figures, it is apparent that the decrease in the Q_{sca} at $\tilde{\nu}_0 = 2600$ cm^{-1}is much greater than the increase in the Q_{abs}, making out the inverted peak in Q_{ext} in Fig. 3.10. At $\tilde{\nu} = 1807$ cm^{-1}, the increase in Q_{abs} is greater than the decrease in Q_{sca}, making the peak seen at this wavenumber in Q_{ext} in Fig. 3.10.

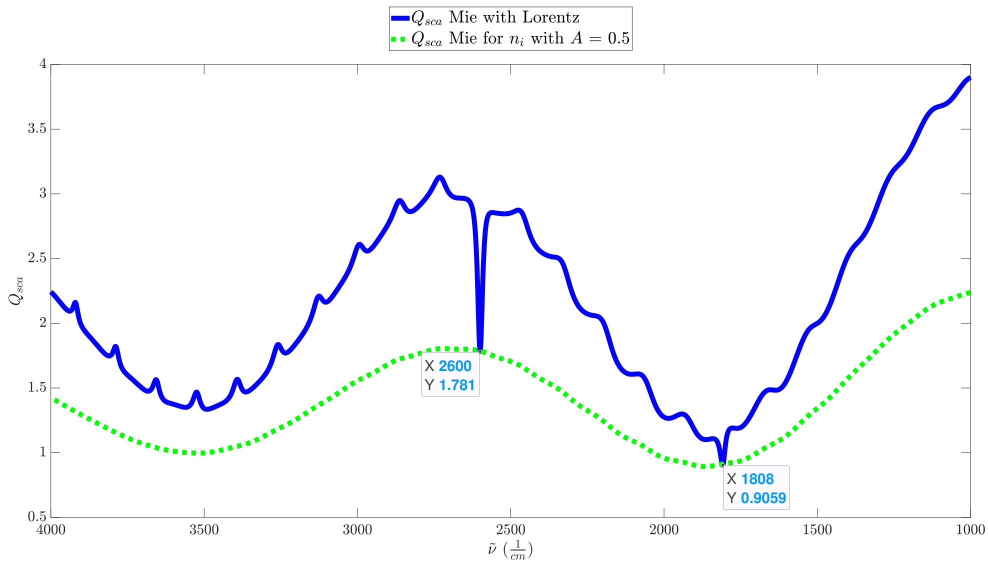

Figure 3.11: Two Q_{sca} is plotted for cylinder1. The dotted green line is Q_{sca} with $A = 0.5$ for all wavenumbers $\tilde{\nu}$, and the solid blue line is Q_{sca} with Lorentzian n_i. The Lorentzian n_i was calculated by two Lorentz functions summed together, one with $\tilde{\nu}_0 = 1807$ cm^{-1} and the other with $\tilde{\nu}_0 = 2600$ cm^{-1}. Both had $\Gamma = 15$ cm^{-1} and $\Lambda = 2300$ cm^{-2}.

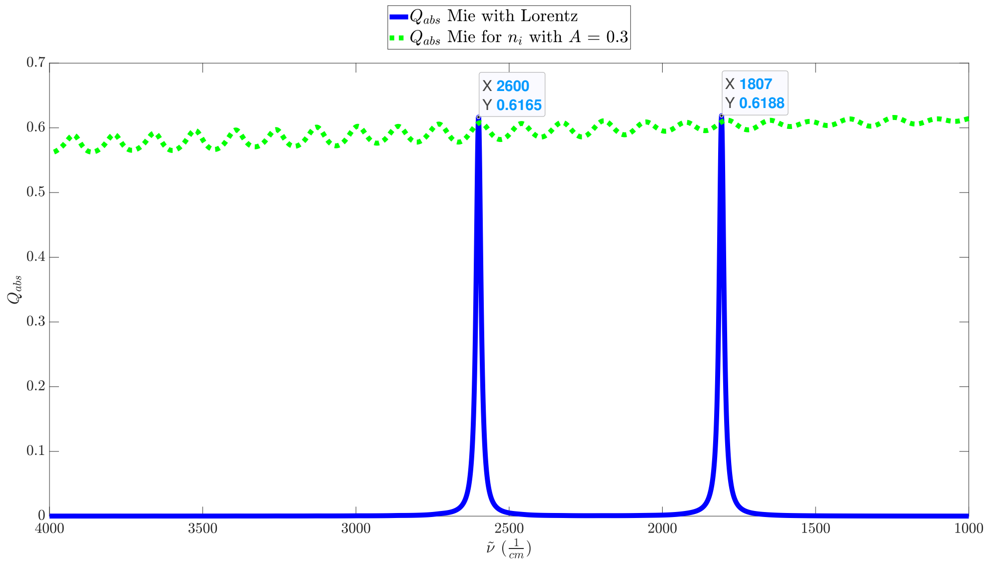

Figure 3.12: Two Q_{abs} is plotted for cylinder1. The dotted green line is Q_{abs} with $A = 0.5$ for all wavenumbers $\tilde{\nu}$, and the solid blue line is Q_{abs} with Lorentzian n_i. The Lorentzian n_i was calculated by two Lorentz functions summed together, one with $\tilde{\nu}_0 = 1807$ cm^{-1} and the other with $\tilde{\nu}_0 = 2600$ cm^{-1}. Both had $\Gamma = 15$ cm^{-1} and $\Lambda = 2300$ cm^{-2}.

The Q_{ext} for cylinder2 with constant $A = 0.5$ (green dotted line) and Lorentzian n_i (blue solid line) are plotted versus the left y-axis in Fig. 3.13, calculated by Eq. (2.28). Λ becomes 6300 cm^{-2} with $A = 0.3$. The center for the Lorentz functions are the ripples at $\tilde{\nu} = 2696$ cm^{-1} and $\tilde{\nu} = 3287$ cm^{-1}. Against the right y-axis, the $\Re(b_{12})$ with constant A (magenta dotted line), $\Re(b_{12})$ with Lorentzian n_i (cyan solid line), $\Re(b_{15})$ with constant A (yellow dotted line) and $\Re(b_{15})$ with Lorentzian n_i (black solid line) are plotted. They were calculated by Eq. (2.33). With absorbance, the wiggles of Q_{ext} are damped. Both sharp ripples have disappeared at the wavenumbers $\tilde{\nu}_0 = 2696$ cm^{-1} and $\tilde{\nu}_0 = 3287$ cm^{-1}. This is seen also by the collapse of the $\Re(b_n)$'s corresponding to these ripples. At $\tilde{\nu}_0 = 2696$ cm^{-1} there is a peak in the Lorentzian Q_{ext}, but not as sharp as the original ripple there. This peak has been created by the absorption band there, from the bottom of a wiggle. At $\tilde{\nu}_0 = 3287$ cm^{-1}, there is an inverted peak from the top of a wiggle in the Lorentzian Q_{ext}. Both inverted and regular peak reaches the same value as that of the Q_{ext} with constant $A = 0.5$, shown by the data tips.

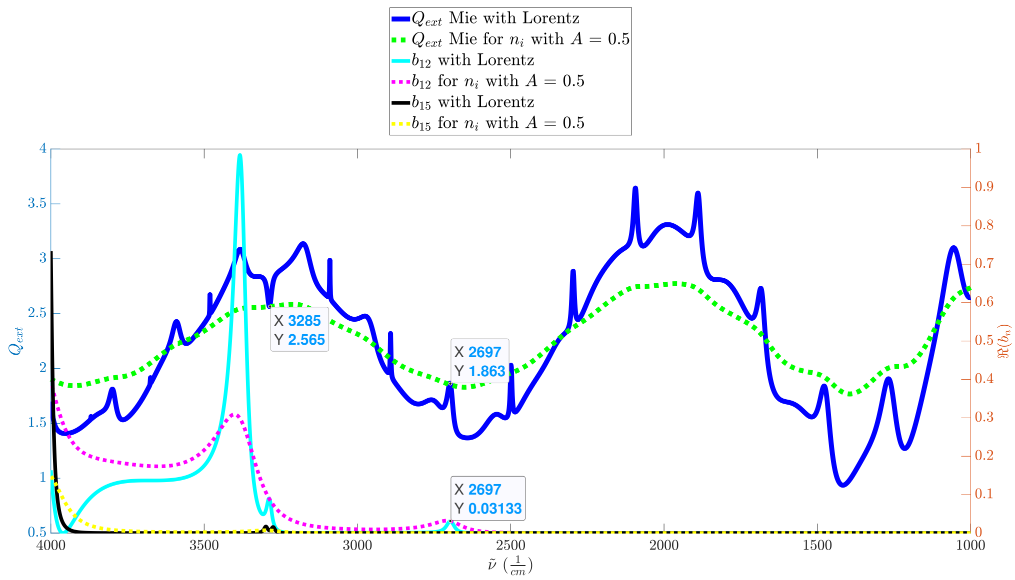

Figure 3.13: Two Q_{ext} for cylinder2 is plotted against the left y-axis. The dotted green line is Q_{ext} with $A = 0.5$ for all wavenumbers $\tilde{\nu}$, and the solid blue line is Q_{ext} with Lorentzian n_i. The $\Re(b_n)$'s are plotted against the right y-axis for $n = 12$ and $n = 15$ for cylinder2. $\Re(b_{12})$ with constant $A = 0.5$ is in dotted magenta line, and in solid cyan for Lorentzian n_i. $\Re(b_{15})$ with constant $A = 0.5$ is plotted in a dotted yellow line, and in a solid black line for the Lorentzian n_i. The Lorentzian n_i was calculated by two Lorentz functions summed together, one with $\tilde{\nu}_0 = 2696$ cm^{-1} and the other with $\tilde{\nu}_0 = 3287$ cm^{-1}. Both had $\Gamma = 15$ cm^{-1} and $\Lambda = 6300$ cm^{-2}.

The Q_{sca} for cylinder2 with $A = 0.5$ constantly (green dotted line), together with Lorentz functions reaching peaks corresponding to $A = 0.5$ (blue solid line) are calculated by Eq. (2.29) and plotted in Fig. 3.14. Finally, using Eq. (2.32), the Q_{abs} of cylinder2 with constant $A = 0.5$ (green dotted line) and with Lorentzian n_i are calculated, and plotted in Fig. 3.15. The increase in the Lorentzian Q_{abs} in Fig. 3.15 is quite similar for both $\tilde{\nu}_0 = 2696$ cm^{-1} and $\tilde{\nu}_0 = 3287$ cm^{-1}, but the decrease in the Lorentzian Q_{sca} in Fig. 3.14 at $\tilde{\nu}_0 = 3287$ cm^{-1}is much greater than the decrease at $\tilde{\nu}_0 = 2696$ cm^{-1}. Thus there is created a peak at $\tilde{\nu}_0 = 2696$ cm^{-1} in the Lorentzian Q_{ext} in Fig. 3.13, and an inverted one at $\tilde{\nu}_0 = 3287$ cm^{-1}.

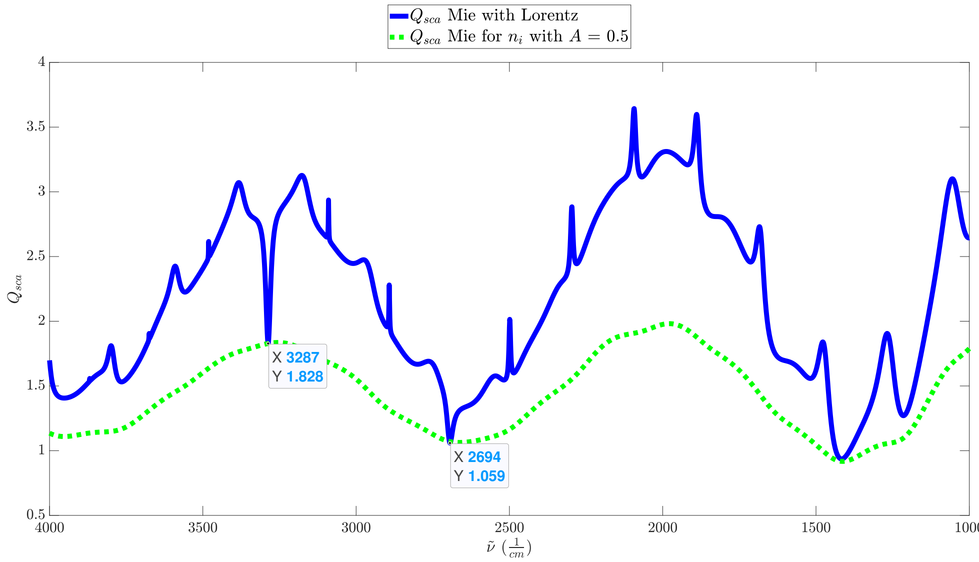

Figure 3.14: Two Q_{sca} is plotted for cylinder2. The dotted green line is Q_{sca} with $A = 0.5$ for all wavenumbers $\tilde{\nu}$, and the solid blue line is Q_{sca} with Lorentzian n_i. The Lorentzian n_i was calculated by two Lorentz functions summed together, one with $\tilde{\nu}_0 = 2696$ cm^{-1} and the other with $\tilde{\nu}_0 = 3287$ cm^{-1}. Both had $\Gamma = 15$ cm^{-1} and $\Lambda = 6300$ cm^{-2}.

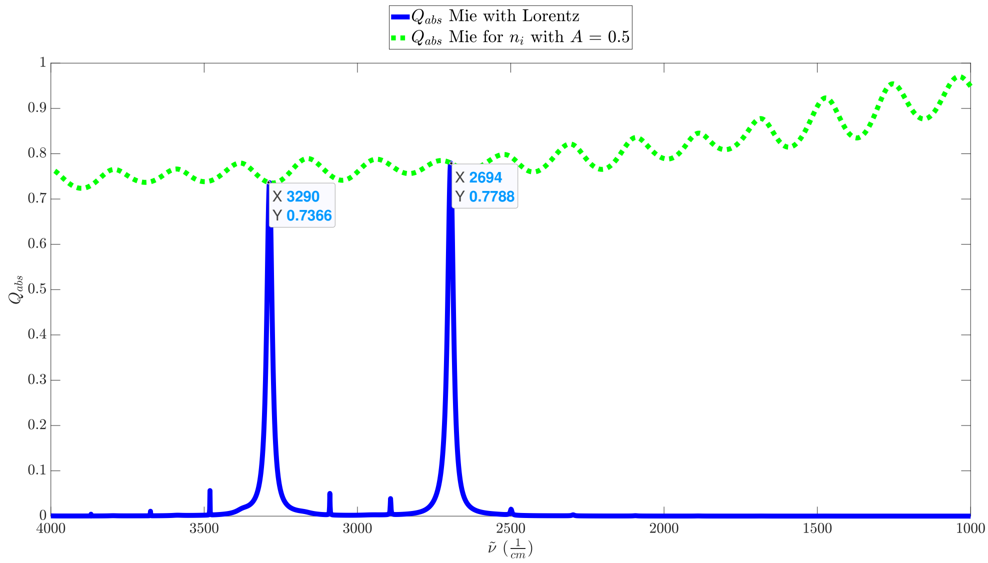

Figure 3.15: Two Q_{abs} is plotted for cylinder2. The dotted green line is Q_{abs} with $A = 0.5$ for all wavenumbers $\tilde{\nu}$, and the solid blue line is Q_{abs} with Lorentzian n_i. The Lorentzian n_i was calculated by two Lorentz functions summed together, one with $\tilde{\nu}_0 = 2696$ cm^{-1} and the other with $\tilde{\nu}_0 = 3287$ cm^{-1}. Both had $\Gamma = 15$ cm^{-1} and $\Lambda = 6300$ cm^{-2}.

3.1.4 Infinite cylinder case II

In this case, the incident light is perpendicular onto a cylinder, with the ***B***-field parallel with the cylinder axis and the ***E***-field perpendicular to the cylinder axis, as shown in 2.3. Only cylinder1 will be used as example system in this section. Figure 3.16 shows Q_{ext} (black line) as a function of wavenumber versus the left y-axis together with a_n calculated by Eq. (2.38) for $n = 18$ (dotted cyan line) and $n = 24$ (dotted magenta line) as a function of wavenumber versus the right y-axis. n is selected so that the peak in a_n corresponds to the ripples at $\tilde{\nu} = 2650$ cm^{-1} and $\tilde{\nu} = 3445$ cm^{-1}in Q_{ext} as indicated by the data tips in Fig. 3.16, making two *a_n-ripple pairs.* The cylinder is non-absorptive, i.e. $n_i = 0$.

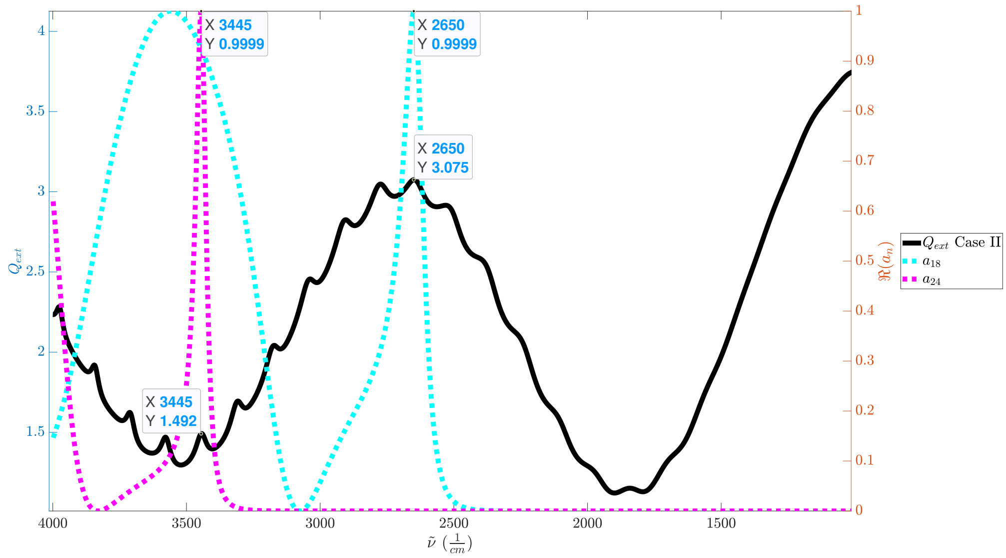

Figure 3.16: a_n-ripple pair for cylinder1 in case II with $n_i = 0$, as indicated by the data tips. Q_{ext} is the solid black line, and plotted versus the left y-axis. The $\Re(a_n)$ with $n = 18$ and $n = 24$ are plotted versus the right y-axis.

How the imaginary part of the refractive index, n_i, vary as a function of wavenumber for (i) a constant $A = 0.3$ (Eq. (2.13)) and (ii) in the case of two absorption bands centered at $\tilde{\nu} = 3445$ cm^{-1}and at $\tilde{\nu} = 2650$ cm^{-1}(Eq. (2.17)) are plotted in Fig. 3.17. For calculating the two Lorentz functions of the absorption bands, $\Gamma = 15$ cm^{-1} and $\Lambda = 1400$ cm^{-2} are used with $\tilde{\nu}_0 = 3445$ cm^{-1} and $\tilde{\nu}_0 = 2650$ cm^{-1}, respectively. Then, they are added together for all $\tilde{\nu}$ and the n_i is calculated by Eq. 2.16. The n_i with constant absorbance $A = 0.3$ (green dashed line) is increasing exponentially with lesser $\tilde{\nu}$, due to the inverse proportionality from Eq (2.13). the Lorentzian n_i (blue solid line) is generally zero, with peaks corresponding to the center of the absorption bands, reaching the same values as for constant $A = 0.3$, as highlighted by the data tips.

This gives two different Q_{ext}, which both are plotted versus the left y-axis together with

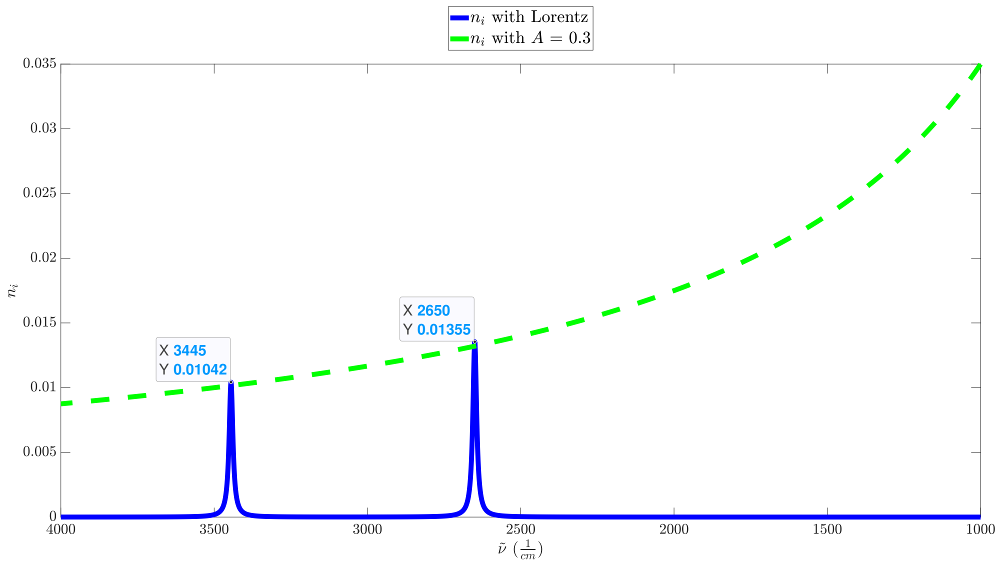

Figure 3.17: Imaginary part of the refractive index, n_i, for cylinder1 in case II with constant $A = 0.3$ (green dashed line) and Lorentz functions centered on $\tilde{\nu} = 2650$ cm^{-1} and $\tilde{\nu} = 3445$ cm^{-1} (blue solid line). $\Gamma = 15$ cm^{-1} and $\Lambda = 1400$ cm^{-2} are used.

the chosen coefficients $\Re(a_{18})$ and $\Re(a_{24})$ versus the right y-axis in Fig. 3.18. For (i) the Q_{ext} is a dashed green line, $\Re(a_{18})$ is a dotted magenta line and $\Re(a_{24})$ is a yellow dotted line. For (ii) the Q_{ext} is a solid blue line, $\Re(a_{18})$ is a dotted cyan line and $\Re(a_{24})$ is a dotted black line. The Q_{sca} and Q_{abs} for the same scenario are plotted in Figs. 3.19 and 3.20 in green dotted line for (i) and blue solid line for (ii). Figure 3.18 shows that for (ii), an inverted peak is created in Q_{ext} at $\tilde{\nu} = 2650$ cm^{-1}, which was a ripple situated at the top of a wiggle. A great decrease in Q_{sca} for this scenario is seen in Fig. 3.19, explaining the inverted peak in Q_{ext}. At $\tilde{\nu} = 3445$ cm^{-1}however, a peak is created in (ii) Q_{ext}. This is at the bottom of a wiggle, and the decrease in (ii) Q_{sca} is lesser than the increase of Q_{abs} for this scenario.

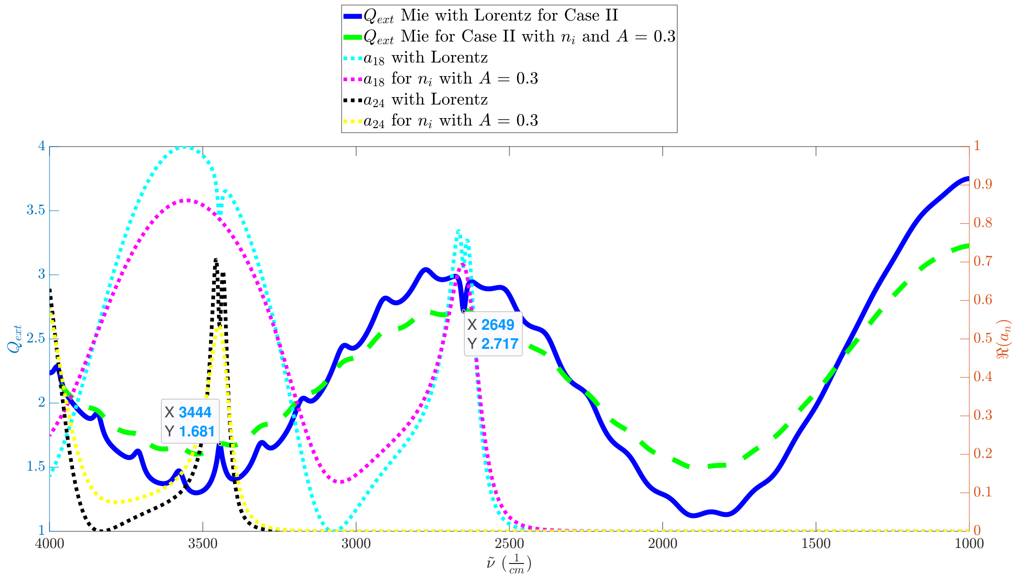

Figure 3.18: Q_{ext} and $\Re(a_n)$'s for cylinder1 in case II with constant $A = 0.3$ and Lorentz functions centered on $\tilde{\nu}_0 = 2650$ cm^{-1} and $\tilde{\nu}_0 = 3445$ cm^{-1}. $\Gamma = 15$ cm^{-1} and $\Lambda = 1400$ cm^{-2} are used.

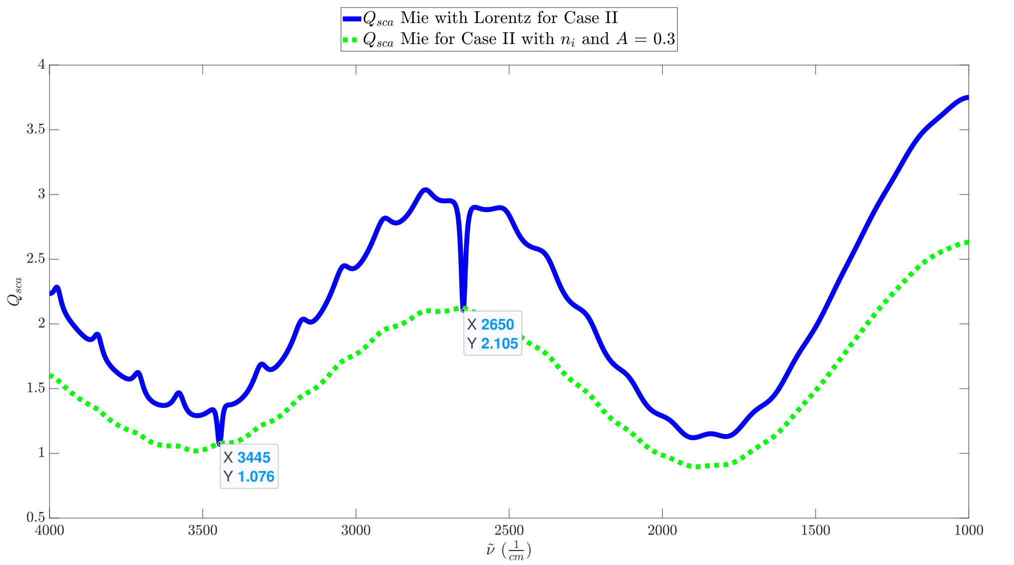

Figure 3.19: Q_{sca} and $\Re(a_n)$'s for cylinder1 in case II with constant $A = 0.3$ and Lorentz functions centered on $\tilde{\nu}_0 = 2650$ cm^{-1} and $\tilde{\nu}_0 = 3445$ cm^{-1}. $\Gamma = 15$ and $\Lambda = 1400$ cm^{-2} are used.

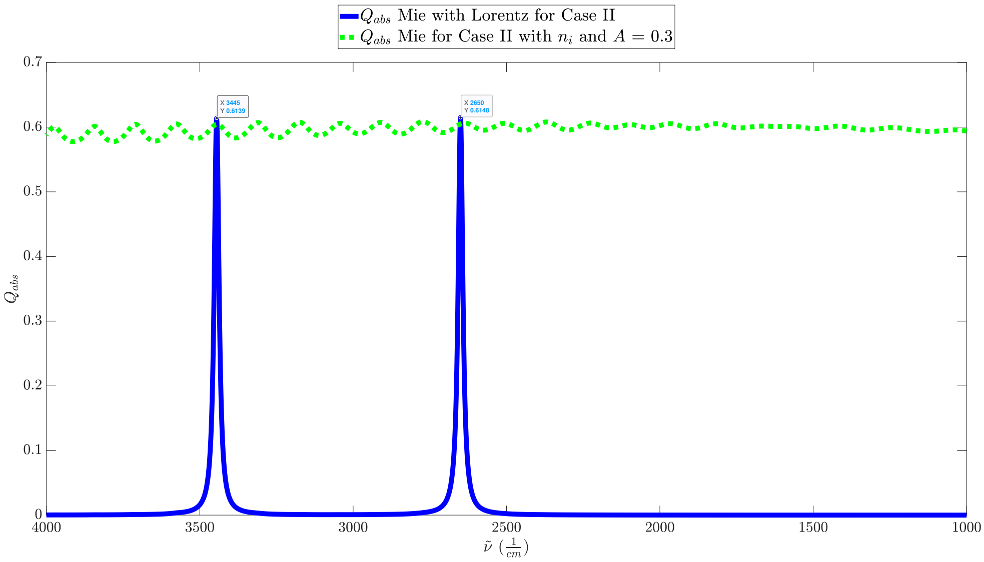

Figure 3.20: Q_{abs} and $\Re(a_n)$'s for cylinder1 in case II with constant $A = 0.3$ and Lorentz functions centered on $\tilde{\nu}_0 = 2650$ cm^{-1} and $\tilde{\nu}_0 = 3445$ cm^{-1}. $\Gamma = 15$ cm^{-1} and $\Lambda = 1400$ cm^{-2} was used.

3.1.5 The effect of the size of the numerical aperture on Q_{ext} and Q_{sca}

In order for the study of the different sizes of NA is legit, Eqs. 2.40 and 2.29 have to produce the same result. The Figs. 3.21 and 3.22 show a comparison of the two results for different values of m. Figure 3.21 shows Q_{ext}, since $Q_{ext} = Q_{sca}$ for non-absorbing particles, for cylinder1 from section 3.1.3. For Fig. 3.22, the n_i is increased from 0 to 0.02, showing Q_{sca}. The Q_{sca} from the exact expression Eq. (2.29) is calculated by the MatLab script B (blue dashed line in both Figs.), and the MatLab script C calculates Q_{sca} by numerical integration (red dashed line in both Figs.), Eq. (2.46).

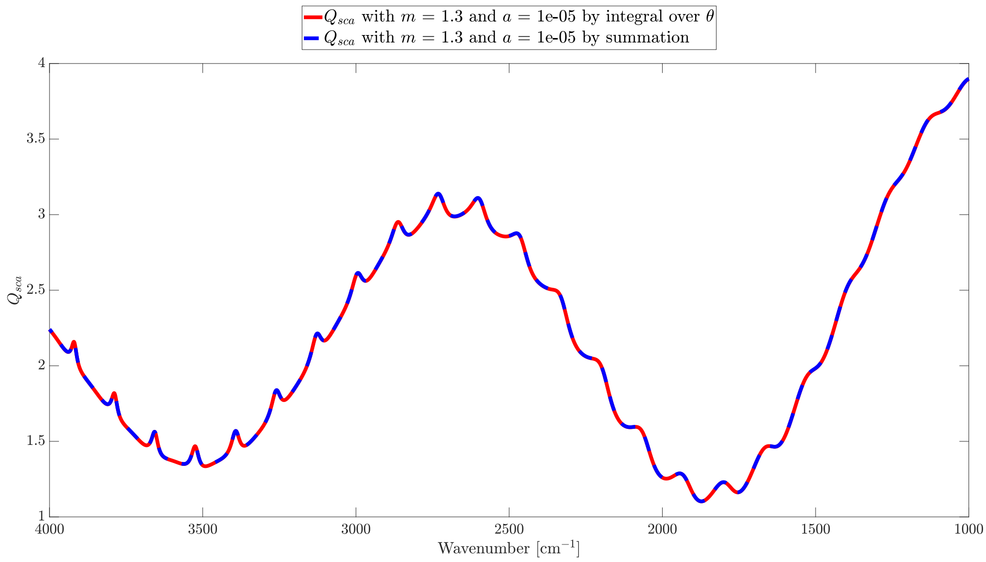

Figure 3.21: Comparison of the calculation of the scattering efficiency factor, Q_{ext}. The integral over θ from 2.40 is in red and the summation approximation from 2.29 is in blue. The radius of the cylinder, a, is 10 μm and the complex refractive index, m, is 1.3-0i.

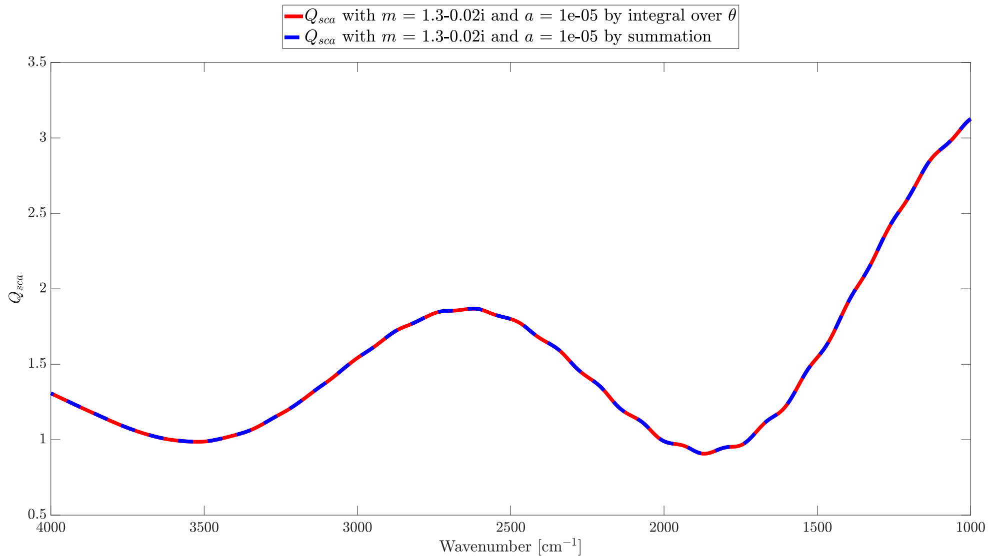

Figure 3.22: Comparison of the calculation of the scattering efficiency factor, Q_{sca}. The integral over θ from 2.40 is in red and the summation approximation from 2.29 is in blue. The radius of the cylinder, a, is 10 μm and the complex refractive index, m, is 1.3-0.02i.

3.1.6 Q_{ext} calculated by integral with regard to different sizes of NA

The Q_{ext} calculated by integration, by help of Eqs. (2.46) and (2.22) for the case of a non-absorptive scatterer (i.e. $Q_{abs} = 0$). The selected NA-values are 0, 0.2, 0.35, 0.5 and 0.65. The real part of the refractive index, n_r, is constant. Q_{ext} for cylinder1 is plotted in Fig. 3.23, where the dark blue line corresponds to NA = 0, which is identical with the exact formula for Q_{ext} Eq. (2.28). The Q_{ext} with the same NAs for cylinder2 is shown in Fig. 3.24. The dark blue line corresponds to NA = 0, i.e. Q_{ext} exact from Eq. (2.28). In both Figs. 3.23 and 3.24 the cyan line corresponds to NA = 0.2, the green line to NA = 0.35, the yellow line to NA = 0.5 and the orange line to NA = 0.65. The Q_{ext} is generally decreased with increasing NA, as expected since the integration area is lessened. However, the structures, i.e. ripples and wiggles, are intact. The ripples representing the Whispering Gallery Modes (WGMs) are just as sharp for each size of NA.

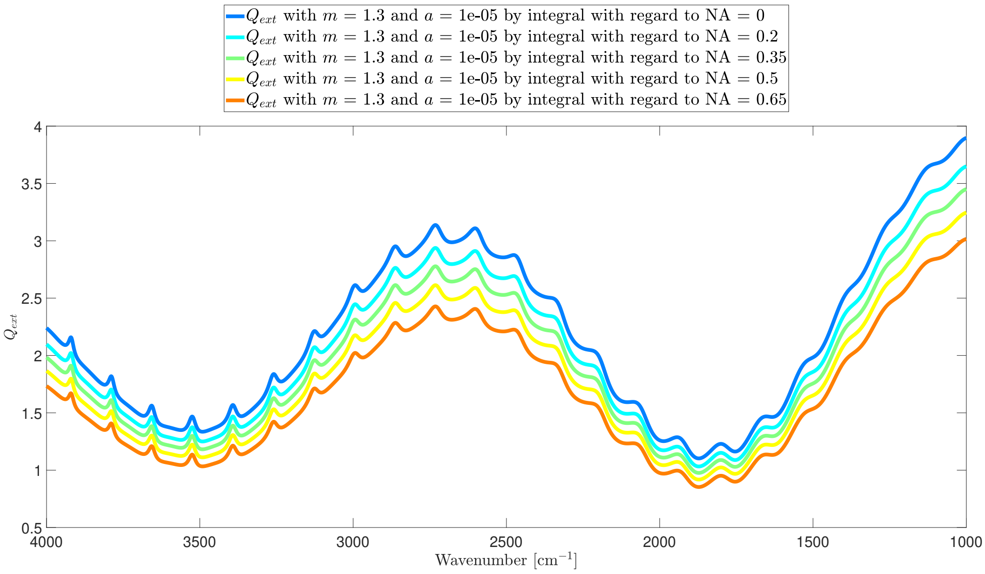

Figure 3.23: The extinction efficiency factor Q_{ext} for cylinder1 by integration with regard to different NA values with no absorbance. The dark blue line corresponds to NA = 0, the cyan line to NA = 0.2, the green line to NA = 0.35, the yellow line to NA = 0.5 and the orange line to NA = 0.65.

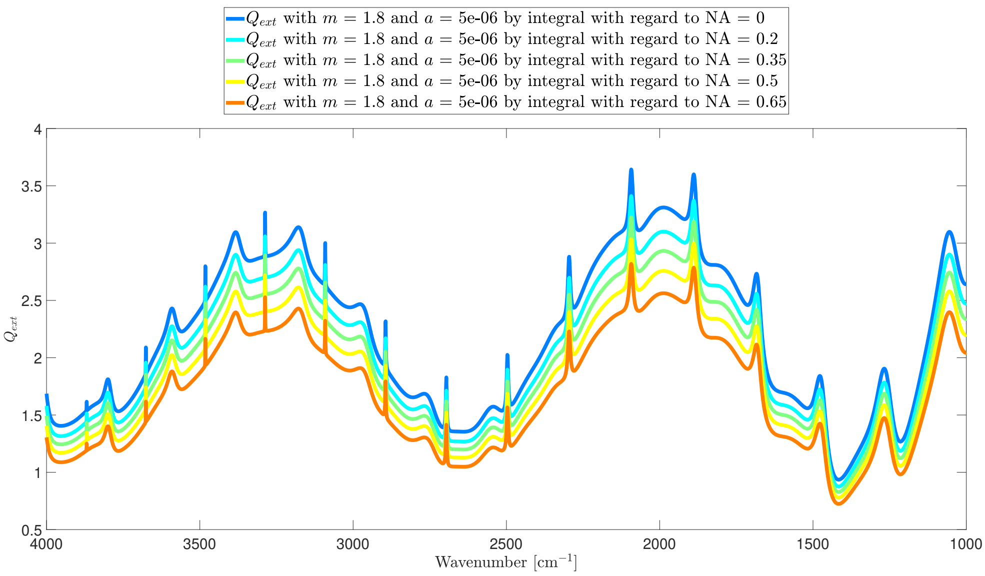

Figure 3.24: The extinction efficiency factor Q_{ext} for cylinder2 by integration with regard to different NA values with no absorbance. The dark blue line corresponds to NA = 0, the cyan line to NA = 0.2, the green line to NA = 0.35, the yellow line to NA = 0.5 and the orange line to NA = 0.65.

3.1.7 Q_{sca} calculated by integral with regard to different NA values with Lorentz

In this section we evaluate how the scattering efficiency is affected when we include both an absorption band and the increase of the size of the numerical aperture. The calculation the scattering efficiency factor Q_{sca} in this section is done by the MatLab script D from Eq. (2.46) with an imaginary refractive index calculated from Eqs. (2.17) and (2.16). In all the Figs. in this section are the dark blue line corresponding to NA = 0, the cyan line to NA = 0.2, the green line to NA = 0.35, the yellow line to NA = 0.5 and the orange line to NA = 0.65.

The Q_{sca} for cylinder1 with a Lorentz-shaped absorption band, with a peak for A = 0.3, i.e. Λ = 1400 cm^{-2} for a FWHM determined by Γ = 15 cm^{-1} at wavenumber $\tilde{\nu}_0 = 3128$cm^{-1} is given in Fig. 3.25. The Q_{sca} is generally lessened at each wavenumber $\tilde{\nu}$ with increasing NA. However, the structures, i.e. wiggles and ripples, stays intact for this scenario as well. The same observation holds true for the Q_{sca} with absorption bands centered at $\tilde{\nu}_0$ = 2600 cm^{-1}for cylinder1, and $\tilde{\nu}_0$ = 2696 cm^{-1}and $\tilde{\nu}_0$ = 3287 cm^{-1}for cylinder2 in Figs. 3.27, 3.26 and 3.28.

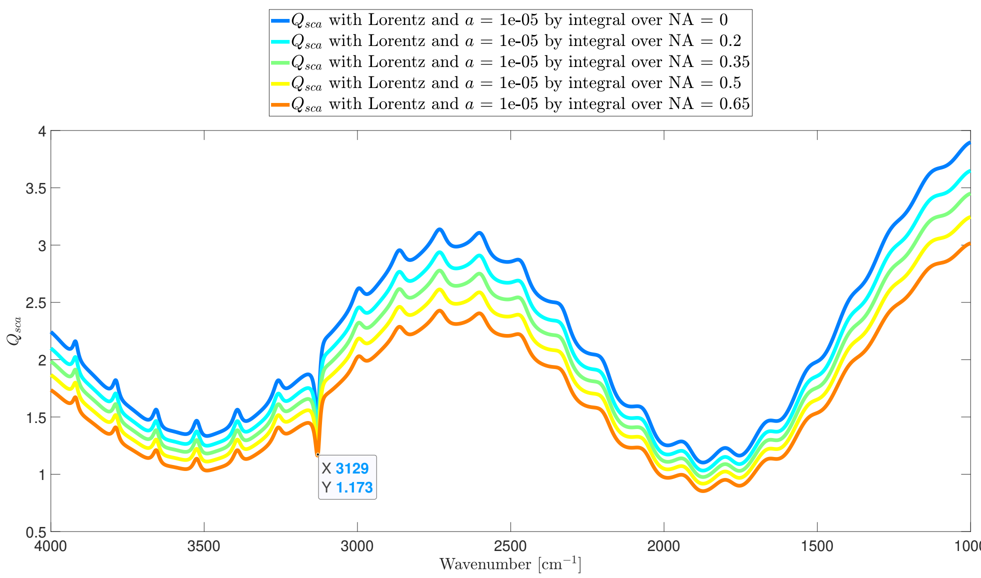

Figure 3.25: The Q_{sca} for cylinder1 by integration with regard different sizes of NA with a Lorentz-shaped absorption band at $\tilde{\nu}_0$ = 3128 cm^{-1} with Γ = 15 cm^{-1} and Λ = 1400 cm^{-2}. The peak of the Lorentz function reaches an imaginary refractive index n_i which corresponds to A = 0.3. The dark blue line corresponds to NA = 0, the cyan line to NA = 0.2, the green line to NA = 0.35, the yellow line to NA = 0.5 and the orange line to NA = 0.65.

For cylinder2, the Lorentz function has Γ = 15 cm^{-1} and Λ = 3800 cm^{-2} in order to have a peak value corresponding to A = 0.3. The scattering efficiency factor Q_{sca} with the Lorentz function at the wavenumber $\tilde{\nu}_0$ = 2696 cm^{-1} is in Fig. 3.26.

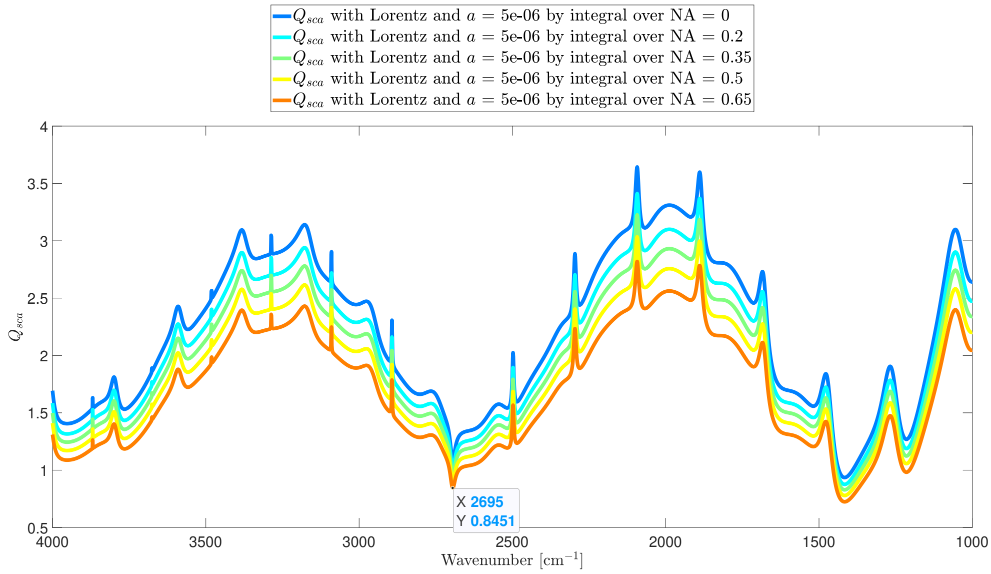

Figure 3.26: The Q_{sca} for cylinder2 by integration with regard different sizes of NA with a Lorentz-shaped absorption band at $\tilde{\nu}_0 = 2696$ cm^{-1} with $\Gamma = 15$ cm^{-1} and $\Lambda = 3800$ cm^{-2}. The peak of the Lorentz function reaches an imaginary refractive index n_i which corresponds to $A = 0.3$. The dark blue line corresponds to NA = 0, the cyan line to NA = 0.2, the green line to NA = 0.35, the yellow line to NA = 0.5 and the orange line to NA = 0.65.

Increasing the peak pure absorbance from $A = 0.3$ to 0.5, the Λ must be increased to 2300 cm^{-2}for absorbance band with $\Gamma = 15$ cm^{-1} for cylinder1. The scattering efficiency factor Q_{sca} for cylinder1 with $\tilde{\nu}_0 = 2600$ cm^{-1} is plotted in Fig. 3.27.

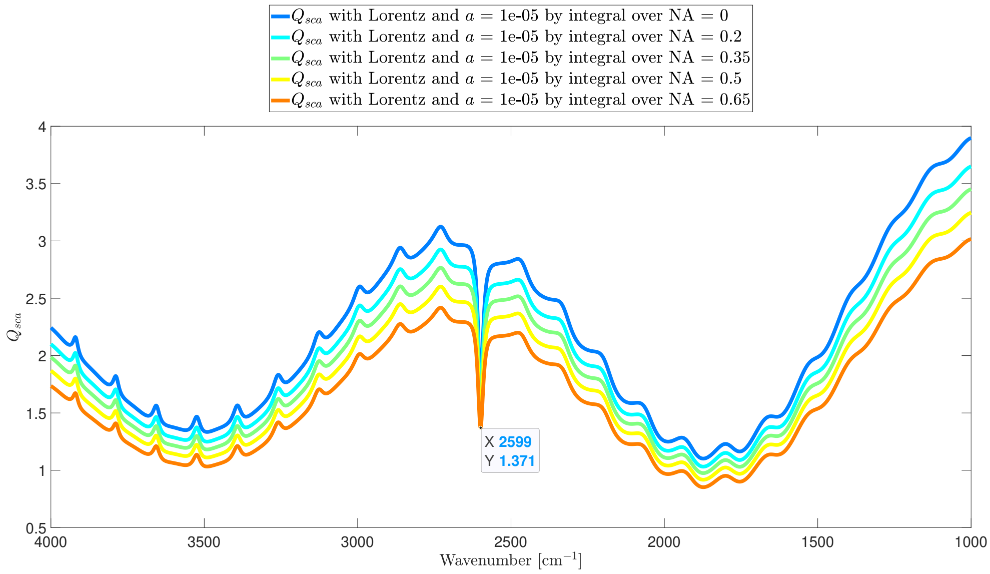

Figure 3.27: The Q_{sca} for cylinder1 by integration with regard different sizes of NA with a Lorentz-shaped absorption band at $\tilde{\nu}_0 = 2600$ cm^{-1} with $\Gamma = 15$ cm^{-1} and $\Lambda = 2300$ cm^{-2}. The peak of the Lorentz function reaches an imaginary refractive index n_i which corresponds to $A = 0.5$. The dark blue line corresponds to NA = 0, the cyan line to NA = 0.2, the green line to NA = 0.35, the yellow line to NA = 0.5 and the orange line to NA = 0.65.

For cylinder2 with the peak value of the Lorentz-function at $\tilde{\nu}_0 = 3287$ cm^{-1}corresponding pure absorbance $A = 0.5$, the Γ is increased to 6300 cm^{-2}, and the scattering efficiency factor Q_{sca} becomes that of Fig. 3.28.

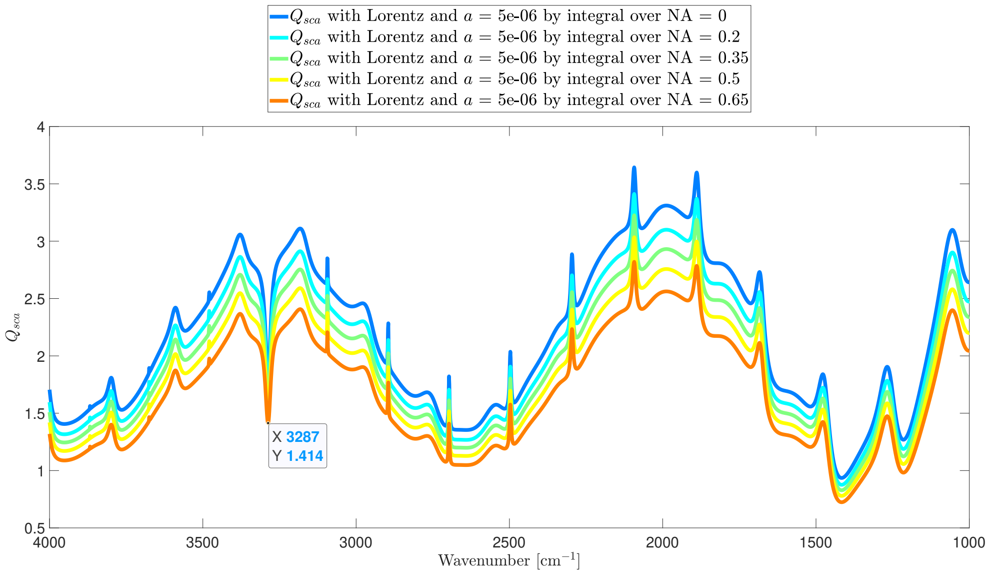

Figure 3.28: The Q_{sca} for cylinder2 by integration with regard different sizes of NA with a Lorentz-shaped absorption band at $\tilde{\nu}_0 = 3287$ cm^{-1} with $\Gamma = 15$ cm^{-1} and $\Lambda = 6300$ cm^{-2}. The peak of the Lorentz function reaches an imaginary refractive index n_i which corresponds to $A = 0.5$. The dark blue line corresponds to NA = 0, the cyan line to NA = 0.2, the green line to NA = 0.35, the yellow line to NA = 0.5 and the orange line to NA = 0.65.

3.2 Disk

3.2.1 Wave function for cylinder1 as a disk

The wave function from Eqs. (2.49) and (2.51) are calculated by the MatLab script E together with the MatLab functions F and G, all made by PhD candidate Maren Anna Brandsrud. This gives the exact result for the plane wave scattered from a disk, which is cylinder2 as "seen" by the $\boldsymbol{E}$-field in Case I, with the $\boldsymbol{E}$-field parallel to the cylinder-axis. The incoming plane wave is traveling from left to right in the disk images. The result of the wave function for the scattered plane wave from this disk at the wavenumber corresponding to the ripple for cylinder1 at $\tilde{\nu} = 1807$ cm^{-1} is given in the Fig. 3.29 for $n_i = 0$, i.e. non-absorptive disk. The ripples corresponds to a resonance, a Whispering Gallery Modes (WGMs), which is due to a standing wave inside the boundary of the disk.

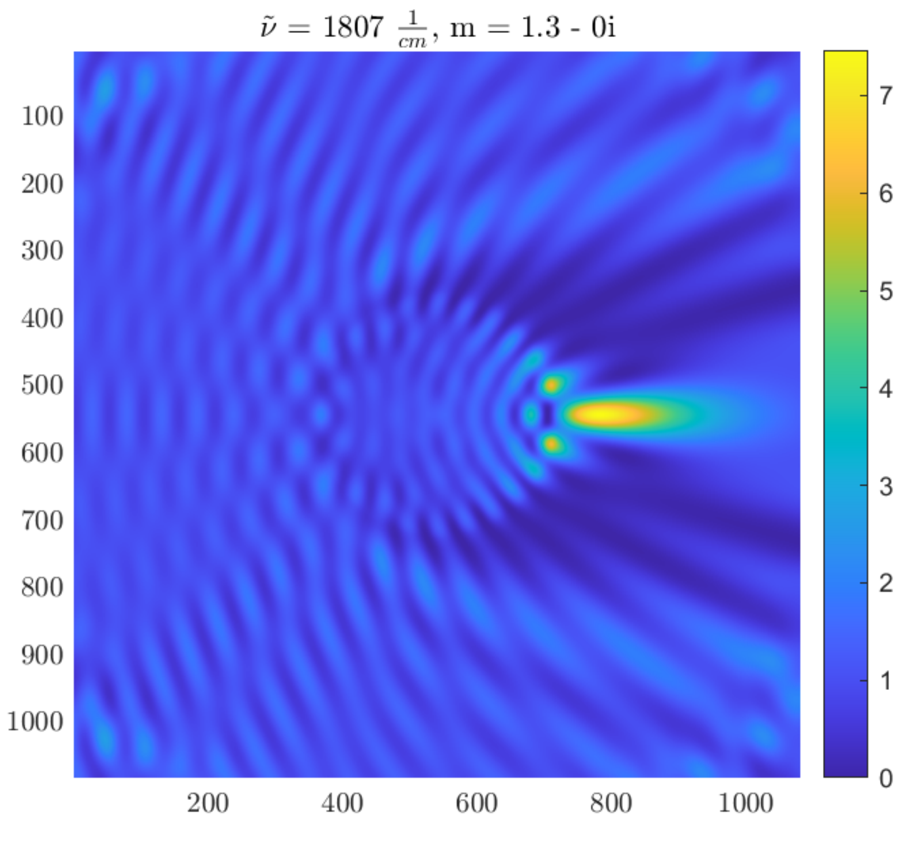

Figure 3.29: The absolute square of the wave function for the scattered plane wave for a disk with $n_r = 1.3$, radius $a = 10\mu$m and $n_i = 0i$ at the wavenumber $\tilde{\nu} = 1807$ cm^{-1}. The scale is rising from a dark blue to a bright yellow for the highest values. The incoming plane wave is traveling from left to right in the image. The sides of the frame are three times longer than the radius of the disk.

Assuming a pure absorbance $A = 0.3$, yields an imaginary refractive index, $n_i = 0.02$

from equation (2.13) at $\tilde{\nu} = 1807$ cm^{-1}. This in turn changes the the scattered wave in Fig. 3.29 to that of Fig. 3.30. The wave function is lessened, and so is the scale. We do still observe remains of the WGM. Increasing the pure absorbance A to 0.5, the imaginary refractive index n_i becomes 0.032 from Eq. (2.13) $\tilde{\nu} = 1807$ cm^{-1}, and the wave function of the scattered wave becomes that of Fig. 3.31. Now, the area where the WGMs originally where are as strong as the field around the disk, indicating that they have disappeared.

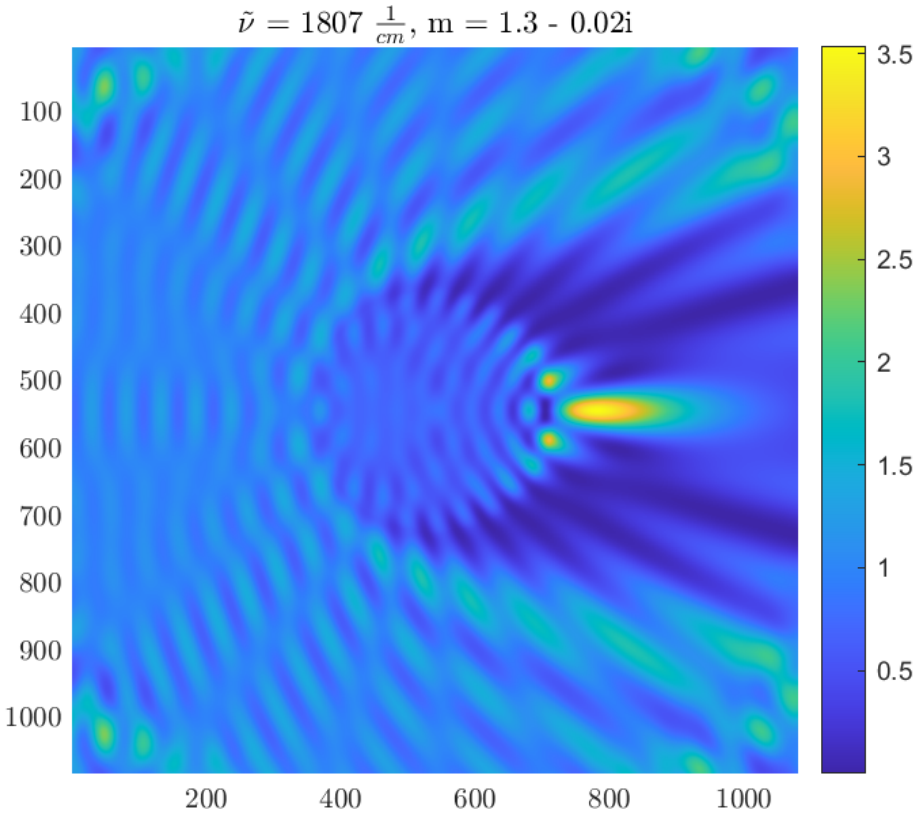

Figure 3.30: The absolute square of the wave function for the scattered plane wave for a disk with $n_r = 1.3$, radius $a = 10\mu$m and $n_i = 0.02i$ at the wave number $\tilde{\nu} = 1807$ cm^{-1}. The scale is rising from a dark blue to a bright yellow for the highest values. The incoming plane wave is traveling from left to right in the image. The sides of the frame are three times longer than the radius of the disk.

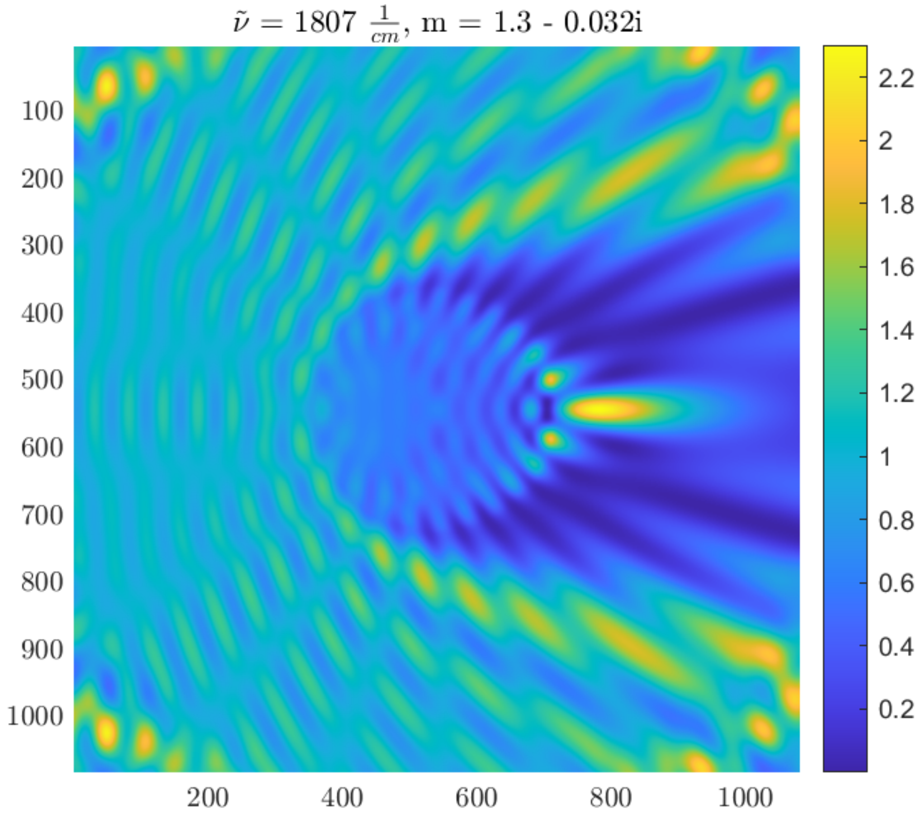

Figure 3.31: The absolute square of the wave function for the scattered plane wave for a disk with $n_r = 1.3$, radius $a = 10\mu$m and $n_i = 0.032i$ at the wave number $\tilde{\nu} = 1807$ cm^{-1}. The scale is rising from a dark blue to a bright yellow for the highest values. The incoming plane wave is traveling from left to right in the image. The sides of the frame are three times longer than the radius of the disk.

The scale in Figs. 3.30 and 3.31 are adjusted to give a nice and clear image, but can be a bit misleading in terms of the different intensities. Hence, Figs. 3.32 and 3.33 provides the same images, but with the same scale as in Fig. 3.29, the non-absorptive disk. From these images, it is apparent that the WGMs already disappear with $A = 0.3$.

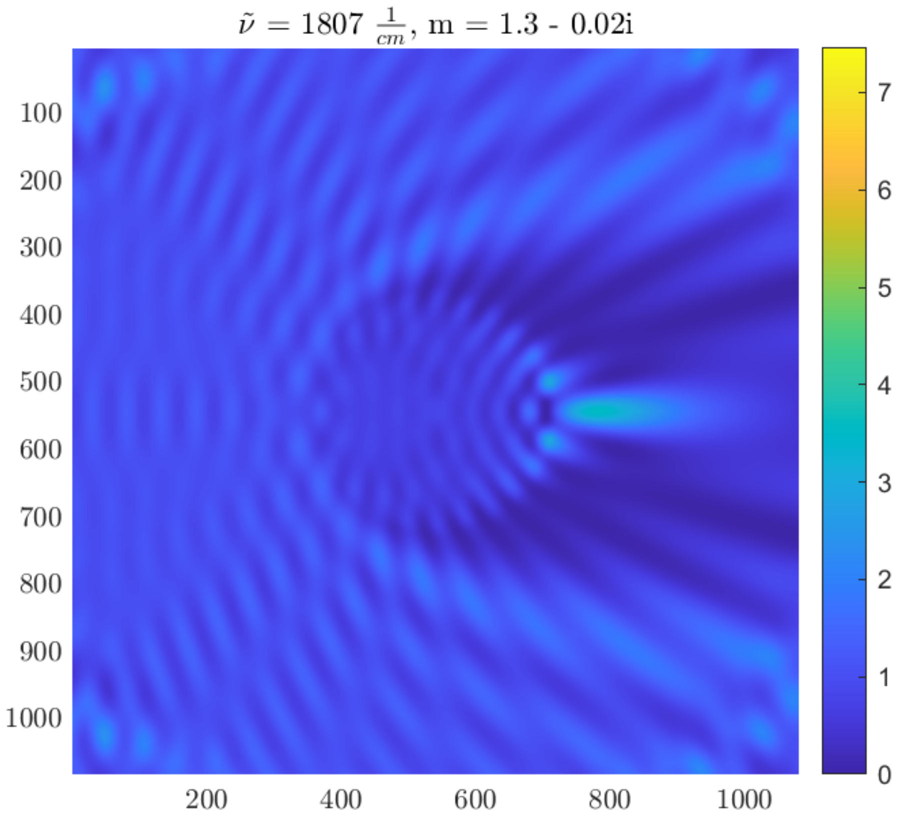

Figure 3.32: The absolute square of the wave function for the scattered plane wave for a disk with $n_r = 1.3$, radius $a = 10\mu$m and $n_i = 0.02i$ at the wave number $\tilde{\nu} = 1807$ cm^{-1}. The scale is rising from a dark blue to a bright yellow for the highest values. The incoming plane wave is traveling from left to right in the image. The sides of the frame are three times longer than the radius of the disk.

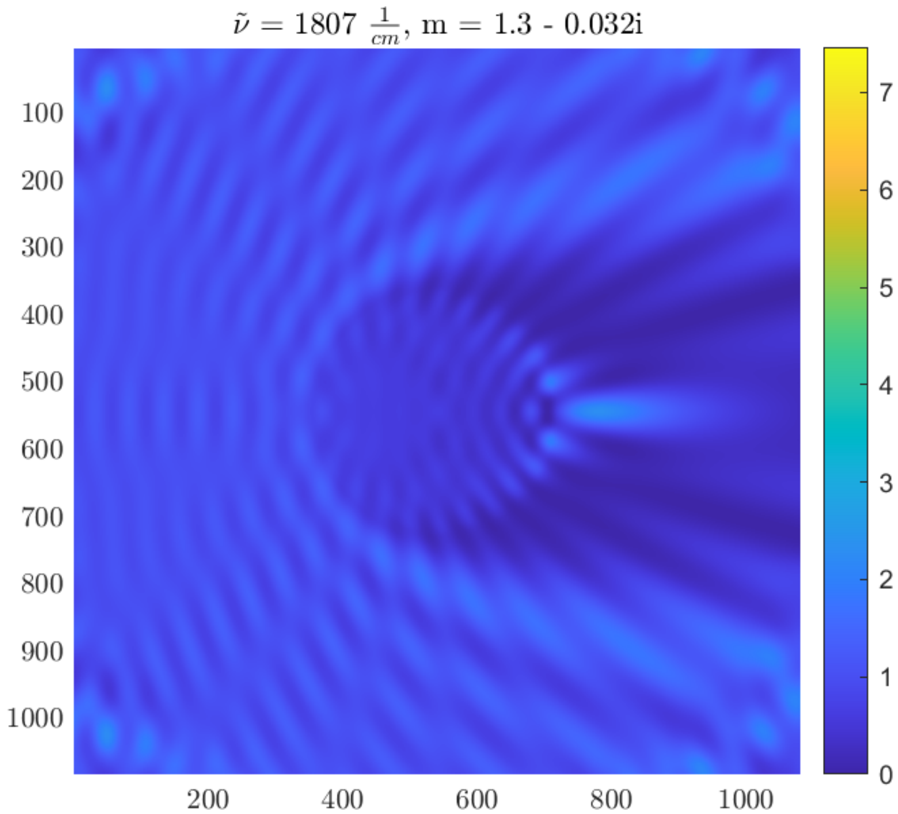

Figure 3.33: The absolute square of the wave function for the scattered plane wave for a disk with $n_r = 1.3$, radius $a = 10\mu$m and $n_i = 0.032i$ at the wave number $\tilde{\nu} = 1807$ cm^{-1}. The scale is rising from a dark blue to a bright yellow for the highest values. The incoming plane wave is traveling from left to right in the image. The sides of the frame are three times longer than the radius of the disk.

3.2.2 Wave function for cylinder2 as a disk

For a disk with the same properties as cylinder2, as in $n_r = 1.8$ and radius $a = 5\mu$m, the absolute square of the wave function for the scattered plane wave is calculated by Eqs. (2.49) and (2.51), and given in Fig. 3.34 for imaginary refractive index $n_i = 0$, i.e. non-absorptive disk, at the ripple in $\tilde{\nu} = 3287$ cm^{-1}. Here, the WGMs are clear around the disk, as expected with this high real refractive index.

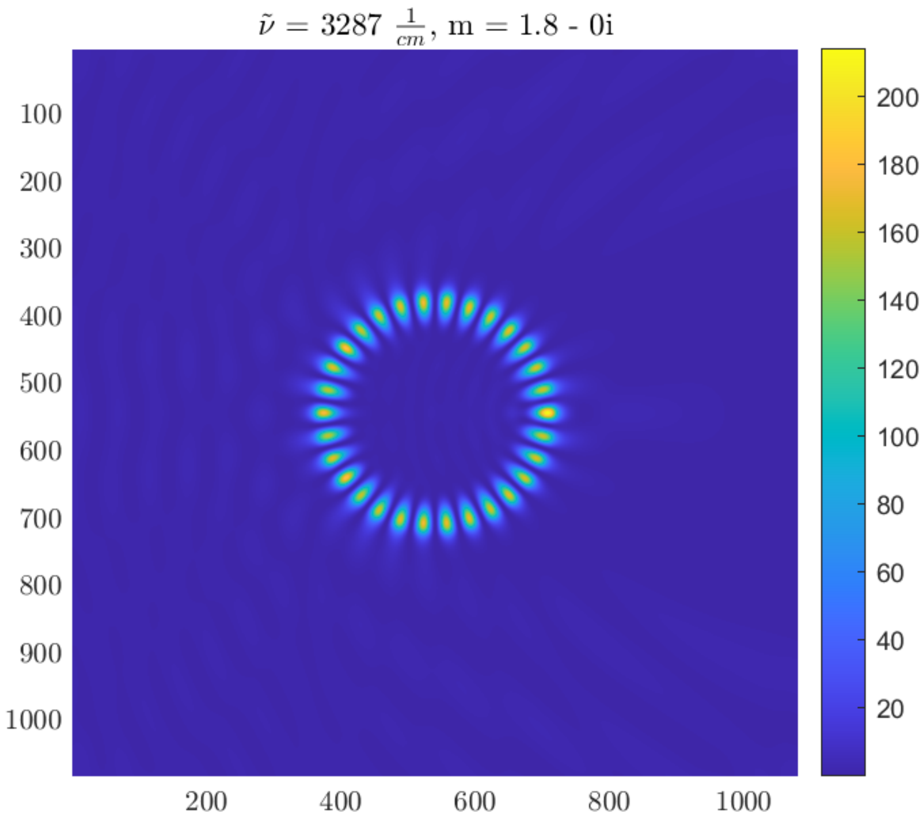

Figure 3.34: The absolute square of the wave function for the scattered plane wave for a disk with $n_r = 1.8$, radius $a = 5\mu$m and $n_i = 0i$ at the wave number $\tilde{\nu} = 3287$ cm^{-1}. The scale is rising from a dark blue to a bright yellow for the highest values. The incoming plane wave is traveling from left to right in the image. The sides of the frame are three times longer than the radius of the disk.

Increasing the pure absorbance to $A = 0.3$ at the same $\tilde{\nu} = 3287$ cm^{-1}, corresponding to imaginary refractive index $n_i = 0.02$ from Eq. (2.12), the absolute square of the wave function for the scattered wave becomes as shown in Fig. 3.35. The scale is drastically lessened, from maximum ≈ 200 in Fig. 3.34, to ≈ 4 in Fig. 3.35. The WGMs have clearly disappeared. Since the scale is lowered, the field around becomes more clear. With pure absorbance $A = 0.5$, Eq. 2.12 gives a imaginary refractive index $n_i = 0.036$. This leads to the near-field around the disk looking as in Fig. 3.36. The scale is lessened a bit more, giving a more clear image of the pattern of the field.

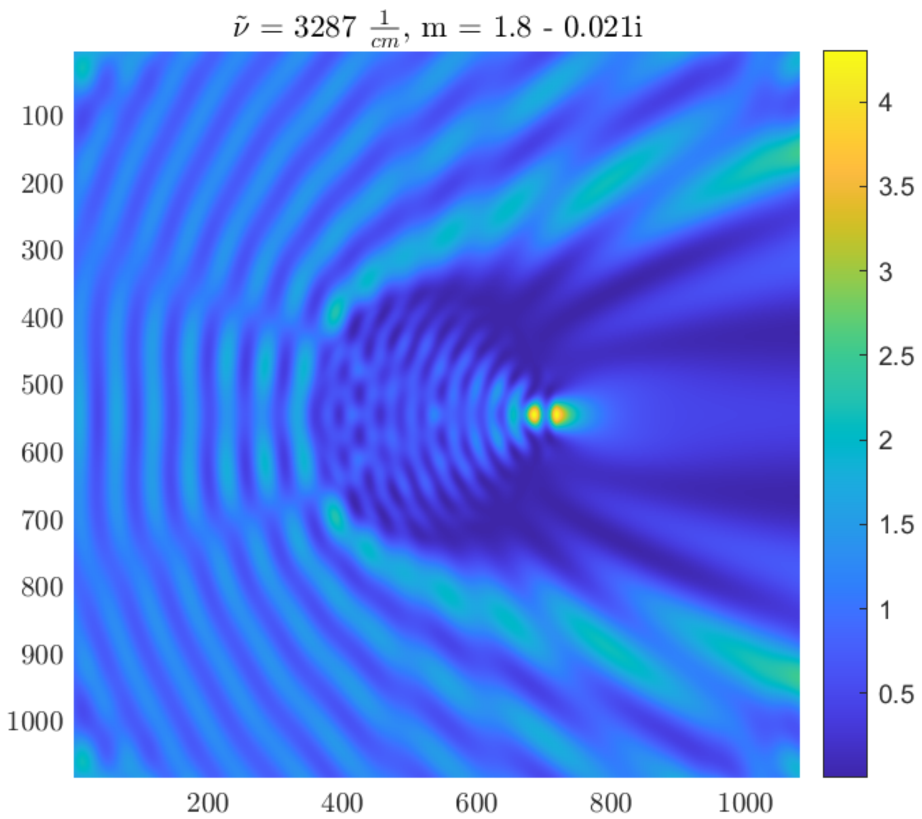

Figure 3.35: The absolute square of the wave function for the scattered plane wave for a disk with $n_r = 1.8$, radius $a = 5\mu$m and $n_i = 0.02i$ at the wave number $\tilde{\nu} = 3287$ cm^{-1}, corresponding to $A = 0.3$. The scale is rising from a dark blue to a bright yellow for the highest values. The incoming plane wave is traveling from left to right in the image. The sides of the frame are three times longer than the radius of the disk.

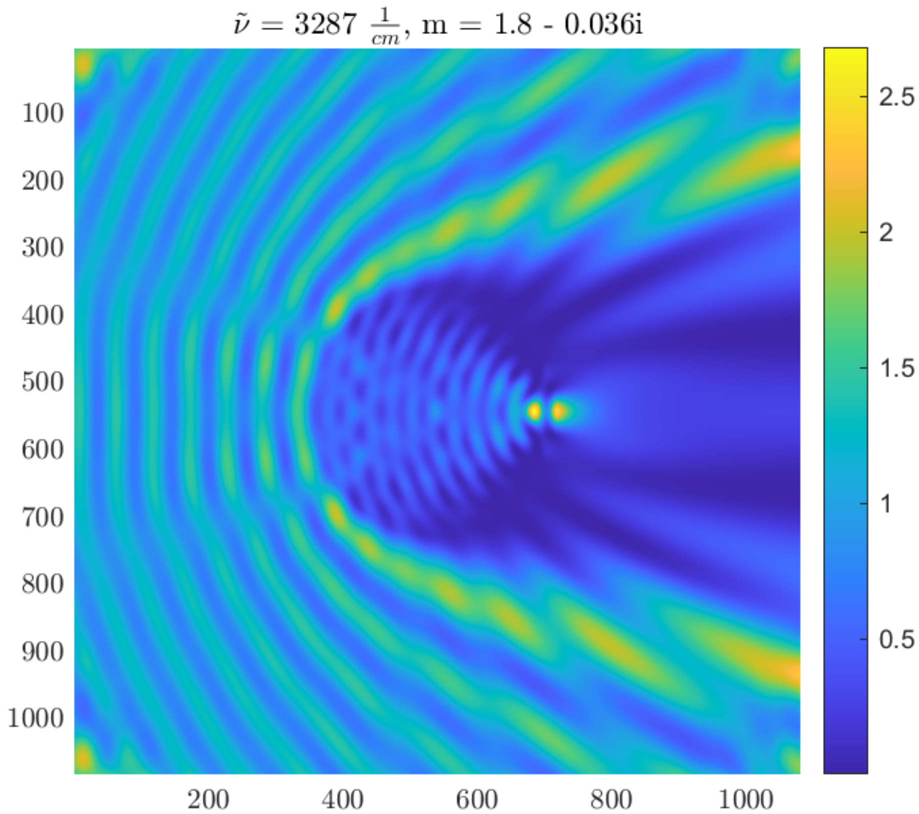

Figure 3.36: The absolute square of the wave function for the scattered plane wave for a disk with $n_r = 1.8$, radius $a = 5\mu$m and $n_i = 0.036i$ at the wave number $\tilde{\nu} = 3287$ cm^{-1}, corresponding to $A = 0.5$. The scale is rising from a dark blue to a bright yellow for the highest values. The incoming plane wave is traveling from left to right in the image. The sides of the frame are three times longer than the radius of the disk.

The adjustment of the scale can be a bit misleading. To show the drastic changes from the non-absorptive disk in Fig. 3.34 to $A = 0.3$ at $\tilde{\nu} = 3287$ cm^{-1}, Fig. 3.37 shows the same scenario as Fig. 3.35, but with the same scale as Fig. 3.34 (maxima ≈ 210). This shows very well the disappearance of the WGMs.

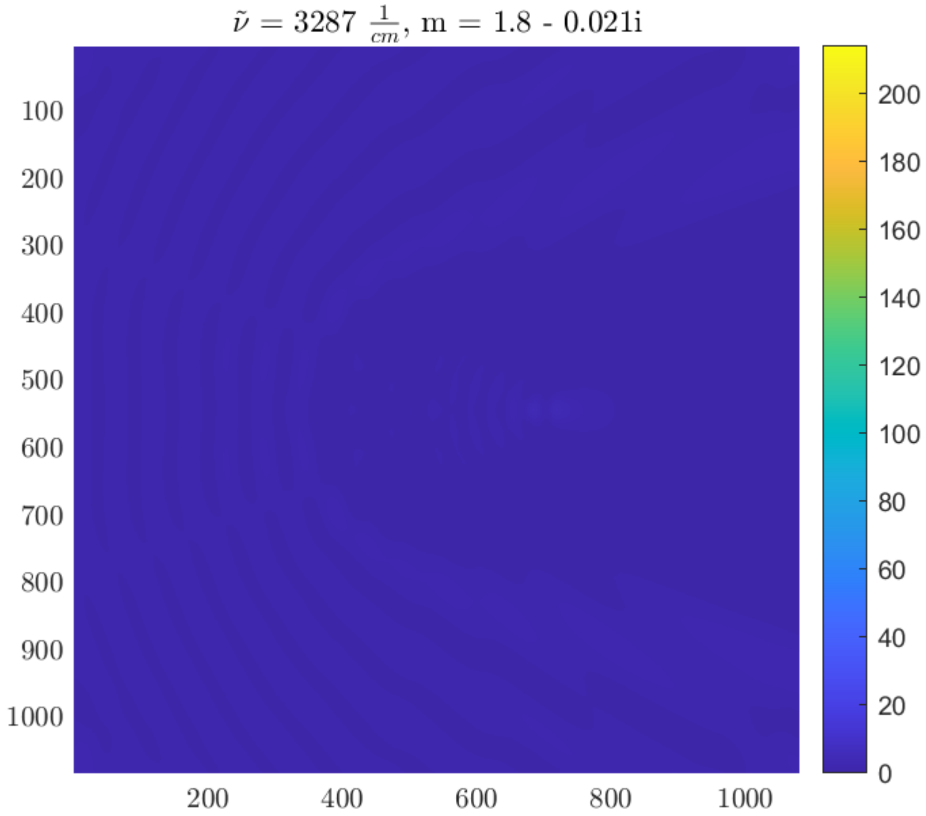

Figure 3.37: The absolute square of the wave function for the scattered plane wave for a disk with $n_r = 1.8$, radius $a = 5\mu$m and $n_i = 0.021i$ at the wave number $\tilde{\nu} = 3287$ cm^{-1}. The scale is rising from a dark blue to a bright yellow for the highest values. The incoming plane wave is traveling from left to right in the image. The sides of the frame are three times longer than the radius of the disk.

3.3 Sphere

3.3.1 Q_{ext} for a sphere with wavenumber independent n_i

The sphere investigated in this thesis is a sphere with radius $a = 5\mu$m and real refractive index $n_r = 1.5$, which corresponds to approximately the refractive index of a PMMA-sphere in the infrared region. Figure 3.38 shows how Q_{ext} changes when the imaginary part of the refractive index n_i is increased. The solid black line is Q_{ext} for a non-absorptive sphere, the green dotted line is Q_{ext} with $n_i = 0.002$, the dashed magenta line is Q_{ext} with $n_i = 0.005$, the dotted red line is Q_{ext} with $n_i = 0.01$ and the dashed cyan line is Q_{ext} with $n_i = 0.02$. The ripples chosen for investigation at $\tilde{\nu} = 1610$ cm^{-1} and $\tilde{\nu} = 3530$ cm^{-1} are indicated with data tips. This figure shows how the wiggles in Q_{ext} are damped as n_i increases.

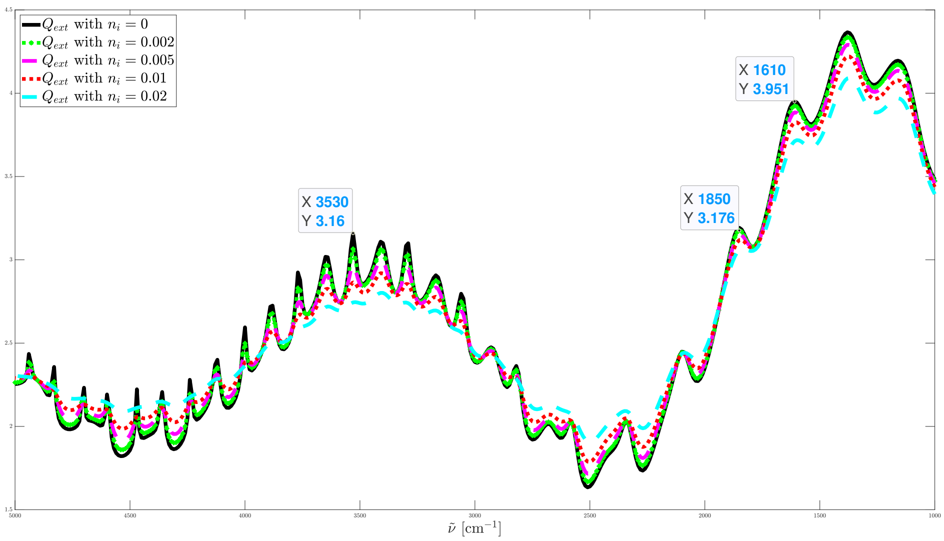

Figure 3.38: The Q_{ext} for a sphere with $n_r = 1.5$ and $a = 5\mu$m and wavelength independent n_i. The data tips indicate the chosen ripples at $\tilde{\nu} = 1610$ cm^{-1}and $\tilde{\nu} = 3530$ cm^{-1}. The Q_{ext} with $n_i = 0$ is the solid black line, Q_{ext} with $n_i = 0.002$ is the green dotted line, Q_{ext} with $n_i = 0.005$ is the dashed magenta line, Q_{ext} with $n_i = 0.01$ is the dotted red line and Q_{ext} with $n_i = 0.02$ is the dashed cyan line.

3.3.2 Efficiency factors for a sphere with Lorentz-shaped absorption band in ripples

A sphere with a Lorentz-shaped absorption band with a constant absorbance A, i.e. variable n_i, is evaluated in this section. $\Gamma = 15$ cm^{-1} was used with a peak value of n_i at $\tilde{\nu}_0 = 1610$ cm^{-1} corresponding to $A = 0.3$ according to Eq. (2.12). The effective thickness used for calculations were approximated to the same as the cylinder, Eq. (2.14). To make the Lorentz function reach this peak value, Λ was set to 3100 cm^{-2}, from Eq. (2.17). The imaginary part of the complex refractive index n_i found by Eq. (2.16) from the Lorentz function is plotted as the blue dotted line in Fig.3.39 versus the right y-axis together with the Q_{ext} (black line) versus the left y-axis, calculated by Eq. (2.53). An inverted peak is created in the Q_{ext} at this wavenumber.

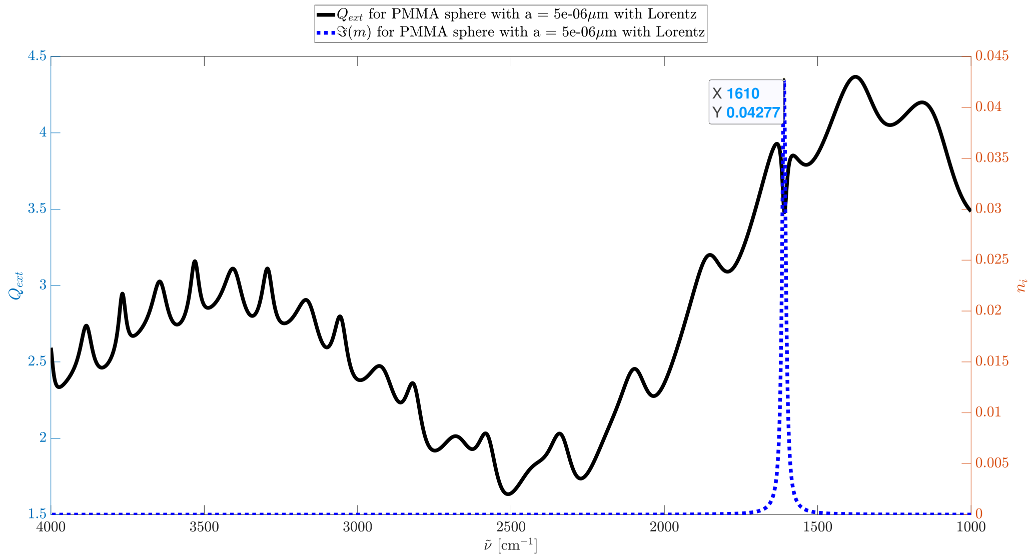

Figure 3.39: The Q_{ext} plotted in a solid black line versus the left y-axis for a sphere with $n_r = 1.5$, $a = 5\mu$m and Lorentzian n_i. The n_i is given by a Lorentz function with $\Gamma = 15$ cm^{-1} and $\Lambda = 3100$ cm^{-2} plotted in a dotted blue line versus the right y-axis with a peak at $\tilde{\nu} = 1610$ cm^{-1} with $A = 0.3$ as indicated by the data tip.

The Q_{sca} for the same scenario is calculated by the Eq. (2.54) given in Fig. 3.40. As for the cylinder, knowing Q_{sca} and the Q_{ext} for the sphere gives the Q_{abs} from Eq. (2.22). The result of Q_{abs} is plotted in Fig. 3.41. A great decrease from the top of the wiggle in Q_{sca} is shown, explaining the inverted peak in Q_{ext} as well.

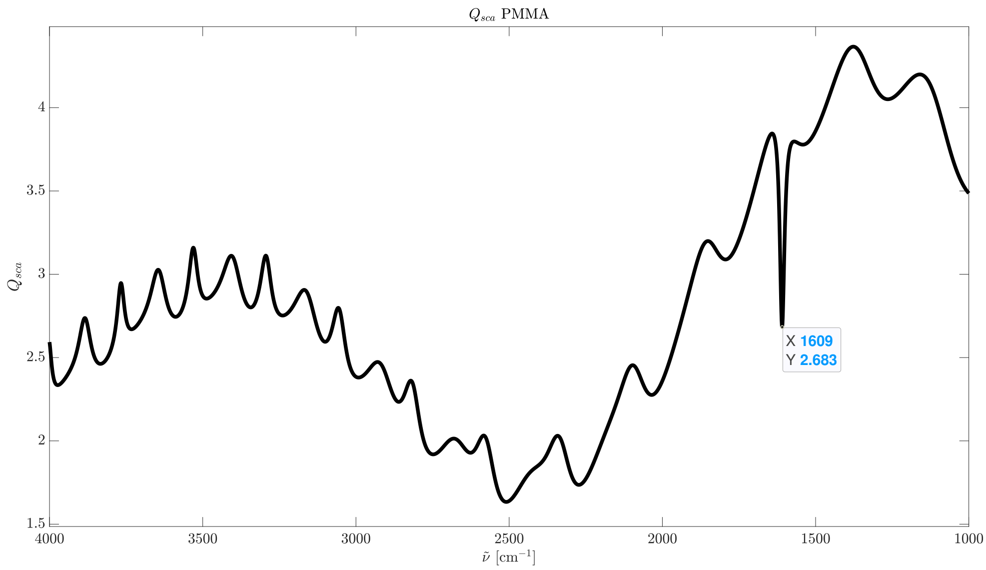

Figure 3.40: The Q_{sca} for a sphere with $n_r = 1.5$, $a = 5\mu$m and Lorentzian n_i with $\Gamma = 15$ cm^{-1}, $\Lambda = 3100$ cm^{-2}, $\tilde{\nu}_0 = 1610$ cm^{-1} and peak corresponding to $A = 0.3$.

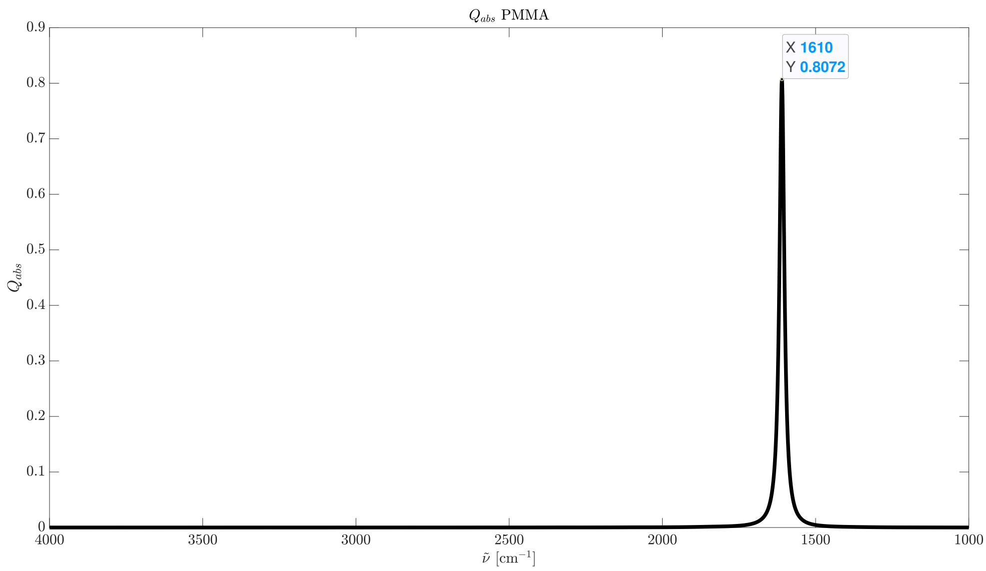

Figure 3.41: The Q_{abs} for a sphere with $n_r = 1.5$, $a = 5\mu$m and Lorentzian n_i with $\Gamma = 15$ cm^{-1}, $\Lambda = 3100$ cm^{-2}, $\tilde{\nu}_0 = 1610$ cm^{-1} and peak corresponding to $A = 0.3$.

Moving this absorption band to $\tilde{\nu}_0 = 3530$ cm^{-1}and increasing the peak of pure absorbance from $A = 0.3$ to $A = 0.5$, the Λ becomes 5200 cm^{-2}from Eqs. (2.13), (2.16) and (2.17). This Lorentzian imaginary refractive index n_i (dotted blue line) is plotted versus the right y-axis together with the extinction efficiency factor Q_{ext} (solid black line) versus the left axis in Fig. 3.42. The ripple at $\tilde{\nu} = 3530$ cm^{-1}was situated on the top of a wiggle, and an inverted peak is created in the Q_{ext}, in perfect harmony with the absorption band.

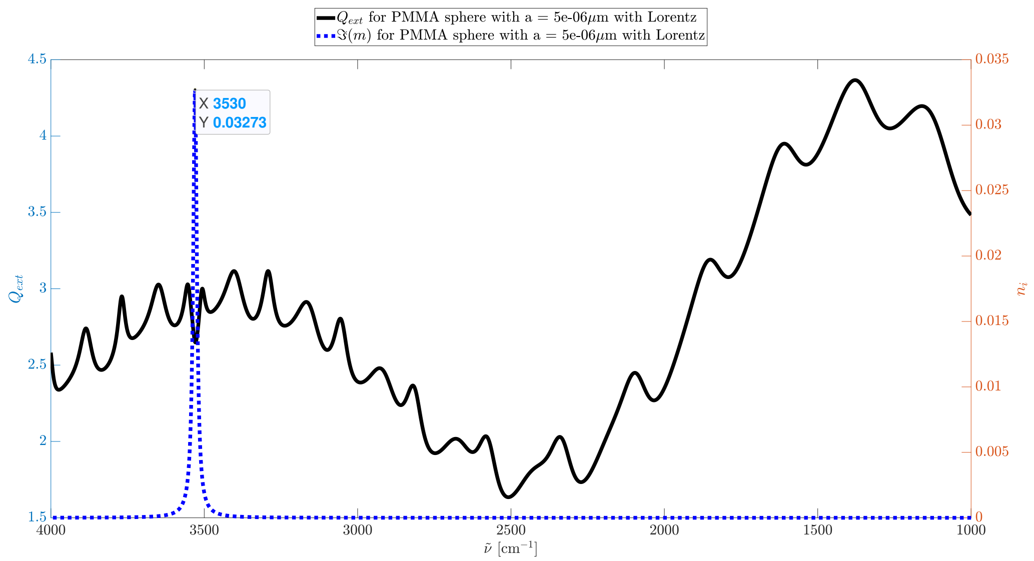

Figure 3.42: The Q_{ext} plotted in a solid black line versus the left y-axis for a sphere with $n_r = 1.5$, $a = 5\mu$m and Lorentzian n_i. The n_i is given by a Lorentz function with $\Gamma = 15$ cm^{-1} and $\Lambda = 5200$ cm^{-2} plotted in a dotted blue line versus the right y-axis with a peak at $\tilde{\nu} = 3530$ cm^{-1} with $A = 0.5$ as indicated by the data tip.

In this scenario the Q_{sca} from Eq. (2.54) and Q_{abs} from Eq. (2.22) are as in Figs. 3.43 and 3.44. A decrease in Q_{sca} far greater than the increase of Q_{abs} is seen also in this scenario.

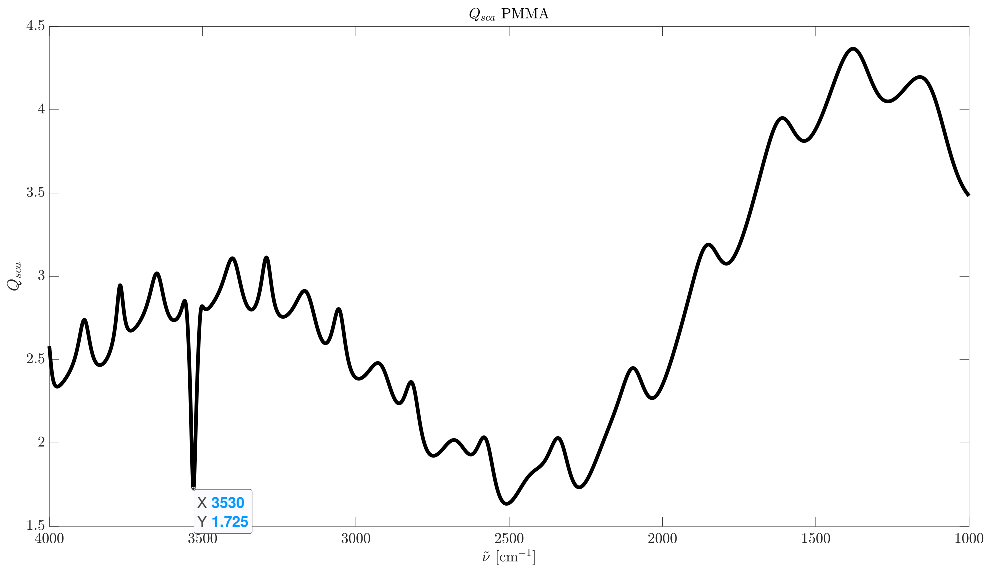

Figure 3.43: The Q_{sca} for a sphere with $n_r = 1.5$, $a = 5\mu$m and Lorentzian n_i with $\Gamma = 15$ cm^{-1}, $\Lambda = 5200$ cm^{-2}, $\tilde{\nu}_0 = 3530$ cm^{-1} and peak corresponding to $A = 0.5$.

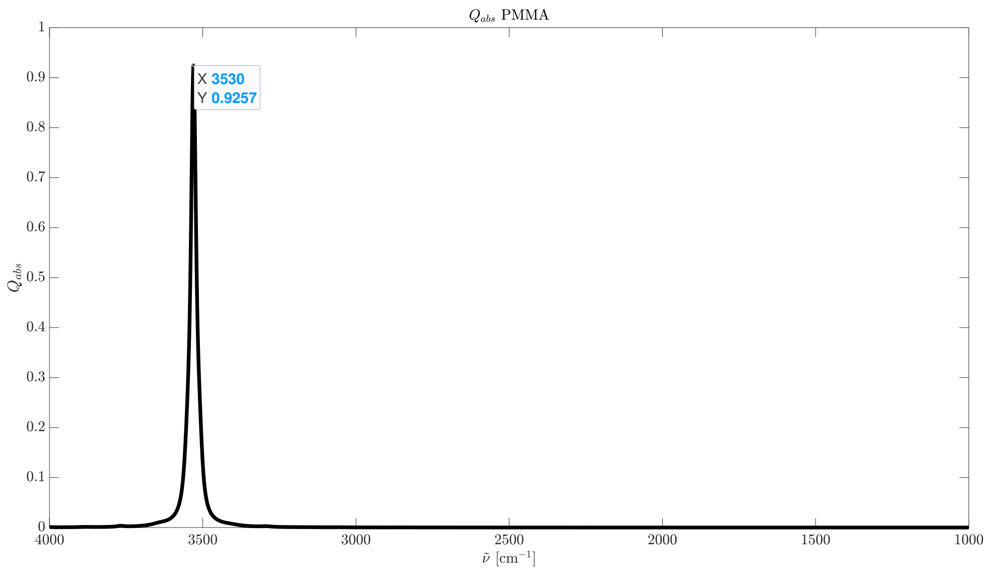

Figure 3.44: The Q_{abs} for a sphere with $n_r = 1.5$, $a = 5\mu$m and Lorentzian n_i with $\Gamma = 15$ cm^{-1}, $\Lambda = 5200$ cm^{-2}, $\tilde{\nu}_0 = 3530$ cm^{-1} and peak corresponding to $A = 0.5$.

3.3.3 Extinction efficiency for a sphere with Lorentz-shaped absorption band outside ripples

As a comparison to how the absorption bands affect the extinction efficiency factor when placed in ripples, two absorbance bands are put outside ripples. The two tested are set at exactly $\tilde{\nu}_0 = 1750$ cm^{-1} and $\tilde{\nu}_0 = 3250$ cm^{-1}. The one at $\tilde{\nu}_0 = 1750$ cm^{-1} represents that of the absorption from stretches between C=O bands (vibrational spectroscopy). This band is related to lipids, and have a FWHM of 15 cm^{-1}, which means Γ is put at 15 cm^{-1}. With an absorbance peak of $A = 0.3$, the Λ becomes 3100 cm^{-2}. The band at $\tilde{\nu}_0 = 3250$ cm^{-1} represents absorption from stretches in a O-H band (vibrational spectroscopy). The FWHM of "several hundreds" is interpreted as $\Gamma = 300$ cm^{-1}. In order to reach a peak absorbance of $A = 0.3$, Λ becomes 63 000cm^{-2}. This absorption band is related to water and carbohydrates (Kohler et al., 2020). The extinction efficiency factor Q_{ext} and the imaginary refractive index n_i becomes as in Figs. 3.46 and 3.45.

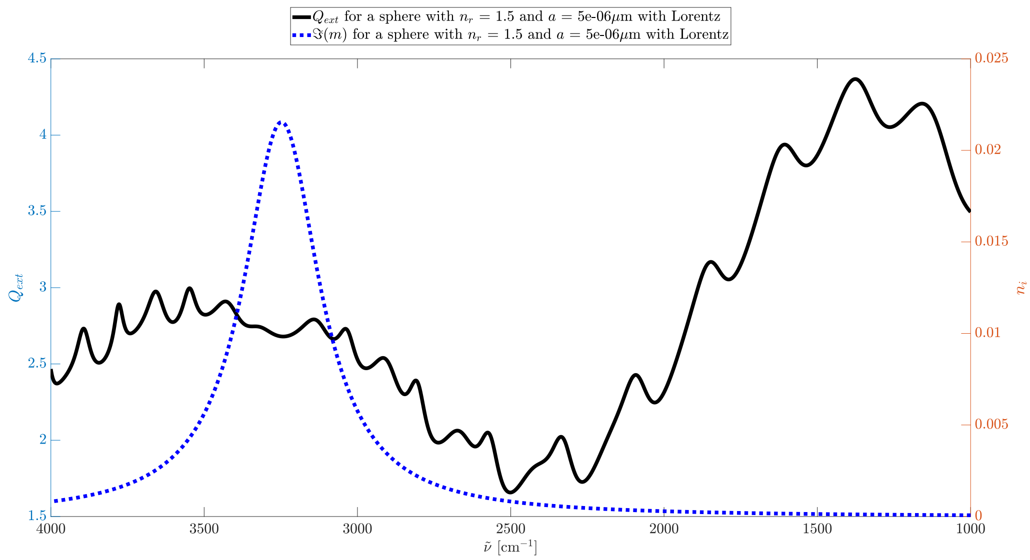

Figure 3.45: The Q_{ext} for a sphere with $n_r = 1.5$ and $a = 5\mu$m. Lorentz peak at $\tilde{\nu}_0 = 3530$ cm^{-1}with $A = 0.3$, Lorentz FWHM $\Gamma = 300$ cm^{-1} and $\Lambda = 63000$cm^{-2}.

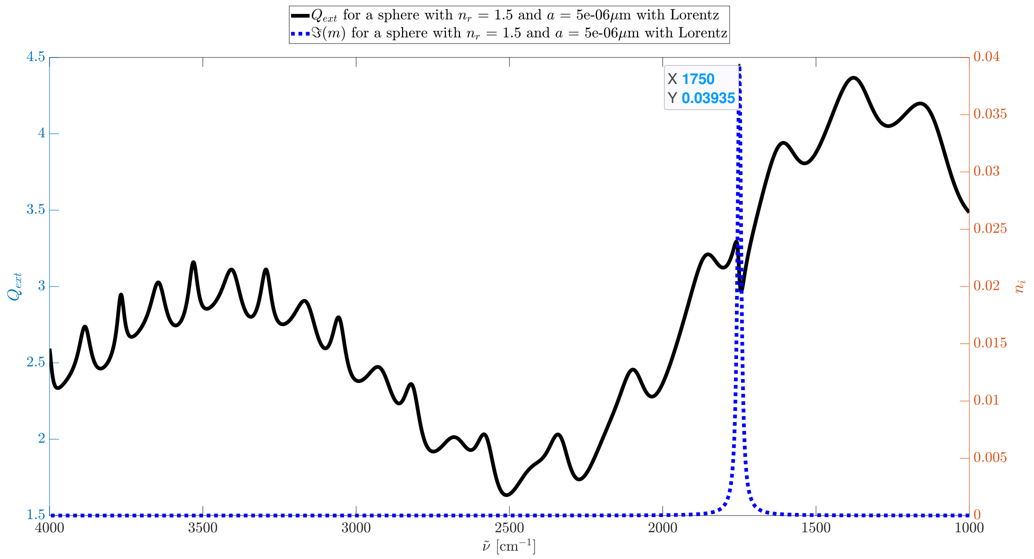

Figure 3.46: The Q_{ext} for a sphere with $n_r = 1.5$ and $a = 5\mu$m. Lorentz peak at $\tilde{\nu}_0 = 1750$cm^{-1}with $A = 0.3$, Lorentz FWHM $\Gamma = 15$ cm^{-1} and $\Lambda = 3100$ cm^{-2}.

3.3.4 Inverted peaks found in experimental data

The inverted peaks created by absorption bands over ripples at high levels of scattering (top of wiggle) as predicted by the results in this thesis (sections 3.1 and 3.3) have been found in experimental data by μFTIR (Fourier-Transform Infrared) imaging. Polyethylene was cooled by liquid nitrogen and milled into micrometer-sized particles with random morphology. The spectroscope used was a Bruker Hyperion 3000 with a 15x objective system, which has a numerical aperture (NA) of 0.4. 64 scans was done with a resolution of 8 cm^{-1}. The microscope slide was a 1 mm ZnSe, and the background was an empty slide.

As a reference spectrum, the pure absorbance (i. e. scatter-free) spectrum of a 25 μm thick polyethylene foil is presented in Fig. 3.47. The only absorbance bands present are those created by C-H stretching vibrations around $\tilde{\nu} = 2900\ \text{cm}^{-1}$, and those of C-C stretching vibrations around $\tilde{\nu} = 1470\ \text{cm}^{-1}$ (both from CH_2 and CH_3 groups).

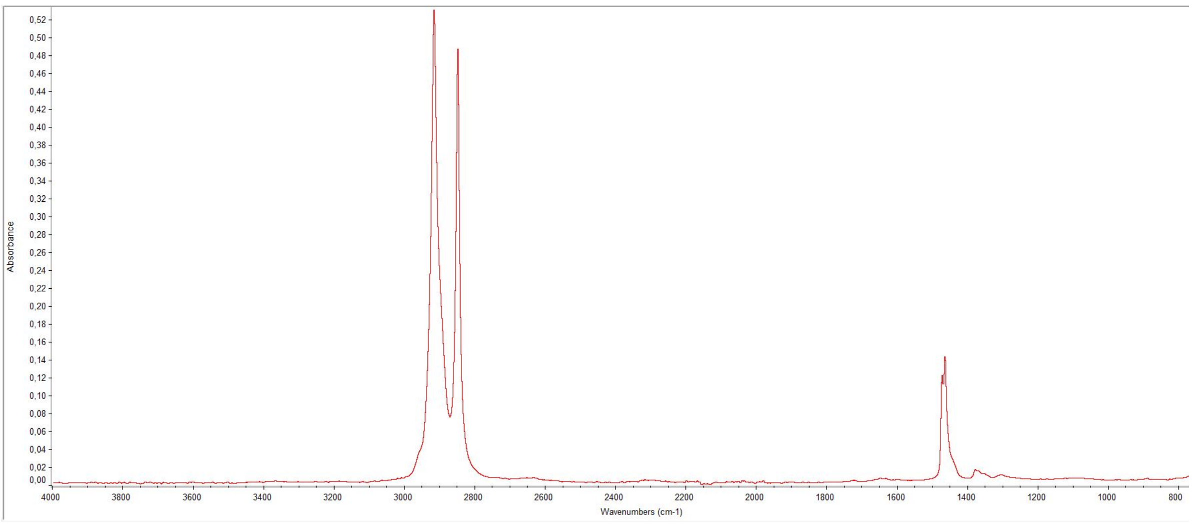

Figure 3.47: Pure absorbance (i.e. scatter-free) spectrum of a 25 μm thick polyethylene foil.

Two apparent absorbance spectra are presented in Figs. 3.48 and 3.49. Since they have randomly created different morphology, they have different scattering signatures (wiggles). Notice that the inverted peaks are only present when the absorption band is in the area of high scattering, i.e. on the top of a wiggle.

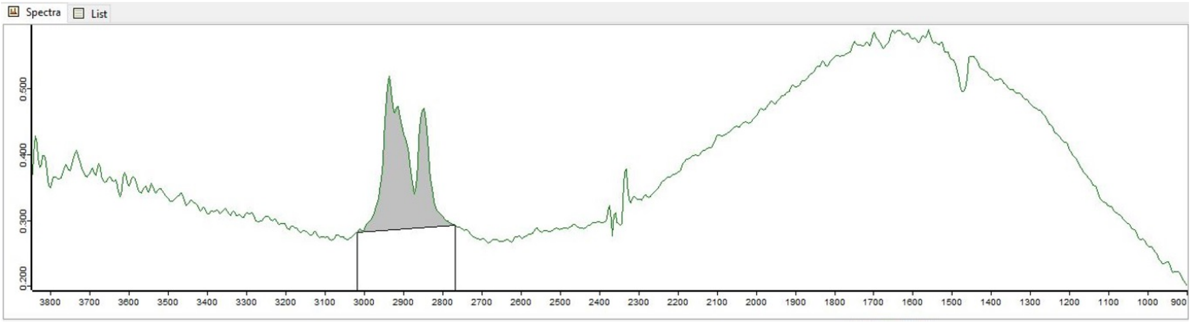

Figure 3.48: Apparent spectrum of a μm-sized polyethylene particle. An inverted peak is present around the high levels of scattering in the area of the $\tilde{\nu} = 1470$ cm^{-1} absorption band.

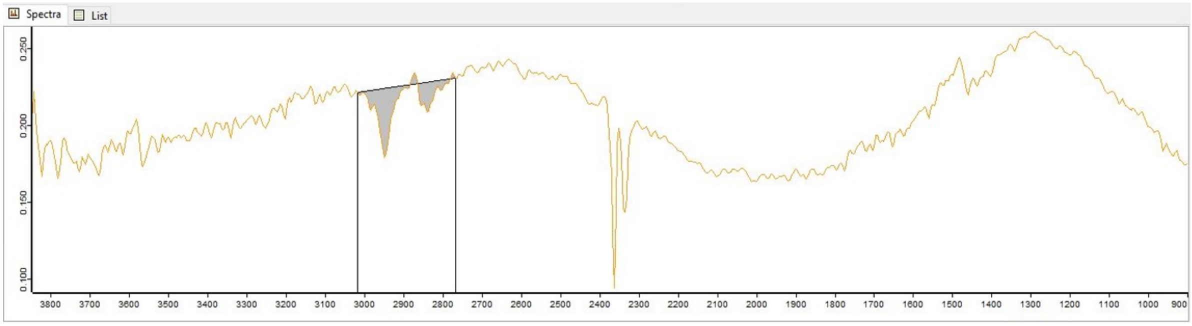

Figure 3.49: Apparent spectrum of a μm-sized polyethylene particle. An inverted peak is present around the high levels of scattering in the area of the $\tilde{\nu} = 2900$ cm^{-1} absorption band.

The experimental data in this section have been provided by researcher Boris Zimmermann.

4. Discussion

For both the cylinder cases, as well as for the spherical particle, a dampening of the wiggles in the extinction efficiency factor Q_{ext} appeared when applying a constant absorbance across the spectrum used ($\tilde{\nu}$ = 1000 cm^{-1}- 4000 cm^{-1}). Thus, when a Lorentzian absorption band was moved into a ripple, Q_{ext} was shoved from its current position towards the damped position. This meant the ripple disappeared if it was placed on the middle-value of a wiggle, making a smooth curve. At the extremity points, the Q_{ext} was clearly pushed towards the damped position, making either a peak from the bottom of a wiggle, or inverted peak from the top of a wiggle. With increasing pure absorbance A, both inverted and normal peaks, grew in size. Thus, they made a more and more clear dent in the usual curve of the wiggles.

It is apparent from the disk figures (Sec. 3.2) that the wave function for the scattered plane wave greatly decreases as soon as absorbance is present. The WGMs representing the ripples disappear, and this is seen also in the Q_{ext} figures as well. With absorbance, the ripples disappear and the wiggles are pressed to smaller amplitudes in Q_{ext} (Secs.3.1 and 3.3).

Upon examining the efficiency factors for scattering and absorbance, Q_{sca} and Q_{abs}, the inverted peaks in Q_{ext} are explained by the fact that Q_{sca} is so greatly decreased from the top of a wiggle when an absorbance band is put there, that although there is absorbance and therefore increase in Q_{ext} from Q_{abs}, the decrease in Q_{sca} is much greater. Another way of looking at it is that since Q_{sca} is exponentially dependent on the coefficient b_n, which is dependent on the complex refractive index, m, and Q_{ext} is only linearly dependent on $\Re(b_n)$ (within the summation). Therefore, Q_{sca} will indeed respond more to changes in the b_n's than Q_{ext}. Remember, Q_{abs} is calculated by the difference between these (Eq. (2.32)).

The Q_{ext} lessened in value across the spectrum when taking into account the numerical aperture, NA, as one would expect when integrating over a smaller area. All though Q_{ext} was generally decreased, the ripples where still intact. Therefore, it seems that the WGMs are still radiating as greatly as before since they are mostly wavenumber dependent, as long as there is no absorbance. With absorbance, the NA will become relevant however, since the absorbance spectra will depend on NA (van Dijk et al., 2013).

It has been shown that for both increasing scaling factor x and imaginary part of the refractive index n_i, the wiggles of Q_{ext} are dampened (Sharma and Somerford, 2006). So, in a way, there really shouldn't be any surprise that when increasing n_i in a smaller area at the top, or bottom of a wiggle, it creates an inverted peak or a normal peak respectively. Inverted peaks have been found in absorbance spectra from μFTIR imaging, Figs. 3.48 and 3.49.The inverted peaks have earlier been discarded as artefacts in absorbance spectra, but they have been predicted by Mie theory in this thesis.

The classical telltale sign for an absorbance band, the derivative shape, is visible when one created by the Lorentz function is placed outside ripples, both in this thesis, Fig. 3.46 and other publications (Lukacs et al., 2015). However, when situated over one, there is either a peak, an inverted peak, or a smooth curve, depending on the placement on the wiggle. The disappearance of a ripple is a a sign of absorbance, even though there might not be a derivative shape present in that area. The increase in light absorbed is close to the same amount that is not being scattered anymore, making little apparent change in Q_{ext}.

In studying raw absorbance spectra, it would be wise to look for regular peaks or inverted peaks as well as the derivative shape in order to determine where there is absorbance. This means algorithms correcting the raw absorbance spectra for Mie extinction, such as the ME-EMSC, should consider to correct for absorbance where there are inverted peaks or regular peaks instead of a derivative shape in the extinction. All though the Q_{ext} is generally decreased somewhat as a consequence of regarding the NA, the ripples stays intact, and studies examining the behavior of ripples, or WGMs could simplify calculations by not regarding the NA.

5. Conclusions

When an absorbance band is put over a ripple at the top of a wiggle, an inverted peak in the extinction efficiency factor Q_{ext} is created due to the great loss in scattering. A regular peak is created in Q_{ext} when an absorbance band is put over a ripple on the bottom of a wiggle. The most difficult case is when the ripple is placed mid-way on the wiggle. In this case, the ripple do disappear, leaving a smooth curve, since the loss in scattering is the same as that gained by absorbance. This observation was true for both cylinders and spheres. An essential assumption done in this thesis is then that cells can be interpreted as either a quasi-spherical or quasi-cylindrical particle, giving the same results as the perfect geometric shapes. In addition, two different cases of incident radiation was studied for the cylinder and the same outcome was yielded in both scenarios. Different sizes of the radius a, refractive index m and absorbance A was tested, all scenarios giving the same result. Inverted peaks have been found in apparent absorbance spectra from μFTIR imaging in the area of expected absorption bands at high levels of scattering (top of wiggle). These have earlier been discarded as artefacts, but are now predicted by Mie theory and therefore a signature for an absorption band. The Q_{ext} is dependent on the NA, but the ripple represented by the WGM are not. Neither is the pattern of Q_{ext}, it is simply the size of it that decreases as NA increases. Therefore, it is legit to do studies of ripples and WGM without calculating for the NA.

References

Bassan, P., Byrne, H., Bonnier, F., Lee, J., Dumas, P., and Gardner, P. (2009). Resonant Mie Scattering in infrared spectroscopy of biological materials - understanding the 'dispersion artefact'. *Analyst* (8).

Bassan, P., Kohler, A., Martens, H., Lee, J., Byrne, H., Dumas, P., Gazi, E., Brown, M., Clarke, N., and Gardner, P. (2010). Resonant Mie Scattering (RMieS) correction of infrared spectra from highly scattering biological samples. *Analyst* (2).

Blümel, R., Lukacs, R., Zimmermann, B., Bağcioğlu, M., and Kohler, A. (2018). Observation of Mie ripples in the synchrotron Fourier transform infrared spectra of spheroidal pollen grains. *Journal of the Optical Society of America* 35 (10): 1769–1779.

Brandsrud, M. A. (2016). Understanding resonant structures of coupled disks for light management in photovoltaics. Norwegian University of Life Sciences.

Hollesbekk, T. and Skaar, J. (2018). Maxwells ligninger. *Store Norske Leksikon*. Last updated: 27.11.2018. URL: https://snl.no/Maxwells_ligninger.

Kohler, A., Sulé-Suso, J., Sockalingum, G., Tobin, M., Bahrami, F., Yang, Y., Pijanka, J., Dumas, P., Cotte, M., van Pittus, D., Parkes, G., and Martens, H. (2008). Estimating and Correcting Mie Scattering in Synchrotron-Based Microscopic Fourier Transform Infrared Spectra by Extended Multiplicative Signal Correction. *Applied Spectroscopy* 62 (3): 259–266.

Kohler, A., Solheim, J. H., Tafintseva, V., Zimmermann, B., and Shapaval, V. (2020). *Comprehensive Chemometrics: Chemical and Biochemical Data Analysis*. 2nd ed. Elsevier. Chap. Model-Based Pre-Processing in Vibrational Spectroscopy.

Kohler, A., Kirschner, C., Oust, A., and Martens, H. (2005). Extended Multiplicative Signal Correction as a Tool for Separation and Characterization of Physical and Chemical Information in Fourier-Transform Infrared Microscopy Images of Cryo-sections of Beef Loin. *Applied Spectroscopy* 59 (6).

Konevskikh, T., Lukacs, R., Blümel, R., Ponossov, A., and Kohler, A. (2016). Mie scatter corrections in single cell infrared microspectroscopy. 187: 235–257.

Lukacs, R., Blümel, R., Zimmerman, B., Bağcioğlu, M., and Kohler, A. (2015). Recovery of absorbance spectra of micrometer-sized biological and inanimate particles. 9. DOI: 10.1039/c5an00401b.

Mohlenhoff, B., Romeo, M., Diem, M., and Wood, B. R. (2005). Mie-type Scattering and Non-Beer-Lambert Absorption Behavior of Human Cells in Infrared Microspectroscopy. *Biophysical Journal* 88: 3635–3640.

Sharma, S. K. and Somerford, D. J. (2006). *Light Scattering by Optically Soft Particles - Theory and application*. Chichester, UK: Springer. ISBN: 3-540-23910-3.

Skaar, J. (2019). Brytningsindeks. *Store Norske Leksikon*. Last updated: 04.12.2019. URL: https://snl.no/brytningsindeks.

Solheim, J., Gunko, E., Petersen, D., Großerüschkamp, F., Gerwert, K., and Kohler, A. (2019). An open-source code for Mie Extinction EMSC for infrared microscopy spectra of cells and tissues. 12 (8).

Tanner, D. B. (2019). *Optical effects in solids*. Cambridge University Press. ISBN: 9781316672778. DOI: 10.1017/9781316672778.

Tipler, P. A. and Mosca, G. (2008). *Physics for scientists and engineers with modern physics*. ISBN-13: 978-0-7167-8964-2. New York, USA: W.H. Freeman and Company.

Torgersen, F. H. M. (2016). Whispering Gallery Resonances in Dielectric Disk. Norwegian University of Life Sciences.

Townsend, J. S. (2010). *Quantum Physics: A fundamental approach to modern physics*. Sausalito, California, USA: University Science Books. ISBN: 978 1 891389 62 7.

van de Hulst, H. C. (1981). *Light Scattering by Small Particles*. Dover Publications, Inc., An unabridged and corrected republication of the work originally published in 1957 by John Wiley Sons, Inc., New York, USA. ISBN: 0-486-64228-3.

van Dijk, T., Mayerich, D., Carney, P. S., and Bhargava, R. (2013). Recovery of Absorption Spectra from Fourier Transform Infrared (FT-IR) Microspectroscopic Measurements of Intact Spheres. *Applied Spectroscopy* 67 (5). DOI: 10.1366/12-06847.

Appendix A. MatLab script: Mie cylinder with constant A and with Lorentz

```
% Exact expression for Qext og Qabs for an infinitely long cylinder.
% Plots Qext and the coefficients bn from Mie with ni=constant, and
% variable ni. The variable ni is modeled with the Lorentz-function.
%
% The incident light travels perpendiculary to the cylinder axis. Case I
% and II from van de Hulst with E-field parallell to the cylinder.
%
% Simen R nnekleiv Eriksen, 10.03.2020, based on M. A. Brandsruds
% excact Qext and Qabs algorithm from 16.09.2019 and A. Kohlers
% algorithm for the dielectic function.
% Theory from van de Hulst chap 15 and Lukacs et al. paper 2015

%%

clear all
close all

%I = case I = E-field parallell to cylinder axis
%II = case II = E-field perpendicular to cylinder axis

set(groot,'defaulttextinterpreter','latex');
set(groot,'defaultLegendInterpreter','latex');
set(groot,'defaultAxesTickLabelInterpreter','latex');

%Input:
nu_array = 1000:1:4000;
Wavenumbers=num2str(nu_array);
```

```
lambda_array = 1./(100*nu_array); %(2:0.01:10)*1e-6;

R = 5e-6; % Radius
    %% Mie for cylinder

%% For the first Lorentz
nu1=2696; % Wavenumber for bn peak corresponding to ripple
gamma=15; % gamma = 15 or 300
omega1=3800; % proportional to absorbance, increases Lorentz peak.

s1 = cal_dielectricSusc_func(Wavenumbers,nu1,gamma,omega1);
%susceptibility

e1 = 3.24 - s1.d; % e=1.69-s.d, 2.25-s.d, or 3.24-s.d
%dielectic function
m1.d = sqrt(e1); %complex refractive index
% nr_array=real(m.d);
% ni_array=-imag(m.d); %the format of this code is m = n_r-i*n_i,
% while the susc-func has m = n_r + i*n_i

%% For the second Lorentz
nu2=3287; % Wavenumber for bn peak corresponding to ripple
gamma=15; % gamma = 15 for nu0 ~= 1750, or 120 for nu0~=3250
omega2=3800; % proportional to absorbance, increases Lorentz peak.

s2 = cal_dielectricSusc_func(Wavenumbers,nu2,gamma,omega2);
%susceptibility

e2 = 3.24 - s2.d; % e=1.69-s.d, 2.25-s.d, or 3.24-s.d
%dielectic function
m2.d = sqrt(e2); %complex refractive index

%% Sum variables for Lorentz in complex refractive index

mv = real(m1.d)+1i.*(imag(m1.d)+imag(m2.d));

x= 2*pi*R./lambda_array;
n_maks = max(ceil(x + 4*x.^(1/3) + 2));
%=39, 24, and 16 for R=10, 5, and 2.5
```

```
b = zeros(length(nu_array), n_maks.*2+1);
a = zeros(length(nu_array), n_maks.*2+1);

    for jj = 1:length(lambda_array)
        x = 2*pi*R./lambda_array(jj);
        y = mv(jj)*x;

        n_min = -ceil(x + 4*x.^(1/3) + 2);

        n = n_min:1:n_maks;

        QextI(jj) = 0;
        QscaI(jj) = 0;
        QextII(jj) = 0;
        QscaII(jj) = 0;

        k = 2*pi/lambda_array(jj);
        rho = 2.*k.*R.*(mv(jj)-1);

        for kk = 1:length(n)
            Jx = besselj(n(kk), x);
            dJx = 0.5*(besselj(n(kk)-1, x) - besselj(n(kk)+1, x));

            Jy = besselj(n(kk), y);
            dJy = 0.5*(besselj(n(kk)-1, y) - besselj(n(kk)+1, y));

            Nx = bessely(n(kk), x);
            dNx = 0.5*(bessely(n(kk)-1, x) - bessely(n(kk)+1, x));

            tan_beta = (mv(jj).*dJy.*Jx - Jy.*dJx) ./ ...
                (mv(jj).*dJy.*Nx - Jy.*dNx);
            tan_alfa = (dJy.*Jx - mv(jj).*Jy.*dJx) ./ ...
                (dJy.*Nx - mv(jj).*Jy.*dNx);

            b(jj, n(kk)+n_maks+1) = tan_beta./(tan_beta - 1i);

            a(jj, n(kk)+n_maks+1) = tan_alfa./(tan_alfa - 1i);

            c(jj, n(kk)+n_maks+1) = b(jj, n(kk)+n_maks+1)-...
```

```
                    a(jj, n(kk)+n_maks+1);

                QextI(jj) = QextI(jj) + (2/x).*real(b(jj,...
                    n(kk)+n_maks+1));
%                 QextI0(i) = QextI0(i) + (2/x).*real(b0(i,...
                    % n(p)+n_maks+1));
                QscaI(jj) = QscaI(jj) + (2/x).*abs(b(jj,...
                    n(kk)+n_maks+1)).^2;%b.*conj(b);
                QextII(jj) = QextII(jj) + (2/x).*real(a(jj,...
                    n(kk)+n_maks+1));
                QscaII(jj) = QscaII(jj) + (2/x).*abs(a(jj,...
                    n(kk)+n_maks+1)).^2;%a.*conj(a);

            end



            QabsI(jj) = QextI(jj) - QscaI(jj);
            QabsII(jj) = QextII(jj) - QscaII(jj);

        end
ReB = real(b);
ImB = imag(b);

ReA = real(a);
ImA = imag(a);
%% Constant A

d_eff = (pi*R)./2;
A = 0.3; %either 0.3 or 0.5
n_i = (A.*log(10))./(4.*pi.*d_eff.*nu_array.*100);
%Formula for imaginary part of m



        mc = 1.8-1i*n_i; % m0=1.3-ni, 1.5-ni or 1.8-ni
        % complex refractive index

        b0 = zeros(length(nu_array), n_maks.*2+1);
        a0 = zeros(length(nu_array), n_maks.*2+1);
```

```
for ii = 1:length(lambda_array)
    x0 = 2*pi*R./lambda_array(ii);
    y0 = mc(ii)*x0;

    QextI0(ii) = 0;
    QscaI0(ii) = 0;
    QextII0(ii) = 0;
    QscaII0(ii) = 0;

    k0 = 2*pi/lambda_array(ii);
    rho0 = 2.*k0.*R.*(mc(ii)-1);

    for pp = 1:length(n)
        Jx0 = besselj(n(pp), x0);
        dJx0 = 0.5*(besselj(n(pp)-1, x0) - besselj(n(pp)+1, x0));

        Jy0 = besselj(n(pp), y0);
        dJy0 = 0.5*(besselj(n(pp)-1, y0) - besselj(n(pp)+1, y0));

        Nx0 = bessely(n(pp), x0);
        dNx0 = 0.5*(bessely(n(pp)-1, x0) - bessely(n(pp)+1, x0));

        tan_beta0 = (mc(ii).*dJy0.*Jx0 - Jy0.*dJx0) ./...
            (mc(ii).*dJy0.*Nx0 - Jy0.*dNx0);
        tan_alfa0 = (dJy0.*Jx0 - mc(ii).*Jy0.*dJx0) ./...
            (dJy0.*Nx0 - mc(ii).*Jy0.*dNx0);

        b0(ii, n(pp)+n_maks+1) = tan_beta0./(tan_beta0 - 1i);

        a0(ii, n(pp)+n_maks+1) = tan_alfa0./(tan_alfa0 - 1i);

        c(ii, n(pp)+n_maks+1) = b(ii, n(pp)+n_maks+1)-a(ii,...
            n(pp)+n_maks+1);

        QextI0(ii) = QextI0(ii) + (2/x0).*real(b0(ii,...
            n(pp)+n_maks+1));
        QscaI0(ii) = QscaI0(ii) + (2/x0).*abs(b0(ii,...
            n(pp)+n_maks+1)).^2;%b.*conj(b);
        QextII0(ii) = QextII0(ii) + (2/x0).*real(a0(ii,...
```

```
                n(pp)+n_maks+1));
            QscaII0(ii) = QscaII0(ii) + (2/x0).*abs(a0(ii,...
                n(pp)+n_maks+1)).^2;%a.*conj(a);

        end



        QabsI0(ii) = QextI0(ii) - QscaI0(ii);
        QabsII0(ii) = QextII0(ii) - QscaII0(ii);

    end
ReB0 = real(b0);
ImB0 = imag(b0);

ReA0 = real(a0);
ImA0 = imag(a0);

%% FIGURES for Case I

bcn1 = 37; % the spesific bn you want to plot,
           % given as the column numnber: n_maks+1+n
bcn2 = 40; % the spesific bn you want to plot,
           % given as the column numnber: n_maks+1+n

f2 = figure('color', [1 1 1]); %Q_ext
yyaxis right
% plot(nu_array, ni_array, 'm')
plot(nu_array, ReB(:,bcn1), ':c', 'Linewidth', 6)
hold on
plot(nu_array, ReB0(:,bcn1), ':m', 'Linewidth', 6)
plot(nu_array, ReB(:,bcn2), ':k', 'Linewidth', 6)
plot(nu_array, ReB0(:,bcn2), ':y', 'Linewidth', 6)
ylabel('$\Re(b_{n})$','Interpreter','Latex','FontSize', 24);
yyaxis left
plot(nu_array, QextI(:), '-b', 'Linewidth', 8)
plot(nu_array, QextI0(:), '--g', 'Linewidth', 8)
xlabel('$\tilde{\nu}$ ($\frac{1}{cm}$)','Interpreter',...
    'Latex','FontSize', 24);
ylabel('$Q_{ext}$','Interpreter','Latex','FontSize', 24);
```

```
set(gca, 'XDir','reverse', 'FontSize', 24)
legendInfo2 = ['$b_{12}$ with Lorentz'];
legendInfo22 = ['$b_{12}$ for $n_{i}$ with $A$ = ' num2str(A)];
legendInfob1 = ['$b_{15}$ with Lorentz'];
legendInfobb1 = ['$b_{15}$ for $n_{i}$ with $A$ = ' num2str(A)];
legendInfob2 = ['$Q_{ext}$ Mie with Lorentz'];
legendInfobb2 = ['$Q_{ext}$ Mie for $n_{i}$ with $A$ = ' num2str(A)];
%vary the bn
legend(legendInfob2, legendInfobb2, legendInfo2, legendInfo22,...
    legendInfob1, legendInfobb1, 'Interpreter','Latex', 'Location',...
    'northoutside', 'FontSize', 28)

%Zoomed figure
%z_values = (501:1501); % for nu0 ~= 1750
%z_values = (1501:3001); % for nu0 ~=3250

%high res (0.05 steps) zoomed figure
% z_values = (10001:30001);
%
% fz = figure('color', [1 1 1]);
% yyaxis left
% plot(nu_array(z_values), QextI(z_values), '-b', 'Linewidth', 8)
% hold on
% plot(nu_array(z_values), QextI0(z_values), ':g', 'Linewidth', 8)
% xlabel('$\tilde{\nu}$ ($\frac{1}{cm}$)','Interpreter','Latex',...
%     'FontSize', 24);
% ylabel('$Q_{ext}$','Interpreter','Latex','FontSize', 24);
% axis( [ min(nu_array(z_values)) max(nu_array(z_values))...
% 0.9*min(min(QextI0(z_values))) 1.1*max(max(QextI0(z_values)))])
% set(gca, 'XDir','reverse','FontSize', 24)
% yyaxis right
% % plot(nu_array, ni_array, 'm')
% plot(nu_array(z_values), ReB(z_values,bcn), '-c', 'Linewidth', 6)
% plot(nu_array(z_values), ReB0(z_values,bcn), ':m', 'Linewidth', 6)
% ylabel('$\Re(b_{n})$','Interpreter','Latex','FontSize', 24);
% leg1 = legend('$Q_{ext}$ Mie with Lorentz',...
%     '$Q_{ext}$ Mie $n_{i} = 0$','$b_{16}$ with Lorentz',...
%     '$b_{16}$ with $n_{i}=0$', 'Location', 'northoutside')
% %vary the bn
```

```
% set(leg1, 'Interpreter', 'Latex', 'Fontsize', 24)

f3 = figure('color', [1 1 1]); %Q_sca
plot(nu_array, QscaI(:), '-b', 'Linewidth', 8)
hold on
plot(nu_array, QscaI0(:), ':g', 'Linewidth', 8)
xlabel('$\tilde{\nu}$ ($\frac{1}{cm}$)','Interpreter','Latex',...
    'FontSize', 24);
ylabel('$Q_{sca}$','Interpreter','Latex','FontSize', 24);
set(gca, 'XDir','reverse', 'FontSize', 24)
legendInfo3 = ['$Q_{sca}$ Mie with Lorentz'];
legendInfo33 = ['$Q_{sca}$ Mie for $n_{i}$ with $A$ = ' num2str(A)];
legend(legendInfo3, legendInfo33, 'Interpreter','Latex', 'Location',...
    'northoutside', 'FontSize', 28)

f4 = figure('color', [1 1 1]); %Q_abs
plot(nu_array, QabsI(:), '-b', 'Linewidth', 8)
hold on
plot(nu_array, QabsI0(:), ':g', 'Linewidth', 8)
xlabel('$\tilde{\nu}$ ($\frac{1}{cm}$)','Interpreter','Latex',...
    'FontSize', 24);
ylabel('$Q_{abs}$','Interpreter','Latex','FontSize', 24);
set(gca, 'XDir','reverse', 'FontSize', 24)
legendInfo4 = ['$Q_{abs}$ Mie with Lorentz'];
legendInfo44 = ['$Q_{abs}$ Mie for $n_{i}$ with $A$ = ' num2str(A)];
legend(legendInfo4, legendInfo44, 'Interpreter','Latex', 'Location',...
    'northoutside', 'FontSize', 28)
%

Lz = -imag(mv); %Lorentz
mci = -imag(mc); %ni with constant A

f5 = figure('color', [1 1 1]); %Lorentz versus ni with constant A
plot(nu_array, Lz, '-b', 'Linewidth', 8)
hold on
plot(nu_array, mci, '--g', 'Linewidth', 8)
xlabel('$\tilde{\nu}$ ($\frac{1}{cm}$)','Interpreter','Latex',...
    'FontSize', 24);
ylabel('$n_{i}$','Interpreter','Latex','FontSize', 24);
```

```
set(gca, 'XDir','reverse', 'FontSize', 24)
legendInfo5 = ['$n_{i}$ with Lorentz'];
legendInfo55 = ['$n_{i}$ with $A$ = ' num2str(A)];
legend(legendInfo5, legendInfo55, 'Interpreter','Latex', 'Location',...
    'northoutside', 'FontSize', 28)

%% FIGURES for Case II

acn1 = 37; % the spesific an you want to plot,
           % given as the column numnber: n_maks+1+n
acn2 = 40; % the spesific an you want to plot,
           % given as the column numnber: n_maks+1+n

f2 = figure('color', [1 1 1]); %Q_ext
yyaxis right
plot(nu_array, ReA(:,acn1), ':c', 'Linewidth', 6)
hold on
plot(nu_array, ReA0(:,acn1), ':m', 'Linewidth', 6)
plot(nu_array, ReA(:,acn2), ':k', 'Linewidth', 6)
plot(nu_array, ReA0(:,acn2), ':y', 'Linewidth', 6)
ylabel('$\Re(a_{n})$','Interpreter','Latex','FontSize', 24);
yyaxis left
plot(nu_array, QextII(:), '-b', 'Linewidth', 8)
plot(nu_array, QextII0(:), '--g', 'Linewidth', 8)
xlabel('$\tilde{\nu}$ ($\frac{1}{cm}$)','Interpreter','Latex',...
    'FontSize', 24);
ylabel('$Q_{ext}$','Interpreter','Latex','FontSize', 24);
set(gca, 'XDir','reverse', 'FontSize', 24)
legendInfo2 = ['$a_{12}$ with Lorentz'];
legendInfo22 = ['$a_{12}$ for $n_{i}$ with $A$ = ' num2str(A)];
legendInfob1 = ['$a_{15}$ with Lorentz'];
legendInfobb1 = ['$a_{15}$ for $n_{i}$ with $A$ = ' num2str(A)];
legendInfob2 = ['$Q_{ext}$ Mie with Lorentz for Case II'];
legendInfobb2 = ['$Q_{ext}$ Mie for Case II with' ...
    '$n_{i}$ and $A$ = ' num2str(A)];
%vary the an
legend(legendInfob2, legendInfobb2, legendInfo2, legendInfo22,...
    legendInfob1, legendInfobb1, 'Interpreter','Latex', 'Location',...
    'northoutside', 'FontSize', 28)
```

```
f3 = figure('color', [1 1 1]); %Q_sca
plot(nu_array, QscaII(:), '-b', 'Linewidth', 8)
hold on
plot(nu_array, QscaII0(:), ':g', 'Linewidth', 8)
xlabel('$\tilde{\nu}$ ($\frac{1}{cm}$)','Interpreter','Latex',...
    'FontSize', 24);
ylabel('$Q_{sca}$','Interpreter','Latex','FontSize', 24);
set(gca, 'XDir','reverse', 'FontSize', 24)
legendInfo3 = ['$Q_{sca}$ Mie with Lorentz for Case II'];
legendInfo33 = ['$Q_{sca}$ Mie  for Case II with $n_{i}$ and $A$ = '...
    num2str(A)];
legend(legendInfo3, legendInfo33, 'Interpreter','Latex', 'Location',...
    'northoutside', 'FontSize', 28)

f4 = figure('color', [1 1 1]); %Q_abs
plot(nu_array, QabsII(:), '-b', 'Linewidth', 8)
hold on
plot(nu_array, QabsII0(:), ':g', 'Linewidth', 8)
xlabel('$\tilde{\nu}$ ($\frac{1}{cm}$)','Interpreter','Latex',...
    'FontSize', 24);
ylabel('$Q_{abs}$','Interpreter','Latex','FontSize', 24);
set(gca, 'XDir','reverse', 'FontSize', 24)
legendInfo4 = ['$Q_{abs}$ Mie with Lorentz for Case II'];
legendInfo44 = ['$Q_{abs}$ Mie  for Case II with $n_{i}$ and $A$ = '...
    num2str(A)];
legend(legendInfo4, legendInfo44, 'Interpreter','Latex', 'Location',...
    'northoutside', 'FontSize', 28)

Lz = -imag(mv); %Lorentz
mci = -imag(mc); %ni with constant A

f5 = figure('color', [1 1 1]); %Lorentz versus ni with constant A
plot(nu_array, Lz, '-b', 'Linewidth', 8)
hold on
plot(nu_array, mci, '--g', 'Linewidth', 8)
xlabel('$\tilde{\nu}$ ($\frac{1}{cm}$)','Interpreter','Latex',...
    'FontSize', 24);
```

```
ylabel('$n_{i}$','Interpreter','Latex','FontSize', 24);
set(gca, 'XDir','reverse', 'FontSize', 24)
legendInfo5 = ['$n_{i}$ with Lorentz'];
legendInfo55 = ['$n_{i}$ with $A$ = ' num2str(A)];
legend(legendInfo5, legendInfo55, 'Interpreter','Latex', 'Location',...
    'northoutside', 'FontSize', 28)
```

Appendix B. MatLab script: bn-ripple-pairs

```
% Exact expression for Qext og Qabs for an infinitely long cylinder.
% Plots Qext and selective coefficients bn from Mie with ni=0.
%
% The incident light travels perpendiculary to the cylinder axis.
% Case I from van de Hulst with E-field parallell to the cylinder.
%
% Simen R nnekleiv Eriksen, date 24.03.2020, based on M. A. Brandsruds
% excact Qext and Qabs algorithm from 16.09.2019
%
% Theory from van de Hulst chap 15.

%%

clear all
close all

%I = case I = E-field parallell to cylinder axis
%II = case II = E-field perpendicular to cylinder axis

set(groot,'defaulttextinterpreter','latex');
set(groot,'defaultLegendInterpreter','latex');
set(groot,'defaultAxesTickLabelInterpreter','latex');

%Input:
nu_array = 1000:1:4000;

lambda_array = 1./(100*nu_array);

R = 10e-6;
```

```
nr = 1.3;
ni = 0.0; %Assume no imaginary refraction

    %% Mie for cylinder

    m = nr - ni*1i;

x= 2*pi*R./lambda_array;
n_maks = max(ceil(x + 4*x.^(1/3) + 2));

b = zeros(length(nu_array), n_maks.*2+1);
a = zeros(length(nu_array), n_maks.*2+1);

    for j = 1:length(lambda_array)
        x= 2*pi*R./lambda_array(j);
        y = m*x;

        nu_min = -ceil(x + 4*x.^(1/3) + 2);
        nu_max = ceil(x + 4*x.^(1/3) + 2);

        n = nu_min:1:nu_max;

        QextI(j) = 0; %Mie ripples
        QscaI(j) = 0;
        QextII(j) = 0;
        QscaII(j) = 0;

        k = 2*pi/lambda_array(j);
        rho = 2*k*R*(m-1);


        for kk = 1:length(n)
            Jx = besselj(n(kk), x);
            dJx = 0.5*(besselj(n(kk)-1, x) - besselj(n(kk)+1, x));

            Jy = besselj(n(kk), y);
            dJy = 0.5*(besselj(n(kk)-1, y) - besselj(n(kk)+1, y));

            Nx = bessely(n(kk), x);
```

```
            dNx = 0.5*(bessely(n(kk)-1, x) - bessely(n(kk)+1, x));

            tan_beta = (m.*dJy.*Jx - Jy.*dJx) ./ (m.*dJy.*Nx - Jy.*dNx);
            tan_alfa = (dJy.*Jx - m.*Jy.*dJx) ./ (dJy.*Nx - m.*Jy.*dNx);

            b(j, n(kk)+n_maks+1) = tan_beta./(tan_beta - 1i);
            a(j, n(kk)+n_maks+1) = tan_alfa./(tan_alfa - 1i);

            c(j, n(kk)+n_maks+1) = b(j, n(kk)+n_maks+1)-a(j,...
                n(kk)+n_maks+1);

            QextI(j) = QextI(j) + (2/x).*real(b(j, n(kk)+n_maks+1));
            %Mie ripples
            QscaI(j) = QscaI(j) + (2/x).*abs(b(j, n(kk)+n_maks+1)).^2;
            %b.*conj(b);
            QextII(j) = QextII(j) + (2/x).*real(a(j, n(kk)+n_maks+1));
            QscaII(j) = QscaII(j) + (2/x).*abs(a(j, n(kk)+n_maks+1)).^2;
            %a.*conj(a);

        end

        QabsI(j) = QextI(j) - QscaI(j);
        QabsII(j) = QextII(j) - QscaII(j);

    end
ReB = real(b);
ImB = imag(b);

ReA = real(a);
ImA = imag(a);

%% FIGURE for case I
%
% f2 = figure('color', [1 1 1]);
% yyaxis right
% % plot(nu_array, ReB(:, :)) %plots all bns
% plot(nu_array, ReB(:,12), ':c', 'Linewidth', 8)
% % Put a column number to represent a bn
% hold on
```

```
% plot(nu_array, ReB(:,14), ':m', 'Linewidth', 8)
% % Put a column number to represent a bn
% ylabel('$\Re(b_{n})$', 'Interpreter', 'Latex', 'FontSize', 24)
% axis([ min(nu_array) max(nu_array) 0 1])
% yyaxis left
% plot(nu_array, QextI(:), '-k', 'Linewidth', 8)
% xlabel('$\tilde{\nu}$ ($\frac{1}{cm}$)','Interpreter',...
% 'Latex','FontSize', 24)
% set(gca, 'XDir','reverse', 'FontSize', 24)
% ylabel('$Q_{ext}$','Interpreter','Latex','FontSize', 24)
% axis([ min(nu_array) max(nu_array) 0.9*min(min(QextI))...
% 1.1*max(max(QextI))])
% leg1 = legend('$Q_{ext}$','$b_{?}$','$b_{?}$', 'Location',...
% 'eastoutside'); %Call the correct bn from n-list
% set(leg1, 'Interpreter', 'Latex', 'Fontsize', 24)

%% FIGURE for case II

f3 = figure('color', [1 1 1]);
yyaxis right
% plot(nu_array, ReB(:, :)) %plots all bns
plot(nu_array, ReA(:,58), ':c', 'Linewidth', 8)
%Put a column number to represent a bn
hold on
plot(nu_array, ReA(:,64), ':m', 'Linewidth', 8)
%Put a column number to represent a bn
ylabel('$\Re(b_{n})$', 'Interpreter', 'Latex', 'FontSize', 24)
axis([ min(nu_array) max(nu_array) 0 1])
yyaxis left
plot(nu_array, QextII(:), '-k', 'Linewidth', 8)
xlabel('$\tilde{\nu}$ ($\frac{1}{cm}$)','Interpreter',...
    'Latex','FontSize', 24)
set(gca, 'XDir','reverse', 'FontSize', 24)
ylabel('$Q_{ext}$','Interpreter','Latex','FontSize', 24)
axis([ min(nu_array) max(nu_array) 0.9*min(min(QextII))...
    1.1*max(max(QextII))])
leg1 = legend('$Q_{ext}$ Case II','$a_{18}$','$a_{24}$',...
    'Location', 'eastoutside'); %Call the correct bn from n-list
set(leg1, 'Interpreter', 'Latex', 'Fontsize', 24)
```

Appendix C. MatLab script: Q_{sca} integral for cylinder case 1

```
%% Qsca integral over numerical aperture for cylinder
clear all
clc

%% Define parameters
v = 1000:1:4000; % List of wavenumbers in cm^-1
lambda = 1./(v*100); % Wavelength in m
a = 10e-6; % Radius of the cylinder in m
x = 2*pi*a./lambda; % Scaling factor array
n_max = max(ceil(x + 4*x.^(1/3) + 2)); % Maximum n
n_min = -max(ceil(x + 4*x.^(1/3) + 2)); % Minimum n
n = n_min:1:n_max; % List of n's
ni = 0;
m = 1.5 - 1i*ni; % Complex refractive index
y = m.*x; % Second scaling factor
NA = [0 0.2 0.35 0.5 0.65]; % List of different numerical apertures

%% The Integral with regard to numerical aperture

for kk = 1:length(NA)
    t_min = asin(NA(kk)); % Start of integration area
    t_max = 2*pi - t_min; % End of integration area
    theta = t_min:0.01:t_max;
    % The angles the integral is calculated over
    bn = zeros(length(v), length(n));

for ii = 1:length(v)
    Qsca(ii, kk) = 0;
```

```
    x = 2*pi*a./lambda(ii); % Scaling factor
    y = m.*x; % Second scaling factor

    for jj = 1:length(n)

        % Functions dependent on x
        Jx = besselj(n(jj), x); % Bessel Function of first kind
        dJx = 0.5.*(besselj(n(jj)-1, x) - besselj(n(jj)+1,x));
        % Derivative of Bessel function of first kind
        Hx = besselh(n(jj), 2, x); % Second Hankel Function
        dHx = 0.5.*(besselh(n(jj)-1, 2, x) - besselh(n(jj)+1, 2, x));
        % Derivative of Second Hankel Function

        %Functions dependent of y
        Jy = besselj(n(jj), y); % Bessel Function of first kind
        dJy = 0.5.*(besselj(n(jj)-1, y) - besselj(n(jj)+1,y));
        % Derivative of Bessel function of first kind
%           Hy = besselh(n, 2, y); % Second Hankel Function
%           dHy = 0.5.*(besselh(n-1, 2, y) - besselh(n+1, 2, y));
% Derivative of Second Hankel Function

        bn(ii, jj) =(m.*dJy.*Jx-Jy.*dJx)./(m.*dJy.*Hx-Jy.*dHx);
        % The coefficient bn

        Qsca(ii, kk) = Qsca(ii, kk) + 1/(pi.*x).*trapz(theta,...
            (abs(bn(ii, jj).*exp(1i.*n(jj).*theta))).^2);
        % Scattering efficiency calculated with trapezoid method

    end

end
end


%% Plot figure

cmap = colormap(jet(length(NA)));

f1 = figure('color', [1 1 1]);
```

```
for kk = 1:length(NA)
    if ni == 0
        Qext = Qsca;
        plot(v, Qext(:, kk),'color', cmap(kk, :), 'Linewidth', 6);
        hold on
        Leg{kk} = ['$Q_{ext}$ with $m$ = ' num2str(m) ' and $a$ = ' ...
            num2str(a) ' by integral with regard to NA = ' ...
            num2str(NA(kk))];
    else
    plot(v, Qsca(:, kk),'color', cmap(kk, :), 'Linewidth', 6);
    hold on
    Leg{kk} = ['$Q_{sca}$ with $m$ = ' num2str(m) ' and $a$ = ' ...
        num2str(a) ' by integral with regard to NA = ' num2str(NA(kk))];
    end
end
legend(Leg, 'Interpreter','Latex', 'Location', 'northoutside',...
    'FontSize', 28)
xlabel('Wavenumber [cm$^{-1}$]','Interpreter','Latex','FontSize',24);
set(gca,'XDir','reverse', 'FontSize', 24);
if ni == 0
    ylabel('$Q_{ext}$','Interpreter','Latex','FontSize',24);
else
ylabel('$Q_{sca}$','Interpreter','Latex','FontSize',24);
end
```

Appendix D. MatLab script: Q_{sca} integral with Lorentz

```
%% Qsca integral over numerical aperture for cylinder
clear all
close all
clc

%% Define parameters for Qsca
v = 1000:1:4000; % List of wavenumbers in cm^-1
lambda = 1./(v*100); % Wavelength in m
a = 10e-6; % Radius of the cylinder in m
x = 2*pi*a./lambda; % Scaling factor array
n_max = max(ceil(x + 4*x.^(1/3) + 2)); % Maximum n
n_min = -max(ceil(x + 4*x.^(1/3) + 2)); % Minimum n
n = n_min:1:n_max; % List of n's
NA = [0 0.2 0.35 0.5 0.65]; % List of different numerical apertures

%% Define parameters for Lorentz
v0 = 3128; % Wavenumber for bn peak corresponding to ripple
Wavenumbers = num2str(v);
Gamma = 15; % gamma = 15 or 300
Lambda = 2300; % proportional to absorbance, increases Lorentz peak.
s = cal_dielectricSusc_func(Wavenumbers, v0, Gamma, Lambda);
%susceptibility
e = 1.69 - s.d; % e=1.69-s.d, 2.25-s.d, or 3.24-s.d
%dielectic function
m.d = sqrt(e); %complex refractive index

%% The Integral with regard to numerical aperture
```

```
for kk = 1:length(NA)
    t_min = asin(NA(kk)); % Start of integration area
    t_max = 2*pi - t_min; % End of integration area
    theta = t_min:0.01:t_max;
    % The angles the integral is calculated over
    bn = zeros(length(v), length(n));

for ii = 1:length(v)
    Qsca(ii, kk) = 0;
    x = 2*pi*a./lambda(ii); % Scaling factor
    y = m.d(ii).*x; % Second scaling factor

    for jj = 1:length(n)

        % Functions dependent on x
        Jx = besselj(n(jj), x); % Bessel Function of first kind
        dJx = 0.5.*(besselj(n(jj)-1, x) - besselj(n(jj)+1,x));
        % Derivative of Bessel function of first kind
        Hx = besselh(n(jj), 2, x); % Second Hankel Function
        dHx = 0.5.*(besselh(n(jj)-1, 2, x) - besselh(n(jj)+1, 2, x));
        % Derivative of Second Hankel Function

        %Functions dependent of y
        Jy = besselj(n(jj), y); % Bessel Function of first kind
        dJy = 0.5.*(besselj(n(jj)-1, y) - besselj(n(jj)+1,y));
        % Derivative of Bessel function of first kind
%          Hy = besselh(n, 2, y); % Second Hankel Function
%          dHy = 0.5.*(besselh(n-1, 2, y) - besselh(n+1, 2, y));
        % Derivative of Second Hankel Function

        bn(ii, jj) =(m.d(ii).*dJy.*Jx-Jy.*dJx)./(m.d(ii).*dJy.*Hx-...
            Jy.*dHx); % The coefficient bn

        Qsca(ii, kk) = Qsca(ii, kk) + 1/(pi.*x).*trapz(theta,...
            (abs(bn(ii, jj).*exp(1i.*n(jj).*theta))).^2);
        % Scattering efficiency calculated with trapezoid method

    end
```

```
end
end


%% Plot figure

cmap = colormap(jet(length(NA)));
f1 = figure('color', [1 1 1]);
for kk = 1:length(NA)
    plot(v, Qsca(:, kk),'color', cmap(kk, :), 'Linewidth', 6);
    hold on
    Leg{kk} = ['$Q_{sca}$ with Lorentz and $a$ = ' num2str(a)...
        ' by integral over NA = ' num2str(NA(kk))];
end
legend(Leg, 'Interpreter','Latex', 'Location', 'northoutside',...
    'FontSize', 28)
xlabel('Wavenumber [cm$^{-1}$]','Interpreter','Latex','FontSize',24);
ylabel('$Q_{sca}$','Interpreter','Latex','FontSize',24);
set(gca,'XDir','reverse', 'FontSize', 24);
```

Appendix E. MatLab script: Disk exact

```
% Disk_Scattering15122016.m

% Calculates the wave function for a two-dimentional system
% Includes correct solution for the diagonal elements of G
% Start in upper left corner for all arrays etc --> agree with reshape()
% Have make functions to do the different parts to make a nicer program
%
% ONLY FOR DISKS!!
% Exact solution of G at diagonal! NB! dx=dy!!

%%

clear all
close all



set(groot,'defaulttextinterpreter','latex');
set(groot,'defaultLegendInterpreter','latex');
set(groot,'defaultAxesTickLabelInterpreter','latex');

addpath('C:\Users\Documents\MATLAB')

%% INPUT:
% nu_array = [1807 2600 3128]; %For disk1
% nu_array = [2696 3287]; %For disk2
nu_array = [3287];
% ni=0.00:0.002:0.032;
% ni = [0.0 0.011 0.014 0.02 0.023 0.032]; %For disk1
ni = [0.0 0.021 0.026 0.036 0.044]; %For disk2
```

```
for jjj = 1:length(nu_array)
wl = 1./(100*nu_array(jjj)); % Wavelength

folder = ['C:\Users\Simen\Documents\MATLAB', num2str(nu_array(jjj))];
if ~exist(folder, 'dir')
   mkdir(folder)
end


for ii = 1:length(ni)
kk = 0;


Nx=1080;                % Resolution in x-direction
Ny=1080;                % Resolution in y-direction
N=Nx*Ny;              % No of elements in matrix.
NCx=1;                % No of disks in x-direction
NCy=1;                % No of disks in y-direction
R = 5e-6;       % Radius R
F = 2;              % Size of frame as fraction of R
n_index=1.8+1i*ni(ii);        % Refractiv index of the disk(s)
n_index_ec = 1;       %Index of energy converting material
lt =0;    %layer thickness as a fraction of R

%Incoming wave
planewave = 1;

% For calculations of psi_exact and s-matrix
nu = (-40:1:40);

potential = 1;

%% Discretization
%Make the grid. Start in upper left corner and make points downwards.
%Center of the disk is at origo.
a=2*NCx*R*(1+F);      % Width
b=2*NCy*R*(1+F+lt);      % Hight
```

```
dx=a/Nx; % spacing in x-direction
dy=b/Ny; % spacing in y-direction

x=zeros(1,N);
y=zeros(1,N);
x_axis=zeros(1,Nx);
y_axis=zeros(1,Ny);
%Make the grid. Start in upper left corner and make points downwards.
%Center of the disk is at origo.

j=0;
for i=1:Nx
    for l=1:Ny
        j = j+1;
        x(j)=-R*(1+F)+(i-0.5)*dx;
        y(j)= R*(1+F+lt)-(l-0.5)*dy;
        y_axis(l)=y(j);
    end
    x_axis(i)=x(j);
end

clear i j l
%% Potential
[v, v_test, v_test_outside,v_test_ec] = createpotential(N, NCx,...
    NCy, R, F, x, y, n_index, n_index_ec, potential, lt);

% %Plot potential
% vMat=reshape(real(v), Ny,Nx);
% figure('Color',[1 1 1])
% h1 = pcolor(vMat);
% set(h1, 'EdgeColor', 'none'); % Uten linjer
% title({['The potential'],[' n_d_i_s_k = ' num2str(n_index)]})
% axis ij
% colorbar

%% Caclulate incoming wave
for m = 1:length(wl)

    lambda = wl(m);
```

```
phi = 0;%3*pi/2;
k = 2*pi/lambda;
kx=k*cos(phi);
ky=k*sin(phi);


%% Calculate the exact wave function
if (planewave)
    psi_exact = psi_exact_planewave(k, x, y, R, nu,...
        n_index, v_test, v_test_outside);
end


psi_exact_reshaped=(reshape(psi_exact,Ny,Nx));
Xplot2=abs(psi_exact_reshaped).*abs(psi_exact_reshaped);


if ii == 1
    cmax = max(max(Xplot2));
end

Eint(ii,m) = sum(sum(psi_exact.*conj(psi_exact)).*v_test*dy*dx);


f2 = figure('Color',[1 1 1]);
h2 = pcolor(Xplot2);
set(h2, 'EdgeColor', 'none'); % Uten linjer
title(['$\tilde{\nu}$ = ' num2str(nu_array(jjj))...
    ' $\frac{1}{cm}$, m = ' num2str(real(n_index))...
    ' - ' num2str(ni(ii)) 'i'],'Interpreter','Latex' )
% This thesis writes m = nr - ni*li
axis ij
colorbar
caxis([0 cmax]) %constant scale
pbaspect([NCx NCy 1])
shading interp;

%savefig(f2,[folder, '/f2_n_i_',num2str(ni(ii)) ,'.fig'])
saveas(f2,[folder, '/a5um_nr' num2str(real(n_index)) '_Disk_v'...
```

```
        num2str(nu_array(jjj)) '_ni_' ,num2str(ni(ii)),'.png'],'png')

    close(f2)

end

end


if(0)
f1 = figure('color', [1 1 1]);
cmap=colormap(jet(length(ni)));
for ii = 1:length(ni)
    plot(wl*1e6, Eint(ii,:),'Color',cmap(ii,:))
    hold on
    legendInfo{ii} = ['$m $ = ' num2str(real(n_index)) ' - '...
        num2str(ni(ii)), 'i'];
end
plot([8.7135 8.7135], [min(min(Eint))*0.9 max(max(Eint))*1.1] , '--k')
legend(legendInfo,'Interpreter','Latex','FontSize', 28)
xlabel('$\lambda$ ($\mu$m)','Interpreter','Latex','FontSize', 32)
ylabel('$\int |E_{disk}|^2 dA$','Interpreter','Latex','FontSize', 28)
end

%% MOVIE
%
% filename = [folder, '/video_', num2str(nu_array(jjj))];
%
% writerObj = VideoWriter(filename);
%
% writerObj.FrameRate = 1;
% open(writerObj);
% for K = 1:length(ni)
%     filename4 = [folder, '\f2_n_i_0.0000', num2str(ni(K)), '.png'];
%     filename3 = [folder, '\f2_n_i_0.000', num2str(ni(K)), '.png'];
%     filename2 = [folder, '\f2_n_i_0.00', num2str(ni(K)), '.png'];
%     filename1 = [folder, '\f2_n_i_0.0', num2str(ni(K)), '.png'];
%     filename0 = [folder, '\f2_n_i_', num2str(ni(K)), '.png'];
%
```

```
%
%        if  isfile(filename4)
%             thisimage = imread(filename4);
%             writeVideo(writerObj, thisimage);
%        elseif  isfile(filename3)
%            thisimage = imread(filename3);
%             writeVideo(writerObj, thisimage);
%        elseif  isfile(filename2)
%             thisimage = imread(filename2);
%             writeVideo(writerObj, thisimage);
%        elseif  isfile(filename1)
%             thisimage = imread(filename1);
%             writeVideo(writerObj, thisimage);
%        elseif  isfile(filename0)
%             thisimage = imread(filename0);
%             writeVideo(writerObj, thisimage);
%        end
% end
% close(writerObj);


end
```

Appendix F. MatLab function: Create Potential

```
function [v, v_test, v_test_outside,v_test_ec] = createpotential(N,...
    NCx, NCy, R, F, x, y, n_index, n_index_ec, potential, lt)

v=zeros(1,N);
v_test=zeros(1,N);
v_test_outside = ones(1,N);
v_test_ec = zeros(1,N);

n_mirror = 1+50*1i;

for m=1:N
    for nx=1:NCx
        for ny=1:NCy
            switch potential

                case 1 %disk in air
                    xcircle=(2*(nx-1))*R*(1+F);
                    ycircle=-(2*(ny-1))*R*(1);
                    rn=sqrt((x(m)-xcircle)*(x(m)-xcircle)+...
                        (y(m)-ycircle)*(y(m)-ycircle));
                    if (rn<=R)
                        v(m)=1.0-n_index*n_index;
                        v_test(m) = 1;
                        v_test_outside(m) = 0;
                    end

                case 2 %fully embedded disk
                    xcircle=(2*(nx-1))*R*(1+F);
```

```
        ycircle=-(2*(ny-1))*R*(1);
        rn=sqrt((x(m)-xcircle)*(x(m)-xcircle)+(y(m) -...
            ycircle)*(y(m)-ycircle));
        if (rn<=R)
            v(m)=1.0-n_index*n_index;
            v_test(m) = 1;
            v_test_outside(m) = 0;
        elseif (v_test(m)== 0)
            v(m) = 1.0-n_index_ec*n_index_ec;
        end

    case 3 %halfly embedded disk
        xcircle=(2*(nx-1))*R*(1+F);
        ycircle=-(2*(ny-1))*R*(1);
        rn(m)=sqrt((x(m)-xcircle)*(x(m)-xcircle)+(y(m) -...
            ycircle)*(y(m)-ycircle));

        if (rn(m)<=R)
            v(m)=1.0-n_index*n_index;
            v_test(m) = 1;
            v_test_outside(m) = 0;
        elseif (y(m)<0) && (v_test(m)== 0)
            v(m) = 1.0-n_index_ec*n_index_ec;
        end

    case 4
        xcircle=(2*(nx-1))*R*(1+F+lt);
        ycircle=-(2*(ny-1))*R*(1+lt);
        rn(m)=sqrt((x(m)-xcircle)*(x(m)-xcircle)+(y(m) -...
            ycircle)*(y(m)-ycircle));

        if (rn(m)<=R)
            v(m)=1.0-n_index*n_index;
            v_test(m) = 1;
            v_test_outside(m) = 0;
        elseif (y(m)<-R) && (v_test(m)== 0) && (y(m)...
                > -(R+lt*R))
            v(m) = 1.0-n_index_ec*n_index_ec;
            v_test_ec(m) = 1;
```

```
                end

            case 5
                xcircle=(2*(nx-1))*R*(1+F+lt);
                ycircle=-(2*(ny-1))*R*(1+lt);
                rn(m)=sqrt((x(m)-xcircle)*(x(m)-xcircle)+(y(m)-...
                    ycircle)*(y(m)-ycircle));

                if (rn(m)<=R)
                    v(m)=1.0-n_index*n_index;
                    v_test(m) = 1;
                    v_test_outside(m) = 0;
                elseif (y(m)<-R) && (v_test(m)== 0) && (y(m)...
                        > -(R+0.5*lt*R))
                    v(m) = 1.0-n_index_ec*n_index_ec;
                    v_test_ec(m) = 1;

                elseif (y(m)<-(R+0.8*lt*R)) && (v_test(m)== 0) &&...
                        (y(m) > -(R+0.9*lt*R))
                    v(m) = 1.0-n_mirror*n_mirror;
                end

            end
        end
    end
end
end
```

Appendix G. MatLab function: Ψ exact plane wave

```
function psi_exact = psi_exact_planewave(k, x, y, R, nu,...
    n_index, v_test, v_test_outside)
phi_prime = angle(x+1i*y);
psi_exact = 0;
K = k*n_index;

for t = 1:length(nu)
    Jnu_inside = besselj(nu(t), K*sqrt(x.^2 + y.^2));
    Jnu_outside = besselj(nu(t), k*sqrt(x.^2 + y.^2));
    Hnu_outside = besselh(nu(t),1, k*sqrt(x.^2 + y.^2));

    Jk = besselj(nu(t),k*R);
    JK = besselj(nu(t),K*R);

    if nu(t) == 0
        dJk = -besselj(1,k*R);     %dJ_0 = -J_1
        dJK = -besselj(1,K*R);
    else
        dJk = 0.5*(besselj(nu(t)-1,k*R)- besselj(nu(t)+1,k*R));
        dJK = 0.5*n_index*(besselj(nu(t)-1,K*R)- besselj(nu(t)+1,K*R));
    end

    H1 = besselh(nu(t),1,k*R);
    dH1 = 0.5*(besselh(nu(t)-1,1,k*R)-besselh(nu(t)+1,1,k*R));

    NominatorB_l(t) = (1i^nu(t))*(dH1*Jk - dJk*H1);
    DenominatorB_l(t) = (dH1*JK - dJK*H1);
    Bl(t) = NominatorB_l(t)/DenominatorB_l(t);
```

```
    NominatorAana(t) = (1i^nu(t))*(dJk*JK-Jk*dJK);
    DenominatorAna(t) = H1*dJK-dH1*JK;
    A_l(t) = NominatorAana(t)./DenominatorAna(t);

    psi_exact= psi_exact + (Bl(t)*Jnu_inside.*exp(1i*nu(t)...
        .*phi_prime)).*v_test + ...
        (1i^nu(t).*Jnu_outside + A_l(t).*Hnu_outside)...
        .*exp(1i*nu(t).*phi_prime).*v_test_outside;
end
```

Appendix H. MatLab script: Mie sphere

```
%close all
clear all

set(groot,'defaulttextinterpreter','latex');
set(groot,'defaultLegendInterpreter','latex');
set(groot,'defaultAxesTickLabelInterpreter','latex');

addpath('C:\Users\simen\Documents\MATLAB\metzler_qext_sphere\functions')

a =5*1e-6; %radius of sphere in m
wn = (1000:10:5000)*100; %wave number in 1/m
x = 2*pi*wn.*a;

nr = 1.5*ones(1, length(wn));
%wavenumber dependent real part of ref. inf
ni0 = 0.0*ones(1, length(wn));
%wave number dependen imag part of ref. ind
ni002 = 0.002*ones(1, length(wn));
ni005 = 0.005*ones(1, length(wn));
ni01 = 0.01*ones(1, length(wn));
ni02 = 0.02*ones(1, length(wn));
%% Plot refractive indices:
% figure('color',[1 1 1])
% plot(wn/100, nr, wn/100, ni)
% set(gca, 'XDir','reverse')
% legendInfo{1} = ['$\Re(n)$'];
% legendInfo{2} = ['$\Im(n)$'];
% title('Refractive index of PMMA','Interpreter','Latex')
% legend(legendInfo,'Interpreter','Latex', 'location',...
```

```
%       'southwest','FontSize', 12)
% xlabel('$\tilde{\nu}$ [cm$^{-1}]$','Interpreter','Latex',...
%       'FontSize', 18)

%% Calculate exact Mie for a complex refractive index

%MieQabs_complex = [];
%MieQsca_complex = [];
MieQext_complex0 = [];
MieQext_complex002 = [];
MieQext_complex005 = [];
MieQext_complex01 = [];
MieQext_complex02 = [];

for jj=1:length(x)
    m0 = nr(jj) + 1i*ni0(jj); %complex refractive index
    MieExt0 = mie(m0,x(jj)); %Mie Ext from Metzler
    MieQext_complex0 = [MieQext_complex0, MieExt0(4)];
    %Qext for a sphere

    %MieQabs_complex = [MieQabs_complex, MieExt(6)];
    %MieQsca_complex = [MieQsca_complex, MieExt(5)];
end
for kk=1:length(x)
    m002 = nr(kk) + 1i*ni002(kk); %complex refractive index
    MieExt002 = mie(m002,x(kk)); %Mie Ext from Metzler
    MieQext_complex002 = [MieQext_complex002, MieExt002(4)];
    %Qext for a sphere

    %MieQabs_complex = [MieQabs_complex, MieExt(6)];
    %MieQsca_complex = [MieQsca_complex, MieExt(5)];
end
for ll=1:length(x)
    m005 = nr(ll) + 1i*ni005(ll); %complex refractive index
    MieExt005 = mie(m005,x(ll)); %Mie Ext from Metzler
    MieQext_complex005 = [MieQext_complex005, MieExt005(4)];
    %Qext for a sphere

    %MieQabs_complex = [MieQabs_complex, MieExt(6)];
```

```
    %MieQsca_complex = [MieQsca_complex, MieExt(5)];
end
for aa=1:length(x)
    m01 = nr(aa) + 1i*ni01(aa); %complex refractive index
    MieExt01 = mie(m01,x(aa)); %Mie Ext from Metzler
    MieQext_complex01 = [MieQext_complex01, MieExt01(4)];
    %Qext for a sphere

    %MieQabs_complex = [MieQabs_complex, MieExt(6)];
    %MieQsca_complex = [MieQsca_complex, MieExt(5)];
end
for dd=1:length(x)
    m02 = nr(dd) + 1i*ni02(dd); %complex refractive index
    MieExt02 = mie(m02,x(dd)); %Mie Ext from Metzler
    MieQext_complex02 = [MieQext_complex02, MieExt02(4)];
    %Qext for a sphere

    %MieQabs_complex = [MieQabs_complex, MieExt(6)];
    %MieQsca_complex = [MieQsca_complex, MieExt(5)];
end

%%

figure('color',[1 1 1])
plot(wn/100, MieQext_complex0, '-k', 'Linewidth', 6)
hold on
plot(wn/100, MieQext_complex002, ':gX', 'Linewidth', 6)
plot(wn/100, MieQext_complex005, '--m', 'Linewidth', 6)
plot(wn/100, MieQext_complex01, ':r', 'Linewidth', 6)
plot(wn/100, MieQext_complex02, '--c', 'Linewidth', 6)
set(gca, 'XDir','reverse')
legendInfo{1} = ['$Q_{ext}$ with $n_{i}=0$'];
legendInfo{2} = ['$Q_{ext}$ with $n_{i}=0.002$'];
legendInfo{3} = ['$Q_{ext}$ with $n_{i}=0.005$'];
legendInfo{4} = ['$Q_{ext}$ with $n_{i}=0.01$'];
legendInfo{5} = ['$Q_{ext}$ with $n_{i}=0.02$'];
%title('$Q_{ext}$ PMMA','Interpreter','Latex')
legend(legendInfo,'Interpreter','Latex', 'location','northwest',...
    'FontSize', 24)
```

```
xlabel('$\tilde{\nu}$ [cm$^{-1}]$','Interpreter','Latex',...
    'FontSize', 24)
```

Appendix I. MatLab script: Mie sphere with Lorentz

```
close all
clear all

set(groot,'defaulttextinterpreter','latex');
set(groot,'defaultLegendInterpreter','latex');
set(groot,'defaultAxesTickLabelInterpreter','latex');

addpath('C:\Users\simen\Documents\MATLAB\metzler_qext_sphere\functions')

a =5*1e-6; %radius of sphere in m
nu_array = 1000:1:4000;
wn = nu_array*100; %wave number in 1/m
x = 2*pi*wn.*a;

nr = 1.5*ones(1, length(wn));
%wavenumber dependent real part of ref. inf
% ni = 0.0*ones(1, length(wn));
%wave number dependen imag part of ref. ind
nu0=3530;
gamma=15;
omega=5200;
Wavenumbers=num2str(nu_array); %Wavenumbers in 1/cm
s = cal_dielectricSusc_func(Wavenumbers,nu0,gamma,omega);
e = nr.^2 + s.d;
m.d = sqrt(e);
%% Plot refractive indices:
% figure('color',[1 1 1])
```

```
% plot(str2num(Wavenumbers), nr, str2num(Wavenumbers), imag(m.d))
% set(gca, 'XDir','reverse')
% legendInfo{1} = ['$\Re(n)$'];
% legendInfo{2} = ['$\Im(n)$'];
% title('Refractive index of PMMA','Interpreter','Latex')
% legend(legendInfo,'Interpreter','Latex', 'location','southwest',...
%     'FontSize', 12)
% xlabel('$\tilde{\nu}$ [cm$^{-1}]$','Interpreter','Latex',...
%     'FontSize', 18)

%% Calculate exact Mie for a complex refractive index

MieQabs_complex = [];
MieQsca_complex = [];
MieQext_complex = [];

for jj=1:length(x)
    %m.d(jj) = nr(jj) + 1i*m.d(jj); %complex refractive index
    MieExt = mie(m.d(jj),x(jj)); %Mie Ext from Metzler
    MieQext_complex = [MieQext_complex, MieExt(4)]; %Qext for a sphere

    MieQabs_complex = [MieQabs_complex, MieExt(6)];
    MieQsca_complex = [MieQsca_complex, MieExt(5)];
end

%%
figure('color',[1 1 1])
plot(str2num(Wavenumbers), MieQabs_complex, '-k', 'Linewidth', 6)
set(gca, 'XDir','reverse','FontSize', 24)
title('$Q_{abs}$ PMMA','Interpreter','Latex', 'FontSize', 24)
%legend(legendInfo,'Interpreter','Latex', 'location','southwest','FontSize'
xlabel('$\tilde{\nu}$ [cm$^{-1}]$','Interpreter','Latex','FontSize', 24)
ylabel('$Q_{abs}$')

figure('color',[1 1 1])
plot(str2num(Wavenumbers), MieQsca_complex, '-k', 'Linewidth', 6)
set(gca, 'XDir','reverse','FontSize', 24)
title('$Q_{sca}$ PMMA','Interpreter','Latex', 'FontSize', 24)
%legend(legendInfo,'Interpreter','Latex', 'location','southwest','FontSize'
```

```
xlabel('$\tilde{\nu}$ [cm$^{-1}]$','Interpreter','Latex','FontSize', 24)
ylabel('$Q_{sca}$')

figure('color',[1 1 1])
yyaxis left
plot(str2num(Wavenumbers), MieQext_complex, '-k', 'Linewidth', 6)
set(gca, 'XDir','reverse','FontSize', 24)
ylabel('$Q_{ext}$')
yyaxis right
plot(str2num(Wavenumbers), imag(m.d), ':b','Linewidth', 6)
legendInfo{2} = ['$\Im(m)$ for PMMA sphere with a = ' num2str(a) '$\mu$m v
legendInfo{1} = ['$Q_{ext}$ for PMMA sphere with a = ' num2str(a) '$\mu$m
%title('$Q_{ext}$ PMMA','Interpreter','Latex')
legend(legendInfo,'Interpreter','Latex', 'location','northoutside','FontS
xlabel('$\tilde{\nu}$ [cm$^{-1}]$','Interpreter','Latex','FontSize', 24)
ylabel('$n_i$')
```

Norges miljø- og biovitenskapelige universitet
Noregs miljø- og biovitskapelege universitet
Norwegian University of Life Sciences

Postboks 5003
NO-1432 Ås
Norway